



UIT

THE ARCTIC  
UNIVERSITY  
OF NORWAY

Faculty of Science and Technology

Department of Geosciences

# Comparison of 3D and 2D rockfall models

*Considering terrain model quality effect on respective model performances*

—

**Håvard Hind**

*Master's thesis in Geology – GEO-3900*

*May 2018*





## **Acknowledgements**

The work leading up to this thesis was supervised by Prof. Lars Harald Blikra (UiT, NVE) PhD, and co-supervised by Louise Mary Vick (UiT), PhD, and Hallvard Haugen Nordbrøden (SVV), MSc. Thank you for your excellent guidance.

*Håvard Hind*

*Tromsø, May 2018*

## **Abstract**

Rockfalls are blocks of rock that bounce and roll down slopes. They are commonly detached from rock-slopes with inclinations over 40-45°. They embody high energy and mobility and are a major cause of landslide related deaths. Rockfalls can be simulated using empirical relationships and modelling, of which 2D and 3D variants exist for the latter. 3D models allow for rock fragment- and surface shape to be used in impact calculations but require more detailed input and longer computation time.

This thesis compares a 3D rockfall model with a 2D equivalent in terms of output values. 2D software Rocfall 6.0 and 3D software RAMMS:Rockfall is used to back calculate 4 historical rockfalls as comparative basis. The comparison involves the study of individual model performances using digital elevation models from aerial LIDAR and terrestrial photogrammetry, resolutions between 10 cm and 10 m, and on 4 different terrains. A final 3D simulation is used to design a mitigative structure to illustrate rockfall modellings capability in rockfall engineering.

The research finds that 3D modelling generally calculates higher bounce heights and total kinetic energies than 2D modelling, particularly on gentle slopes like taluses. Where 2D modelling show rolling/sliding motion, 3D models often calculate bounces. Higher resolutions generally produce higher output kinetic energies and bounce heights for both 2D and 3D software even when run out length is similar. Simulations using digital elevation models with resolution much higher than 1 m output unrealistic settling locations even in steep slope sections. Steep areas in digital elevation models produced with aircraft based LIDAR are gentler than in those produced with terrestrial photogrammetry. The latter cause the calculation of notably higher bounce heights.

# Table of contents

Acknowledgements .....	ii
Abstract .....	iii
1. Background and objective of study .....	1
2. Literature review .....	3
2.1 Rockfalls.....	3
2.1.1 Definition .....	3
2.1.2 Structural conditioning .....	3
2.1.3 Other conditioning factors.....	6
2.1.4 Rockfall dynamics.....	7
2.2 Taluses.....	10
2.3 Modelling rockfalls .....	11
2.3.1 Empirical methods.....	12
2.3.2 Process based models. ....	13
2.3.3 GIS based models.....	13
2.4 Rockfall mitigation.....	14
2.5 Remote sensing and topographic mapping.....	15
3. Description of case areas .....	18
3.1 Aunfjellet.....	19
3.1.1 Terrain description .....	20
3.1.2 Case rockfall.....	23
3.2 Revsnestinden.....	25
3.2.1 Terrain descriptions .....	25
3.2.2 Case rockfall.....	26
3.3 Rakkenes .....	29
3.3.1 Terrain descriptions.....	30
3.3.2 Case rockfalls .....	37

4. Method .....	41
4.1 Rockfall model descriptions .....	41
4.1.1 Rocfall .....	41
4.1.2 RAMMS: Rockfall .....	42
4.2 On-site work .....	43
4.3 Production of DEMs and boulder point clouds by photogrammetry .....	45
4.4 Preparing digital elevation models and 2D slope sections .....	47
4.5 Setting up simulations .....	49
4.5.1 RAMMS:Rockfall .....	49
4.5.2 Rocfall 6.0 .....	58
4.6 Material input calibration and final simulation .....	61
5 Results .....	65
5.1 Back calculation findings .....	65
5.2 Raster math findings .....	65
5.3 Simulation output .....	67
5.3.1 RAMMS: Rockfall simulations .....	67
5.3.2 Rocfall 6.0 simulations .....	86
6 Summary and discussion .....	99
6.1 Resolution control on output .....	99
6.2 Remote sensing technique effect on output .....	105
6.3 2D vs 3D modelling .....	108
6.4 Rakkenes East mitigation suggestion .....	111
7 Conclusion .....	114
Bibliography .....	115
Appendix A – Slope profiles used in Rocfall 6.0 .....	118
Appendix B – Release point coordinates .....	120
Appendix C – Historical rockfall settling locations and size .....	121

Appendix D - RAMMS:Rockfall material input.....	122
Appendix E – Rocfall 6.0 material input.....	126
Appendix F - RAMMS:Rockfall output deposit locations.....	129
Appendix G - Rocfall 6.0 output deposit locations .....	139

# 1. Background and objective of study

Norway is a mountainous area. Its landmass is a formerly submerged peneplain that has been raised up to 1000-1500 m since the Paleogene period, and continue to rise due to the loss of the burdensome ice sheets of the last ice age (Martinsen et al., 2013). The ever-loftier landmass has been eroded by water, rivers, and for the last few million years, glaciers, to form picturesque valleys and fjords from the ancient plain (Vorren et al., 2013). Unfortunately, many of the resulting mountain sides became unstable when the buttressing of glaciers largely vanished after the last ice age, and landslides and rockslides are commonplace in Norway, sometimes with disastrous consequences (Vorren et al., 2013). Consequently, obtaining knowledge on the cause and distribution of these processes remains an important task in the country.

Rockfalls are blocks of rock that bounce and roll down slopes, and are commonly detached from rock-slopes with over 40-45° inclination (Vorren et al., 2013). Although generally limited in volume, they embody high energy and mobility and are by consequence a major cause of landslide related deaths (Agliardi and Crosta, 2003). To quantify, rockfalls killed 63 people in the 20<sup>th</sup> century in Norway (Devoli et al., 2011). With the expansion of infrastructure and growth of population the consequence of natural hazards are expected to become even more severe in the future (Clague and Roberts, 2012, Domaas and Grimstad, 2014). The onset of climate change is further expected to cause increased precipitation that may elevate water pressure in rock fractures and increase the risk of rockfalls and rockslides (Domaas and Grimstad, 2014). The hazard of rockfalls will certainly remain a challenge in the future.

Determining rockfall processes is made difficult by their complexity and stochastic nature (Fratini et al., 2012). Their kinematics are still governed by mechanical laws and can be simulated to various degrees of complexity using empirical relationships or various types of rockfall modelling (Agliardi and Crosta, 2003), of which 2D and 3D solutions exist for the latter (Dorren et al., 2013). The major advantage of 3D models over 2D models is that the former allows for rock fragment- and surface shape to be used in the impact calculations, but it does however require more detailed input and longer computation time (Chen et al., 2013).

Keeping in mind the impracticalities of 3D simulation, this thesis aims to compare a 3D rockfall model with a 2D equivalent in terms of output values and input elevation data requirements.

The comparison will involve the study of individual model performances using digital elevation models from aerial LIDAR and terrestrial photogrammetry, resolutions between 10 cm and 10 m, and on 4 different terrains to provide a good understanding on the models' competence in a variety of plausible case situations. 2D software Rockfall 6.0 and 3D software RAMMS: Rockfall will be used to back calculate 4 historical rockfalls as comparative basis.

As conclusion this thesis want to highlight the models difference in output kinetic energy and bounce height, and provide guideline on optimal resolution and elevation data source for both 3D and 2D models respectively. This will ideally provide some guideline when picking software and input, also considering the available spatial data. A final simulation on a fifth location in northern Norway will be used to design a mitigative structure for a projected tunnel exit in Rakkenes, showing a practical application of a 3D rockfall model and illustrating its capability in rockfall engineering.

## **2. Literature review**

### **2.1 Rockfalls**

#### **2.1.1 Definition**

Speaking broadly, a rockfall is a natural hazard similar to storms, floods, volcanic eruptions and earthquakes etc. (Marshak, 2011). A more specific definition would be that it's a type of mass movement or mass wasting, a term which encompasses a wide array of gravitationally caused downslope transport of rock, regolith (soil, sediment and debris), snow and ice (Marshak, 2011). Definition then become less defined, some sources define rockfalls as free falling rock debris detached from a free face or cliff (Marshak, 2011, Keller, 2011) whilst some define it as one or several blocks detached from a rock body, which total volume does not exceed 100 cubic meters (Domaas and Grimstad, 2014), paying less mind to the character of movement downslope. Either way, both definitions will suit this treatment.

#### **2.1.2 Structural conditioning**

The stability of rock slopes is often significantly influenced by the structural geology of the rock (Wyllie and Mah, 2004). Structural geology in this sense pertains chiefly to the natural occurring planar breaks in rock mass such as faults, joints and bedding planes, generally referred to as discontinuities, that are weaker than intact rock (Wyllie and Mah, 2004). These rocks are mechanically anisotropic in the sense that they have different shear strength in different directions, and failure is therefore more likely to occur on these planes if stress tensors are oriented favorable to these structures (Twiss and Moores, 1992). The orientations of the discontinuities will therefore affect whether failure will occur on a rock slope (Wyllie and Mah, 2004).

There are four main types of block failures associated with different structural conditions; plane failure, wedge failure, toppling failure and circular failure (Wyllie and Mah, 2004). The types of failure and examples of structures that may cause them are outlined in figure 1. A summary of a more extensive treatment in (Wyllie and Mah, 2004) is provided in the following paragraph.

Plane failure is comparatively rare due to its numerous geometric constraints. A plane failure may only occur when a discontinuity plane strikes at an angle no more than about  $20^\circ$  different from the slope strike, have lower dip angle than the slope but higher dip angle than plane angle of friction, have upslope section of sliding surface intersect a tension crack or slope, and the unstable mass must be confined laterally by material that provide negligible resistance to sliding. Wedge failure may occur on a wider scale of geological conditions. It may occur when two set of discontinuities intersect along a line that plunge at an angle steeper than average plane angle of friction, at more gentle angles than the slope dip, and directed away from slope. Toppling failure occurs when block mass center resides outside its base causing rotation about it and failure. Common variants of toppling failure include block toppling, flexural toppling, and block flexure toppling. The different variants are outlined in figure 2. Block toppling may occur when there exists a set of orthogonally oriented discontinuities, one which dips steeply into rock and a second gently dipping joint set (cross joint) that acts to produce columnar structures. Favorable geologic conditions for this type of failure are bedded sandstone and columnar basalt where these structures are common. Flexural toppling may occur along a single set of discontinuities dipping steeply into rock. The rock mass breaks by flexure when bent due to rotation. Favorable lithologies for this type of failure include thinly bedded shales and slates. Block flexure toppling may occur under similar conditions to those that favor block toppling, although here displacement along cross joints contributes to the failure, i.e. it encompass sliding motion. If discontinuities are more or less randomly oriented, closely spaced or the rock is highly weathered, there is no longer a strongly defined structural pattern in the material. The material then behaves similar to soils and failure occurs along the line of least resistance. Generally, this results in a circular failure surface and subsequent sliding is referred to as a circular failure.

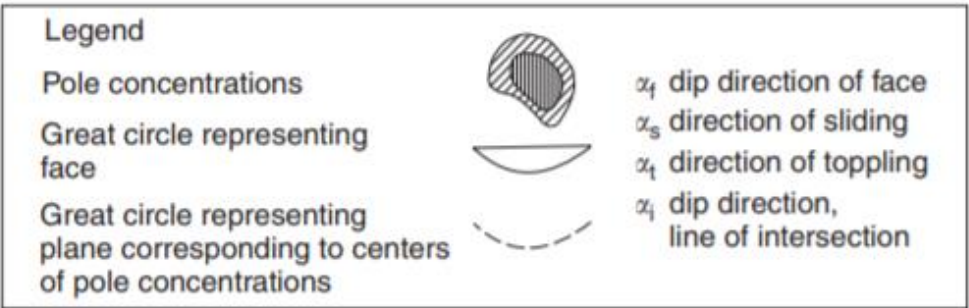
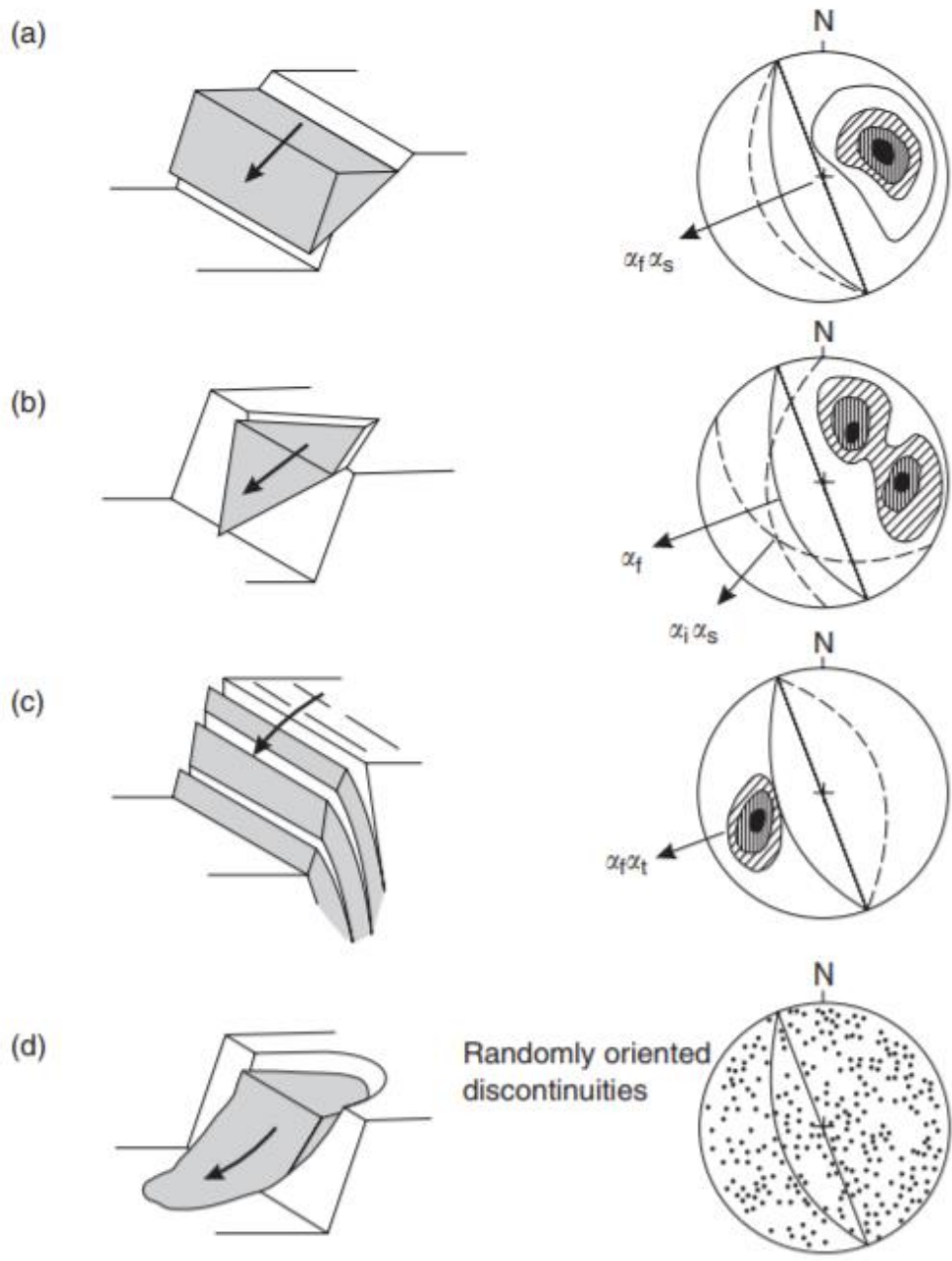


Figure 1: Different modes of slope failures and examples of favorable structural conditions for each. A) Plane failure. B) Wedge failure. C) Toppling. D) Circular failure. From (Wyllie and Mah, 2004).

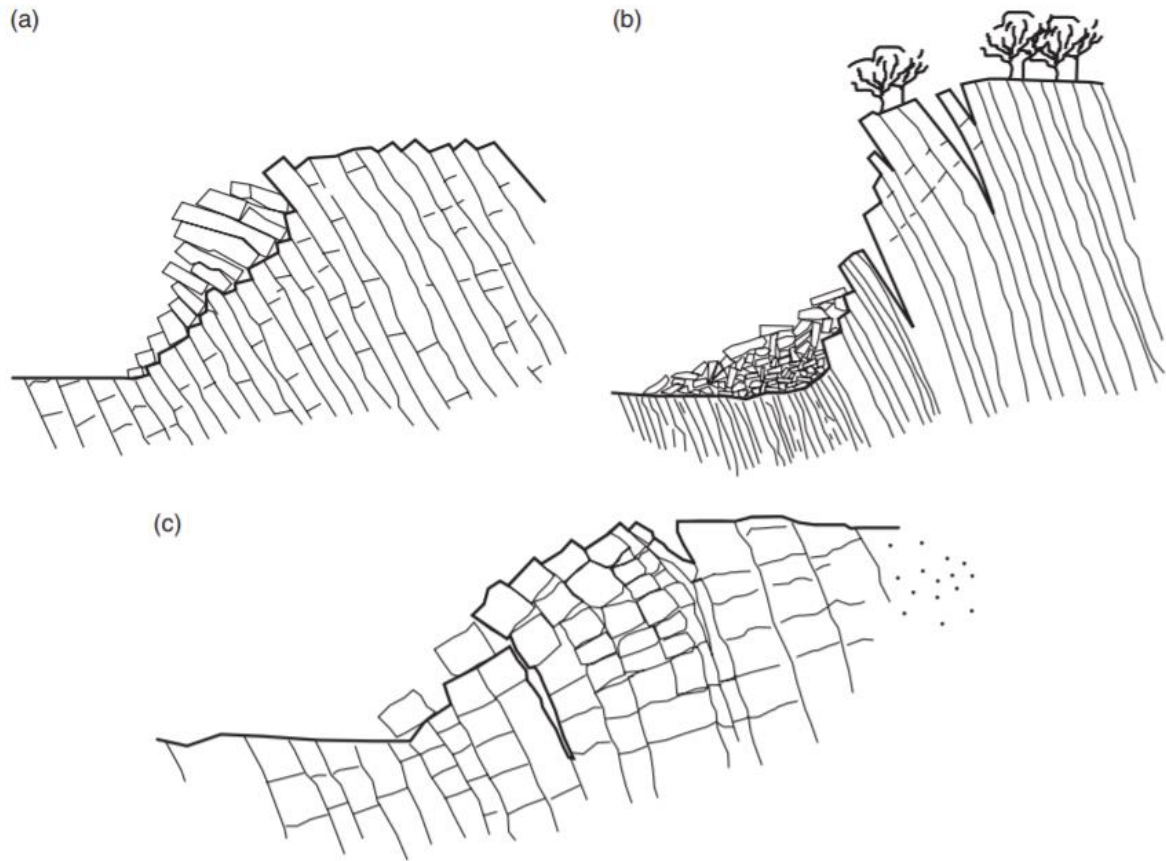


Figure 2: Common variants of toppling failures. A) Block toppling. B) Flexural toppling. C) Block – Flexure toppling. From (Wyllie and Mah, 2004).

### 2.1.3 Other conditioning factors

The structures in rock remain fairly unaltered from day to day and other processes are required to explain the cause of the occasional rockslide or rockfall. The most important mechanisms that cause rockfalls and rockslides are connected to the increase of water pressure in fractures and reduction of fracture plane shear strength (Domaas and Grimstad, 2014). The shear strength of a discontinuity depends on the roughness of its surface, the degree of weathering, extent of debris present, compressive strength of rock material, normal stress on the surface and current water pressure in it (Domaas and Grimstad, 2014). Water is almost always directly or indirectly involved with landslides and its role is particularly important (Keller, 2011). Water pressure both reduce shear strength of potential sliding surfaces by reducing effective normal shear stress on it (less friction), but also adds pressure in tension cracks, increasing forces that induce movement (Wyllie and Mah, 2004). The increase of water pressure may occur during heavy precipitation or melting of snow (Domaas and Grimstad, 2014).

If present water is further allowed to repeatedly freeze and thaw it may displace rock mass, rendering it unstable (Domaas and Grimstad, 2014). The freezing may additionally affect drainage, causing elevated water pressure (Domaas and Grimstad, 2014).

Chemical weathering facilitated by water may over time alter minerals such as feldspars to form weak clay in fractures that allows failure to occur at inclinations as low as under 20° (Domaas and Grimstad, 2014). The feldspar group is the most abundant group of rock forming minerals in the earth's crust (Keller, 2011) illustrating the process' potential importance as conditioning factor. When the thickness of the resulting debris is 25-50 % of the amplitude of fracture plane asperities, there is little to no rock-to-rock contact and fracture shear strength properties becomes that of the infilling, which in turn greatly affects material shear strength (Wyllie and Mah, 2004). Other conditioning factors for rockfalls and rockslides includes; human activity such as blasting and mining, earthquakes, and the expansion of roots during their spring/summer growth season (Domaas and Grimstad, 2014). Even certain animals such as chamois can cause rockfalls when climbing rockfaces (Dorren, 2003).

#### **2.1.4 Rockfall dynamics**

It is common to divide slopes where rockfalls are active into three sections. The upper area where movement is initiated is often called a release area, release zone, starting zone or source zone (Dorren et al., 2013). The second area is called the transit zone which is the area rockfalls have to traverse before reaching the overlapping third area; the deposition zone (Dorren et al., 2013) (see figure 3). Rockfalls propagate through the transit zone as individual blocks that don't interfere significantly with each other (Domaas and Grimstad, 2014). (Ritchie, 1963) described this motion as three main types of movement; free fall, rolling and bouncing in order of increasing slope inclination (see figure 4).

Velocity increase quickly under free fall conditions (Domaas and Grimstad, 2014). When impacting a surface, a fraction of the gained kinetic energy is lost and the remaining fraction is often called the boulders restitution (Domaas and Grimstad, 2014). Restitutions of 0.14 to 0.25 are typical for first impacts (75-86 % energy loss) (Dorren, 2003) and, unless fairly equidimensional, the boulder usually breaks (Luckman, 2013). The value of the restitution then depends somewhat on the stiffness of the substrate, varying between 0.3 and 0.7 for impacts on unconsolidated materials and 0.5 and 0.9 for impacts on bare rock according to a study by (Azzoni and De Freitas, 1995).

As long as the slope is sufficiently steep and restitution sufficiently high the boulder can retain all lost energy between impacts and continue downslope (Domaas and Grimstad, 2014). The value of restitution expected after impact on a certain substrate can be quantified by a coefficient of restitution which is in modelling sometimes treated as a material constant (Frattoni et al., 2012).

Impacts often induce rotation of falling boulders (Domaas and Grimstad, 2014). A study by The Japan Road Association found that rockfall boulder rotational energies could approach values of 40 % of the translational energy, although in half of the experiments this fraction was under 10 % (Heidenreich, 2004). This rotational motion could still allow significant increase of run out length even in flat terrain should rock shape allow this (Domaas and Grimstad, 2014). Flat and rectangular rocks run out may not benefit from this rolling motion unless they are rolling on their sides, as planar side impact may cause up to all rotation to seize (Domaas and Grimstad, 2014). Rolling is otherwise very economical in terms of energy, as only the largest radius of the rock is at any point in contact with the surface and subject to friction (Dorren, 2003). If the rolling block starts to slide, which is common late in transit zone, boulders will usually halt due to friction unless mean slope gradient changes (Bozzolo and Pamini, 1986).

Assigning restitution coefficients to materials is an empirical approach in that its values are based solely on specific datasets, and is for that fact problematic (Agliardi and Crosta, 2003). The actual nature of rockfall energy loss is based on slope roughness, slope geotechnical properties like grain size distribution, water content, void index and elastic moduli, and the boulder shapes and dynamics, but these parameters relationship to energy loss is not fully defined and the relevant parameters are difficult to ascertain in time and space (Agliardi and Crosta, 2003). So while it should be theoretically possible to compute the position and velocity of a rockfall at any time, it is severely complicated in actual conditions (Agliardi and Crosta, 2003).

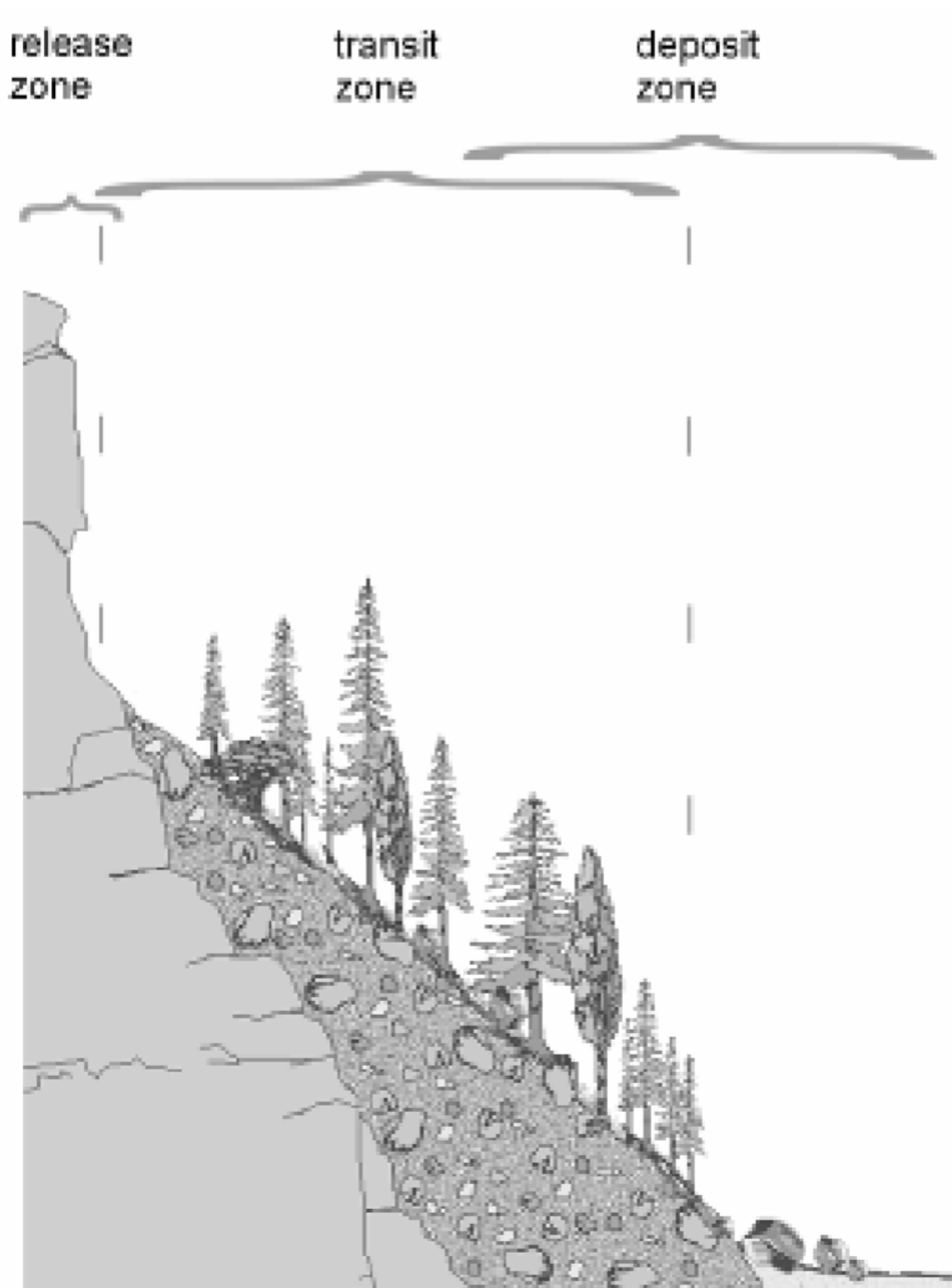


Figure 3: Zones in rockfall areas. From (Dorren et al., 2013).

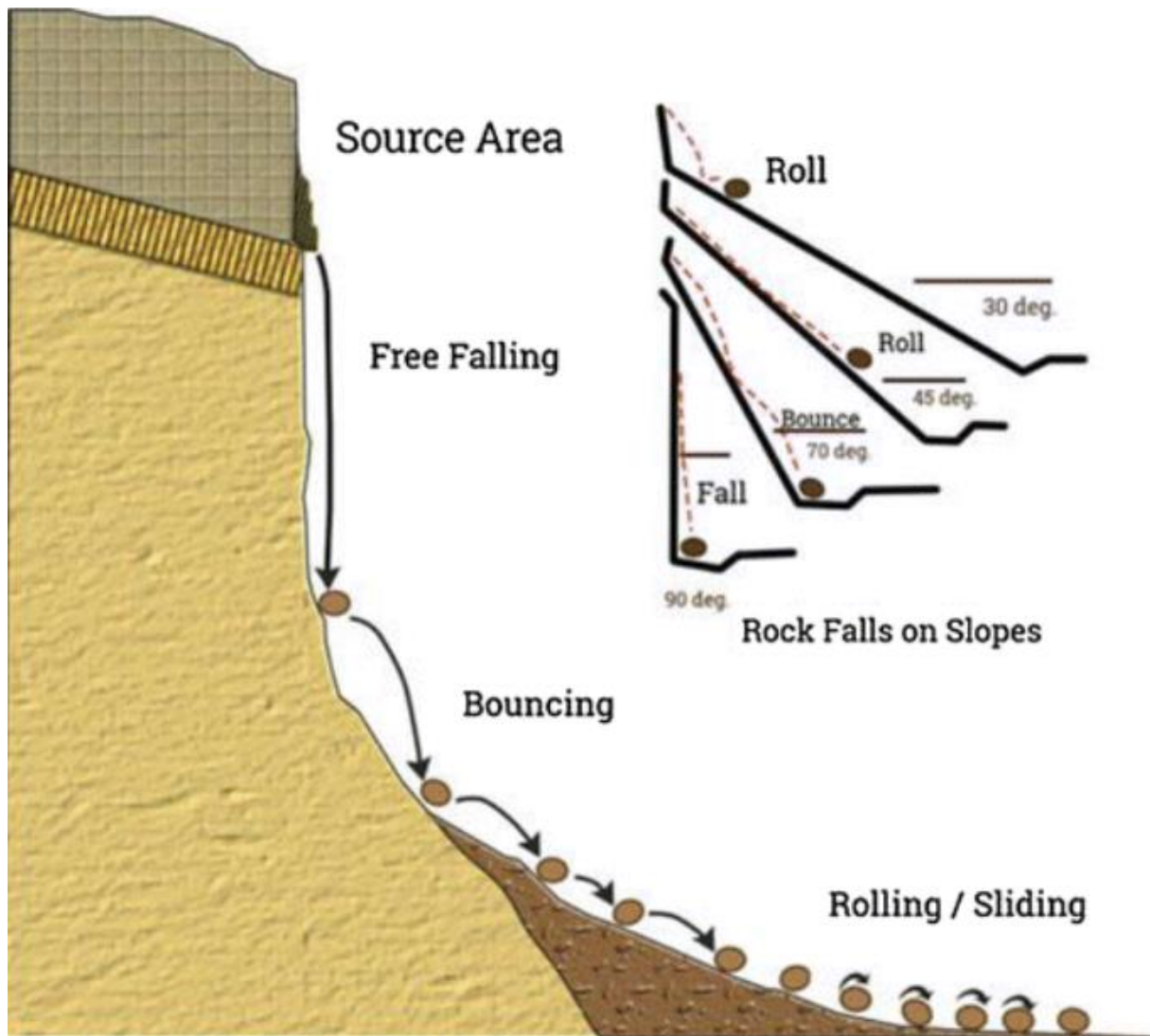


Figure 4: Modes of rockfall motion based on slope angle. (Ritchie, 1963) modified by (Fanos and Pradhan, 2018).

## 2.2 Taluses

The accumulation of debris from mass wasting processes, primarily small rockfalls (1-100 m<sup>3</sup> in volume), creates a characteristic landform and colluvial deposit of loose, usually angular, rocks called a talus or a scree (Luckman, 2013). A good overview of the landform is provided by (Luckman, 2013) and the subchapters statement are provided in this treatment. Taluses occur at the foot of steep bare slopes and generally consist of two main sections; an upper-, and a less steep lower section. Most of the landform usually has 32 to 37 and up to 40° inclinations, but mean inclination may be as low as 25-30° because of a common concavity at the bottom of the slope.

The shape of the landform is otherwise affected by the shape of the deposit area and that of the source area, laterally straight source areas producing straight, so-called sheet taluses, whilst channelized slopes creates cone shaped deposits known as talus cones (see figure 5).

Talus deposits are generally sorted with finer material upslope and coarser material downslope (Upward fining). This pattern, known as fall sorting, owes to the larger momentum of larger falling rocks and their enhanced ability to traverse irregularities in the talus. This sorting is not universal. During winter, larger rocks may be stuck in wet snow and settle in anomalous locations in upper parts of the talus, or reversely, slide down snow-covered slopes and be deposited far from the talus forming a ridge called a nivation ridge. Finer particles may also be transported downslope by avalanches, altering the upward fining sequence. The same process has also been known to transport boulders and deposit them in landforms away from talus edge, called boulder avalanche tongues. Entire taluses may also be transported far from its initial location in areas of permafrost, where they can act like a rocky glacier. Overall though, talus deposits are relatively stable by virtue of their openwork texture that allows them to stay relatively well drained and unaffected by fluvial processes.

Deposition rates on taluses as concluded by a number of studies are presently in the range of under a cm to up to a meter every millennium. These low estimates have led to the suggestion that many taluses are chiefly periglacial in origin and stem from extensive mass wasting after debutting of rock-slopes following the removal of last ice age glaciers.



*Figure 5: Sheet talus slope (left), notice bottom concavity. Talus cone (right). From (Luckman, 2013).*

### **2.3 Modelling rockfalls**

There are many ways to calculate the run out zones for rockfalls and they can broadly be separated into empirical based, process based and GIS based models (Dorren, 2003).

These can further be divided into 2D and 3D models based on whether rockfalls are allowed to deviate from a single slope segment, of which the latter is becoming increasingly more prevalent (Luckman, 2013). Models can also be categorized based on their representation of simulated rock. (Volkwein et al., 2011) distinguished between lumped mass approach, where the rock is calculated as if it was a single dimensionless point, rigid body approach, where rock shape is included in calculation of motion, and hybrid approach where free fall is simulated using lumped mass objects and rigid body mechanics are used when simulating impact, rebound and rolling.

### **2.3.1 Empirical methods**

Empirical methods, sometimes known as statistical methods, uses topographic relationships to infer run out length and are good for producing a simple and quick approximation of it (Dorren, 2003). Some are based on inferred logarithmic relationships between material volume- and vertical distance ratio and run out- length or area (Dorren 2003). Other involve the construction of lines of empirically derived inclination, propagating from points in topography and intersecting downslope topography in expected maximum run out (Dorren, 2003). These are called energy lines or shadow energy lines based on whether the origin of the line is topography- or talus apex respectively, the latter assuming that most energy is lost on first impact (Dorren, 2003). Different shadow angles and energy lines have been suggested by various authors and some examples are presented in figure 6.

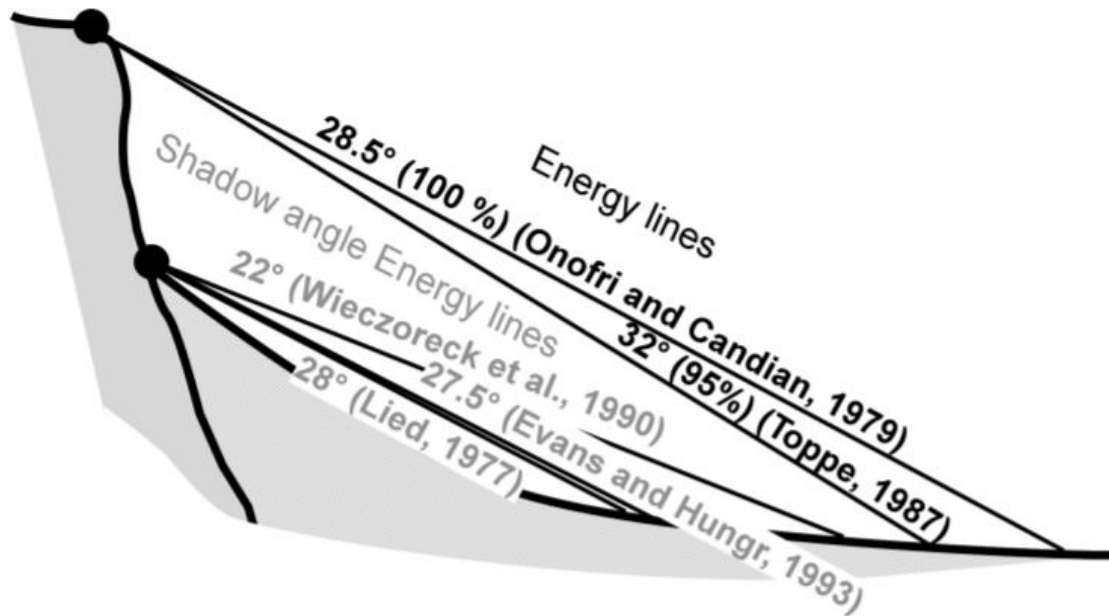


Figure 6: Shadow angles and energy lines as suggested by various authors. From (Jaboyedoff and Labiouse, 2011).

### 2.3.2 Process based models.

Process based models encompass a wide variety of models that simulates or describes the motion of rocks on simulated surfaces (Dorren, 2003). An extensive review of rockfall modelling methods has been published by (Dorren, 2003), and this subchapter summarize its treatment of process based models.

They differ in how they treat movement mode from considering all movement to be sliding, considering motion to be a series of single impacts to discriminating between rolling, sliding and bouncing motions. They further differ in their calculation of surface interaction from applying friction coefficients and rock and soil deformation laws, to simplified bulk or tangential (surface parallel) and normal (surface perpendicular) coefficients of restitution. Some further introduce stochastic variation to input to account for material property variation across slope, adding probabilistic elements to calculations.

### 2.3.3 GIS based models.

GIS (Geographical Information Systems) based models uses a GIS environment or a raster produced from GIS analysis (Dorren, 2003).

Broadly they perform three tasks; the identification of source area, the identification of fall track and the calculation of run out (Dorren, 2003). Some apply empirical models like the previously discussed shadow angle energy line to approximate maximum run out distance (Dorren, 2003).

## **2.4 Rockfall mitigation**

The hazard of rockfalls can be reduced by different techniques broadly categorizing into active and passive mitigation measures. Active measures are those that aim stabilize rock while passive measures are those that aim to either halt or deflect already detached blocks (see figure 7 for examples). Active mitigation measures include the use of shotcrete, meshes or bolts to hinder failure, enhancing drainage to prevent the buildup of water pressure and removing unstable blocks (Domaas and Grimstad, 2014).

The proper design of passive mitigation measures requires knowledge about size, volume, velocity and bounce height of the fragments in questions (Domaas and Grimstad, 2014). The values of the parameters needed for their design can be obtained by computer simulation (Wyllie, 2014). A number of options exists for passive mitigation measures and should be considered based on terrain type and available space. If available space is limited, a concrete wall anchored in substrate or a gabion wall (steel mesh filled with rocks) may be preferable (Domaas and Grimstad, 2014). If more space is available and terrain is sufficiently gentle, embankments may be constructed by local sediments (Domaas and Grimstad, 2014). These structures cannot be much steeper than 34 degrees as this compromise stability, so its height must be scaled considering fragments ability to roll up its sides (Domaas and Grimstad, 2014). Rockfall catching fences, constructions of wire mesh that absorb impact by deformation of mesh and breaking elements, may be preferable if terrain is steep and/or rough (Domaas and Grimstad, 2014). If consequences of failure is sufficiently high, tunnel or shed solutions should be considered (Domaas and Grimstad, 2014).



*Figure 7: Bolting, a active rockfall mitigation measure (left). Rockfall catching fence, a passive rockfall mitigation measure (right). From (Domaas and Grimstad, 2014).*

## **2.5 Remote sensing and topographic mapping**

Developments in the field of remote sensing techniques has made available high-resolution 3D spatial data useful for landslide modelling and susceptibility studies (Fanos and Pradhan, 2018) (see figure 8). Remote sensing is defined as “the acquisition and measurement of information about certain properties of phenomena, objects, or materials by a recording device not in physical contact with the features under surveillance” (Khorram et al., 2012). Remote sensing is geospatial in nature in that measured properties can be assigned geographical coordinates, and its potential (in the form of aerial photography) in producing topographic maps was suggested already in 1840 (Khorram et al., 2012). Since the 1930s the remote sensing technique photogrammetry, defined as the science and technique of interpreting and evaluating the form, dimension and position of objects by analyzing and measuring images of them, has been widely used to produce topographic maps (Redweik, 2012). In practice the technique applies the idea that the spatial attributes (depth) of a scene may be reconstructed by geometrical rules following its observation from two or more perspectives, a technique that has been used by artists since at least the 15<sup>th</sup> century (Redweik, 2012). It is convenient for the effectiveness of its data acquisition phase but results may easily be inhibited by shadows and occlusions (Redweik, 2012).

The application of airborne LIDAR (Acronym for Light detection and ranging (Hodgson and Bresnahan, 2004, Fanos and Pradhan, 2018, Khorram et al., 2012)) is now being used by many countries for topographic mapping (Hodgson and Bresnahan, 2004).

LIDAR calculates distance based on the travel time of emitted, high rate laser pulses reflected of objects and can produce topographic information with typical vertical accuracies of  $\pm 10-15$  cm (Khorram et al., 2012). However, accuracy is worsened by adverse climatic conditions like rain, fog, hot wind, parallel incident angles, excessive range and uneven or poorly reflective surfaces (Jaboyedoff et al., 2012). Additionally, any horizontal error, for example stemming from GPS systems, will result in enhanced vertical error when technique is used on inclined slopes, an error that increases with slope angle (Hodgson and Bresnahan, 2004).

When data is collected, topography can be presented by a set of discrete elevation points, contour lines of equal elevation, 2 dimensional profiles of height or as a function of horizontal coordinates equal to a height value, the latter generally being called a digital elevation model or DEM (Redweik, 2012). High resolution DEMs are increasingly being used for rockfall modelling (Frattini et al., 2012) hence the emphasis of remote sensing in this thesis.

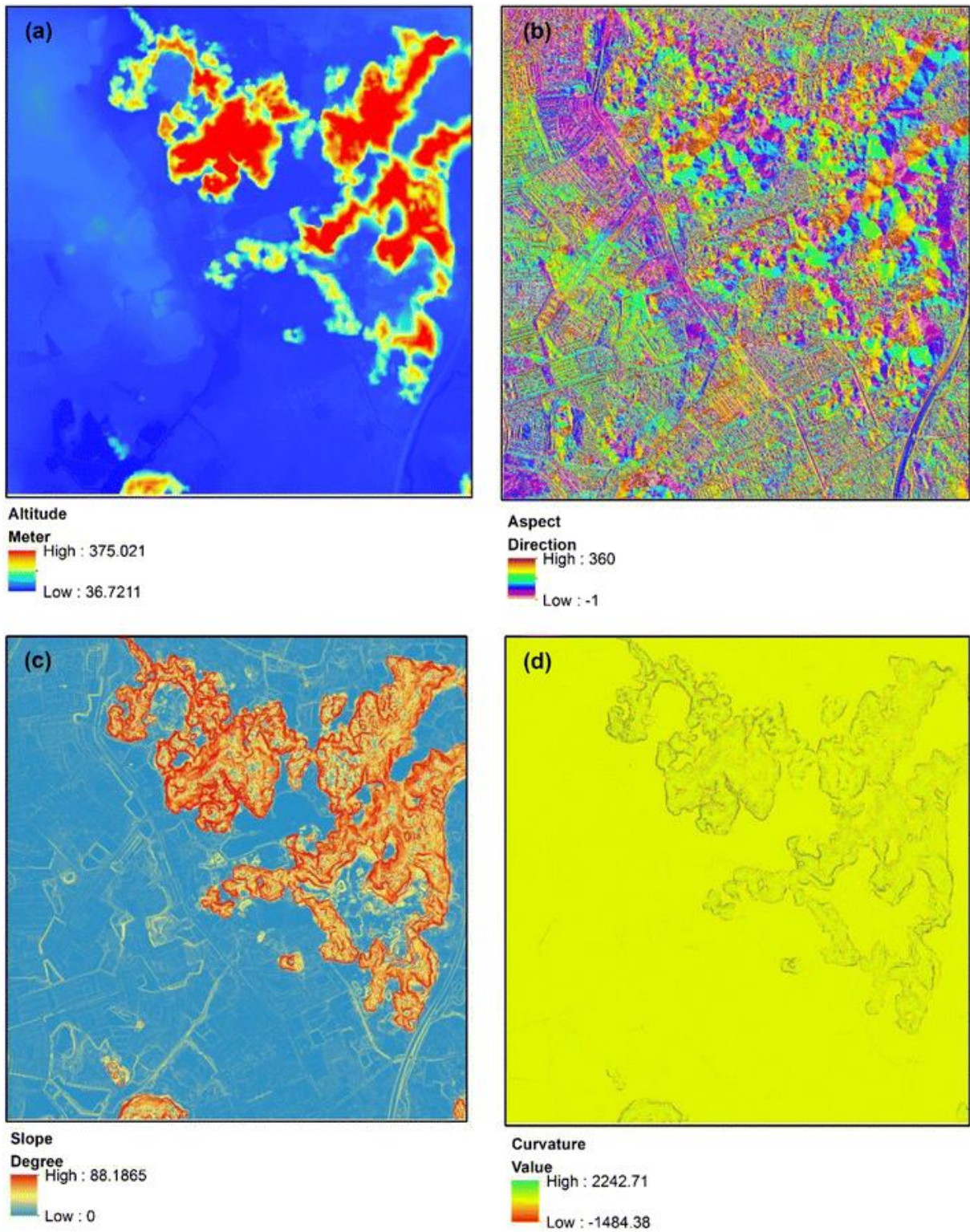


Figure 8: Geomorphic parameters obtained from the remote sensing technique LIDAR. From (Fanos and Pradhan, 2018). a) Altitude. b) Aspect (direction of maximum change rate). c) Slope. d) Curvature (change rate in aspect or slope).

### 3. Description of case areas

Four historical rockfalls will be back calculated using the two chosen models, both in Troms county in Northern Norway. Two are located in the Harstad area (Aunfjellet and Revsnestinden), and two in Rakkenes (see figure 9 and 10). Additionally, a rockfall mitigation system will be designed for a third location in Rakkenes. This chapter describes these locations in terms of terrain and substrate conditions. It also characterizes the historical rockfalls that will be used to calibrate simulation input parameters.

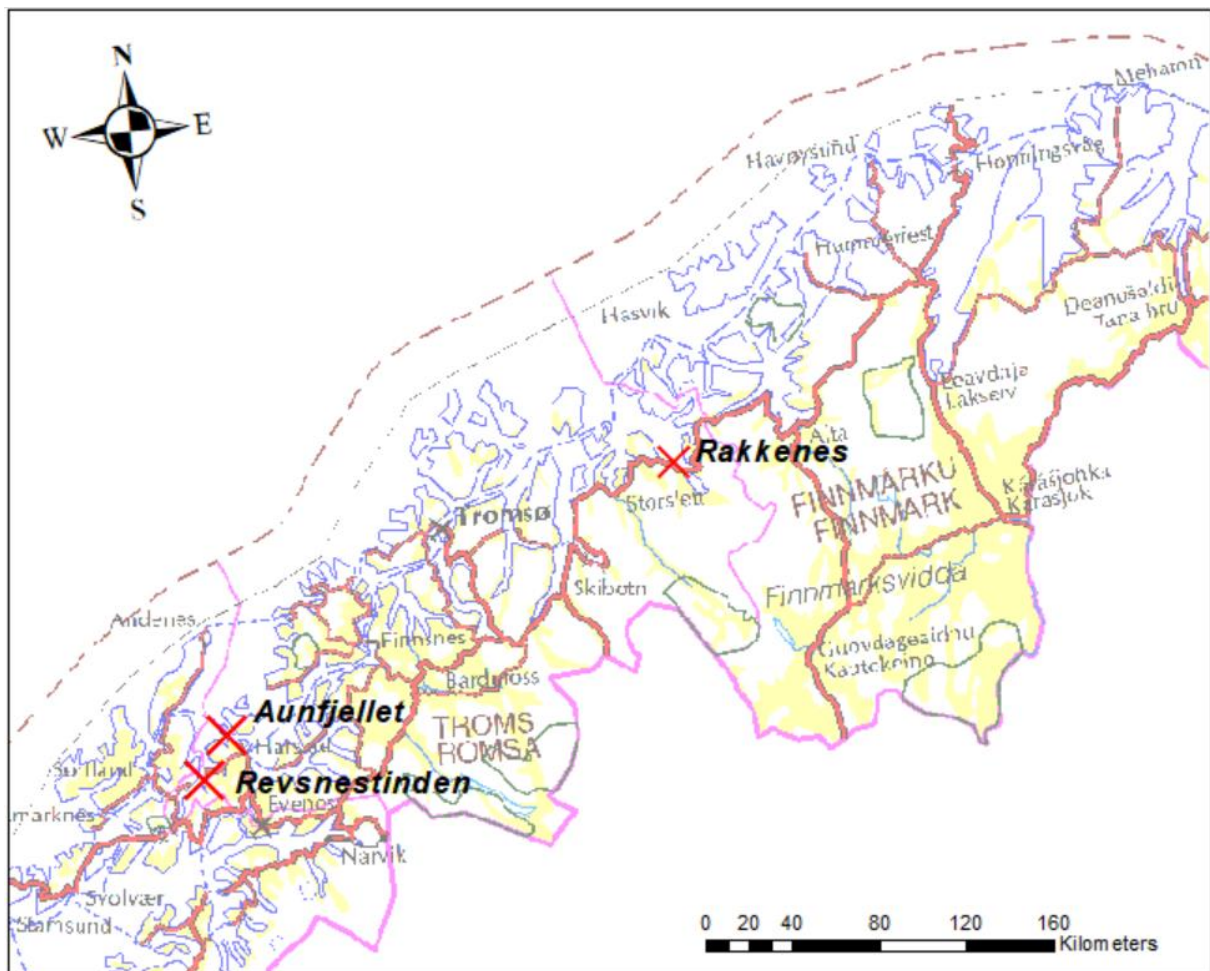


Figure 9: Case area locations in Northern Norway. Modified from (Kartverket).



Figure 10: Harstad Area case areas. Modified from (Kartverket).

### 3.1 Aunfjellet

Aunfjellet is a mountain in Harstad municipality in Troms county. The up to 496 masl (Meter Above Sea Level) mountain lies 13 km northwest of the second most populous city of Troms county, Harstad. Its eastern slope is bypassed by county road 2 and a section of it will be used as case area. See figure 11 for 3D model of area.

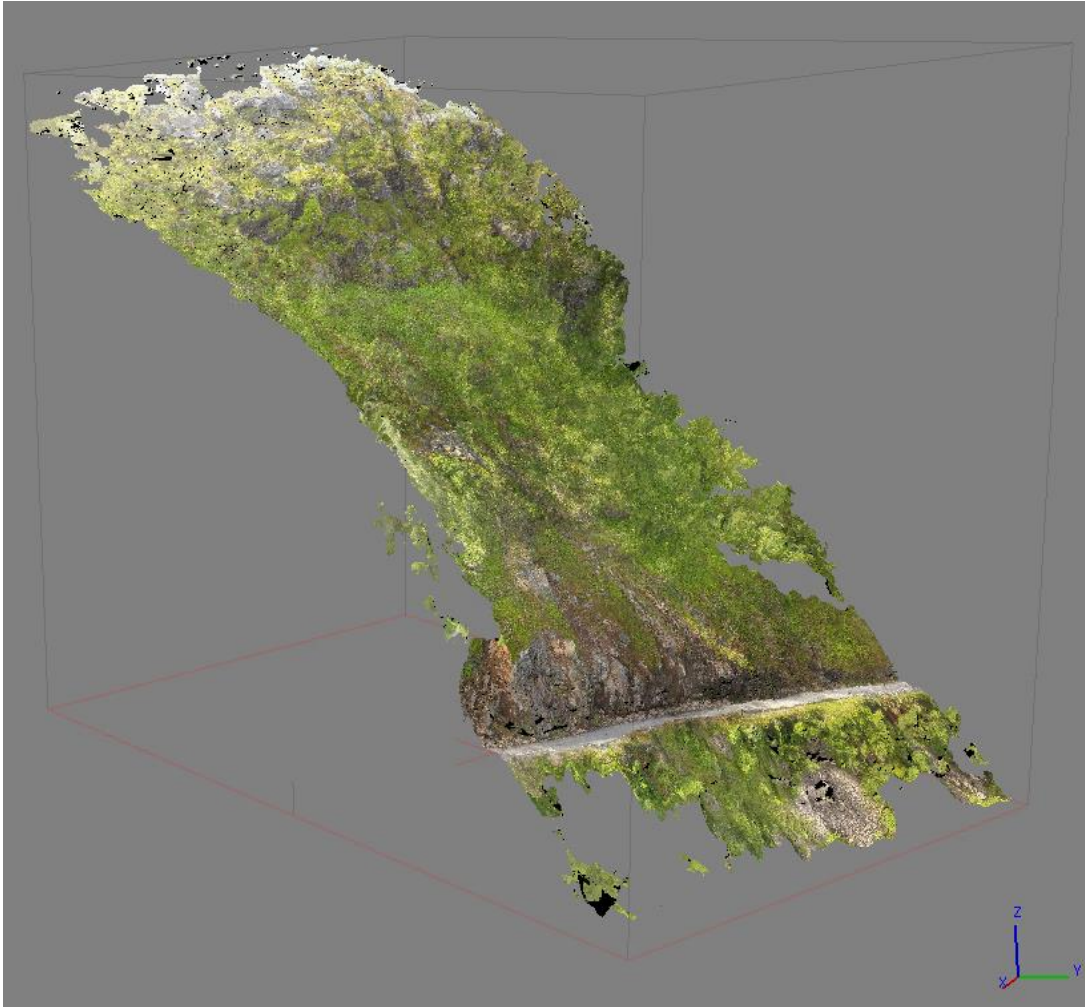


Figure 11: Aunfjellet case area. 3D model produced by photogrammetry.

### 3.1.1 Terrain description

The Aunefjellet case area was visited on a July 11<sup>th</sup> field trip. It was identified as an about 100 m slope with a steepness of 40-45° according to measurements with inclinometer. It terminates with the road cut downslope and a steep cliff like landform upslope (see figure 12). The slope is covered in about 50 cm diameter rock fragments covered in up to 30 cm mossy vegetation. Rock fragments are consistent with talus material. Forestation is also present, with up to 20 cm diameter trunk (at chest height), 10-15-meter-tall, leafy trees distributed across most of the slope (see figure 14). The area is stripped of vegetation in central sections, just above the road and in a discrete area in the south where a concretion of about 1 m diameter boulders can be observed (see figure 13). A number of rock outcrops are present on the slope but these are mostly covered in debris and vegetation in upper sections. A rock outcrop just above the road is stripped bare (see figure 15).



*Figure 12: Steep landform above talus slope. Photo was taken with drone towards the west.*



*Figure 13: Run out area seen from above (drone photo), north is to the left. Notice unvegetated areas in the middle and above road, boulder concretion to the south and rocky outcrops above road.*



*Figure 14: Substrate conditions in upper areas of the Aunfjellet case slope. Photos are taken upslope towards west. Sparse forestation and rock outcrops can be seen. Notice 1 m ruler in right picture for scale.*



*Figure 15: Bare rock just above road cut. The picture is taken towards south. Notice person in upper right quadrant for scale.*

### **3.1.2 Case rockfall**

Aunfjellet has been the location of numerous rockfalls and a catching fence was constructed in 2017 along with other mitigation measures (Vegvesenet, 2017). A rockfall that was initiated by workers during construction phase will be used for back calculation in this case area.

The block had a volume of about 1 cubic meter and “wedge like shape”, was dislodged from bedrock just above talus and settled on the road below (H. H. Nordbrøden 2017, personal communication, 20 October). Pictures that were taken on site show the boulder run out path (see figure 16 and 17).

The bedrock of the case area consist of coarse to medium grained granite and granodiorite (Gustavson, 1974).



*Figure 16: Rockfall source area. Picture is taken towards north. Photo: Hallvard H. Nordbrøden.*



*Figure 17: Case run out area. Picture is taken towards east. Photo Hallvard H. Nordbrøden.*

## 3.2 Revsnestinden

Revsnestinden is a 665-meter-high mountain in Kvæfjord municipality, Troms county in Northern Norway. Its western slope (historical rockfall transit zone) is bypassed by county road 84. See figure 18 for 3D model.



Figure 18: Revsnestinden 3D visualization. North is left in the visualization. From Norgebilder.no (Kartverket).

### 3.2.1 Terrain descriptions

Revsnestinden was visited on July 11<sup>th</sup> and October 14<sup>th</sup> fieldtrips. Observations were made from the lower sections of the slope. Overall observations establish it to be a fairly gentle, large, mostly forested slope with bare upper sections. It is most steep close to summit and fairly gentle in the bottom of the slope close to the road. Lower areas have the character of a talus slope. Substrate downslope consist of about 50 cm diameter rockfragments covered in about 50 cm deep soil and vegetation (see figure 19). The area was mostly covered in leafy forestation with trunk diameters of about 30 cm at chest height. A powerline marked a unforested area oriented North-South. The upper slope is inclined on average at 45°. The talus portion has quite consistent slope angles of 28-30°, before reaching about 20° in lower sections.



*Figure 19: Powerline just above case block settling location. The area has a well-developed soil layer and was covered in vegetation. Picture is taken looking towards the south.*

### **3.2.2 Case rockfall**

A rockfall incident the 20<sup>th</sup> of May 2014 will be used as basis for back calculation in this case area. It was reported and described by a Norwegian Public Roads Administrations (Statens Vegvesen (SVV)) worker (Vegvesenet, 2014a). It was released from the mountain side (see figure 20) and blocked 10 m of the road underneath but did not inflict notable damage as only two boulders with volumes of 5 to 6 m<sup>3</sup> reached the road. The blocks were overall described as having volumes ranging between 2 and 6 m<sup>3</sup> and many settled in talus above road (see figure 21). The source area bedrock was established as granite and granitic gneiss (Vegvesenet, 2014a).

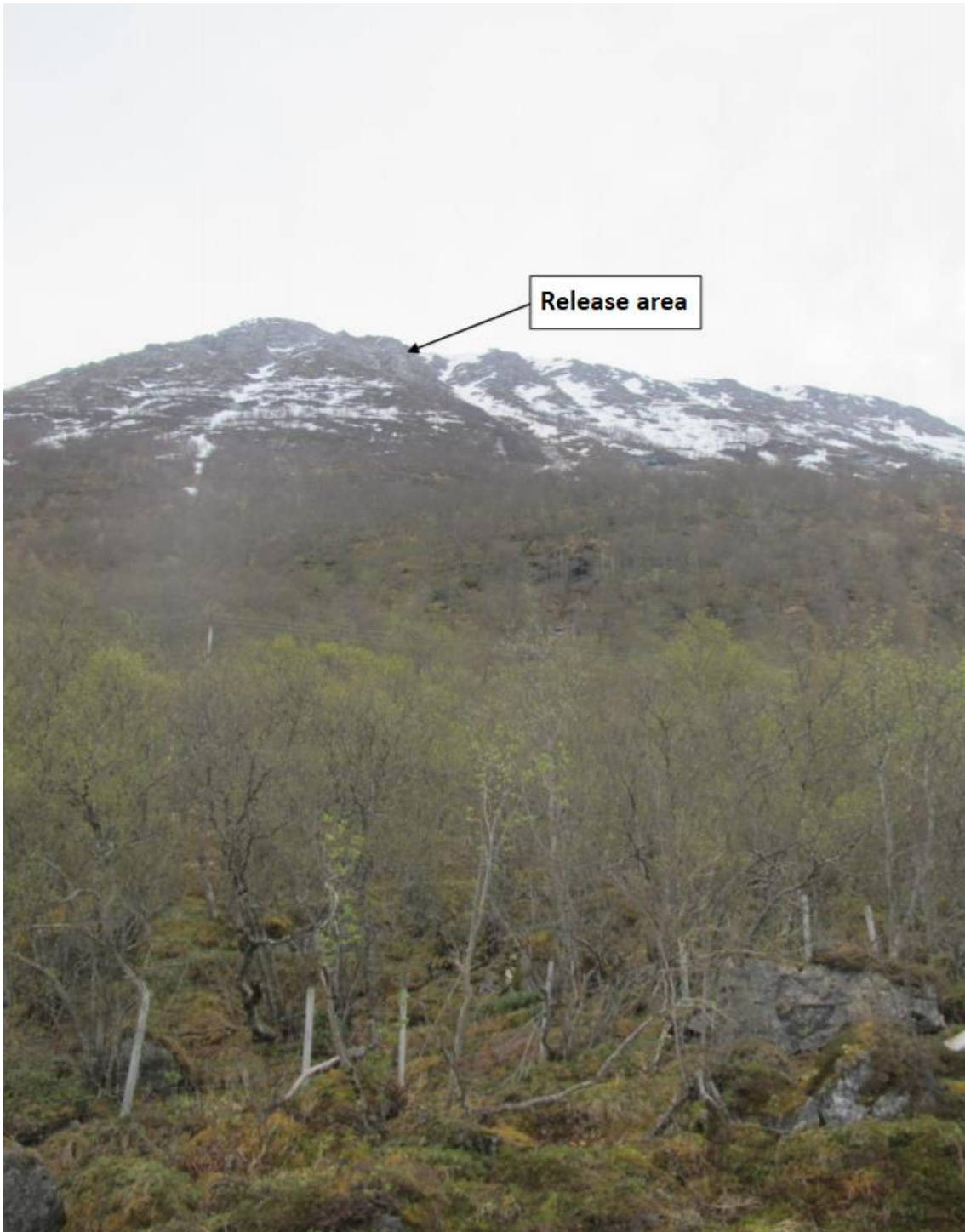


*Figure 20: Source area established by SVV report. Picture is taken towards East. Modified (translated to English) from (Vegvesenet, 2014a).*



*Figure 21: Boulders deposited on the slope as identified in report. Picture is taken towards North. Modified (translated to English) from (Vegvesenet, 2014a).*

Several large boulders were observed in talus during the July 11<sup>th</sup> field trip. Those not significantly covered in vegetation were assumed to be deposited by the 2014 rockfall. One boulder close to the road was chosen for back calculation and was taken photos of for photogrammetry. See figure 22.



Figure 22: Case historical rockfall block. Left and right picture taken towards north and south respectively. Notice shattered forestation beneath boulder in right picture. The folding ruler present in the left picture is 2 m long.

### 3.3 Rakkenes

Rakkenes is an area in Kvænangen municipality, Troms county, Northern Norway that is bypassed by Europe Road 6. Two case rockfalls were used for back calculation in this area. Their locations will hereby be referred to as Rakkenes West and Rakkenes Central respectively. Additionally, a third location was selected for the design of a rockfall mitigation structure based on simulations. This area will be referred to as Rakkenes East (see figure 23 for overview). The bedrock in the area consist chiefly of granodioritic gneisses (Zwaan, 1988).

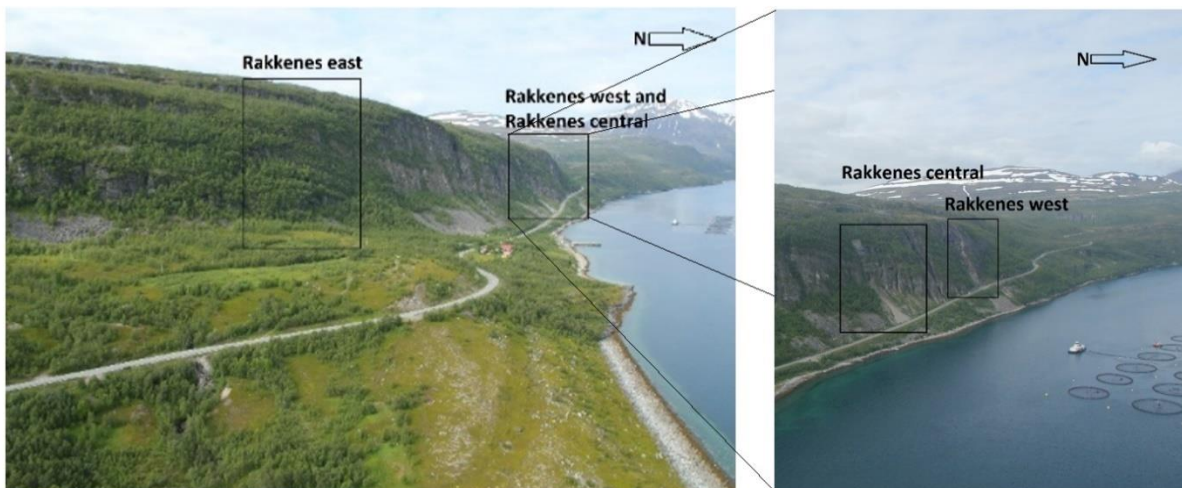


Figure 23: Overview of case areas. Modified from photo: Andreas Person.

### 3.3.1 Terrain descriptions

#### *Rakkenes west*

Rakkenes West was visited on a September 13<sup>th</sup> fieldtrip. The run-out area consisted largely of solid, somewhat brittle rock for the entirety of the slope before terminating downslope with a small ditch and the road (see figure 25). The slope is steep and much of it appear to reside underneath overhanging rock mass (see figure 24 for 3D model). The upper slope is near-vertical and shallows to around 70° at road level.

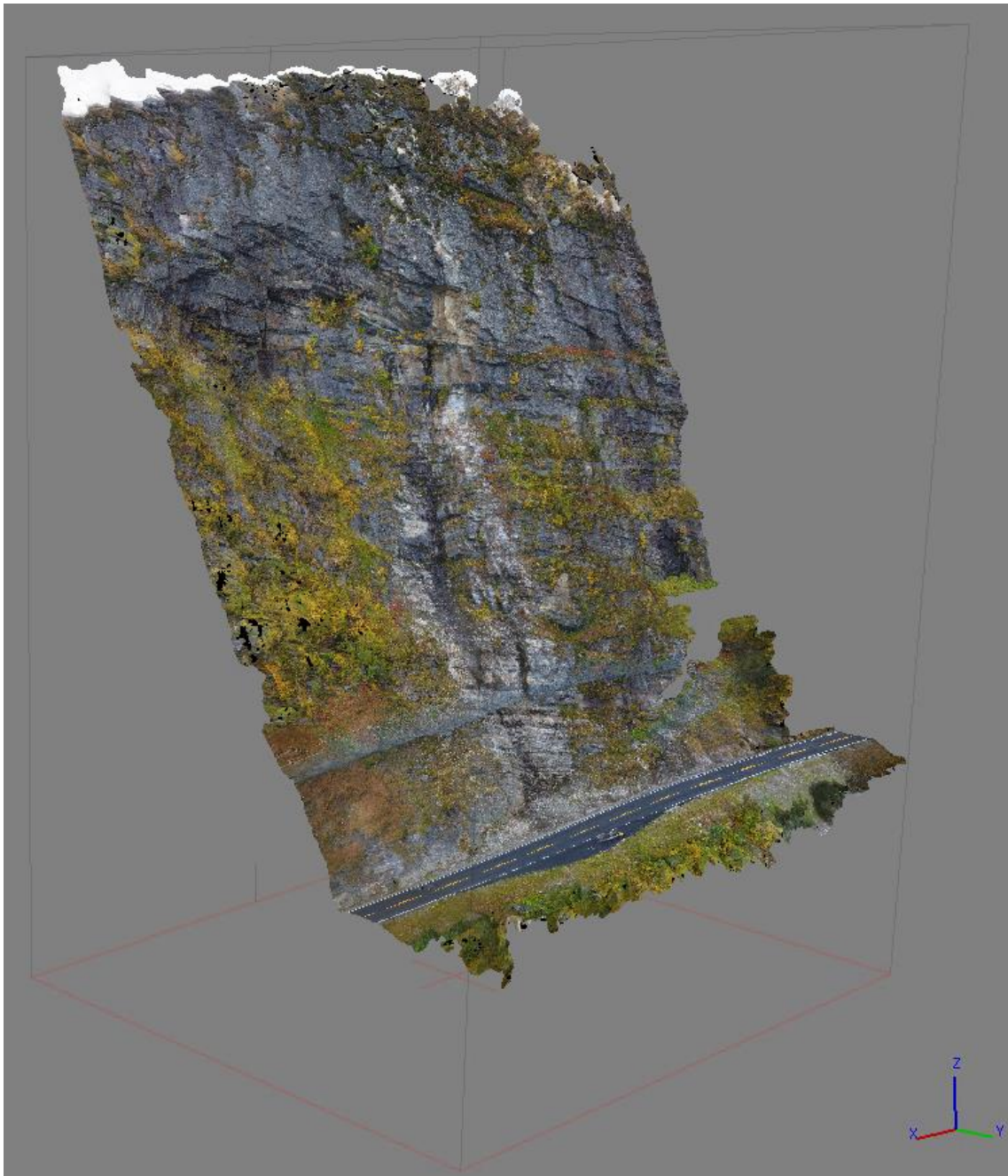


Figure 24: 3D model of the Rakkenes West case area. Model produced by photogrammetry.



*Figure 25: Rakkenes West case area. Picture is taken by drone towards south east. Case area Rakkenes Central can be seen left in the picture. Notice person in lower sections of picture for scale.*

### ***Rakkenes Central***

The area was visited on a September 14<sup>th</sup> field trip. The area consists of a steep, cliff like landform and a gentler slope beneath the cliff and above the road. See figure 26 for 3D model and figure 27 and 28 for aerial photographs. Rock fragments ranging in size from centimeters to over a meter were observed on the slope. Large fragments were mostly present in the periphery of a fan like section emerging from a sub-vertical structure in the cliff (see figure 29). This is consistent with a talus cone. The center of the talus cone consisted largely of fine-grained material. Somewhat dense forestation was visible in eastern sections of case area and minor tree growth could also be observed in the talus cone periphery. The case area terminated downslope with a ditch and road. The upper slope is nearly vertical while the talus is inclined 30 to 40°. The road is sub-horizontal.

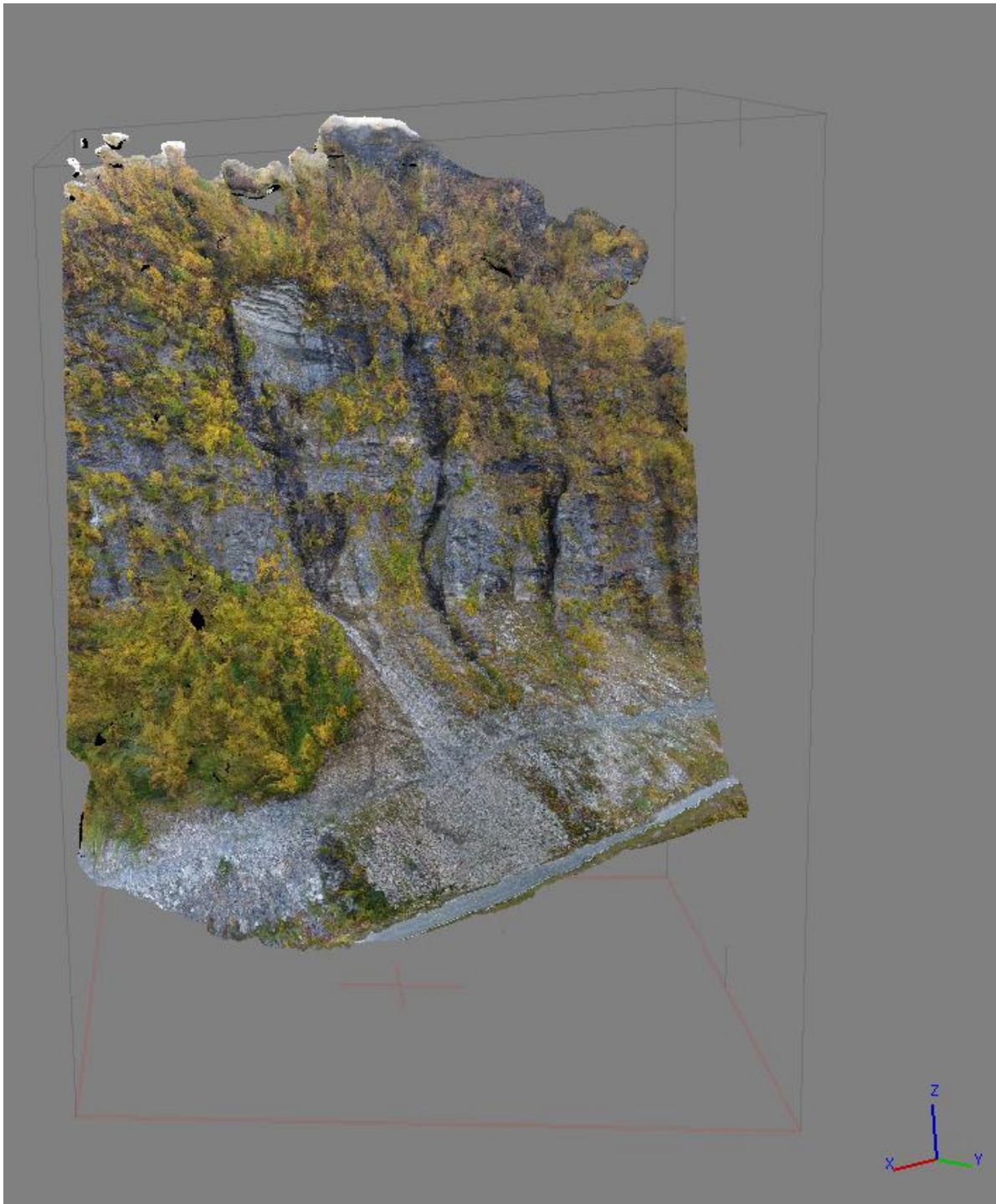


*Figure 26: Rakkenes Central case area 3D model. Model produced by photogrammetry.*



*Figure 27: Cliff like section of the case area. Picture is taken towards the south by drone.*



*Figure 28: Case area seen from above, left is east in the picture. Picture is taken by drone. Notice fan like deposit in central areas.*



*Figure 29: Talus material. Picture taken in eastern section of case area towards south. Notice person in upper right quadrant for scale.*

### ***Rakenes East***

The Rakkenes East case location was visited on a September 14<sup>th</sup> field trip. The area consists of a cliff like landform terminated by a gentler slope beneath that stretches for some tens of meters from cliff foot (see figure 31 and 32). This lower slope is consistent with a talus deposit. The talus terminates with a sub planar soil surface downslope. See figure 30 for 3D model of case area.

The talus consists mostly of meter scale boulders covered in vegetation and 10-15 m tall, 30 cm trunk (at chest height), leafy forestation. Several larger boulders were also observed in the talus, many determined relatively fresh due to the absence of extensive lichen growth. Some had runout traces that could be discerned from shattered wood upslope. The planar soil surface beneath talus had a fairly deep soil layer, few rock fragments and no tree growth.

The cliff area is nearly vertical, but interwoven are terraces with primarily slope angles of 20-30° but also near horizontal sections. The talus mostly has inclinations of 30 to 40° and a down-slope concave section. The soil surface beneath is sub horizontal.

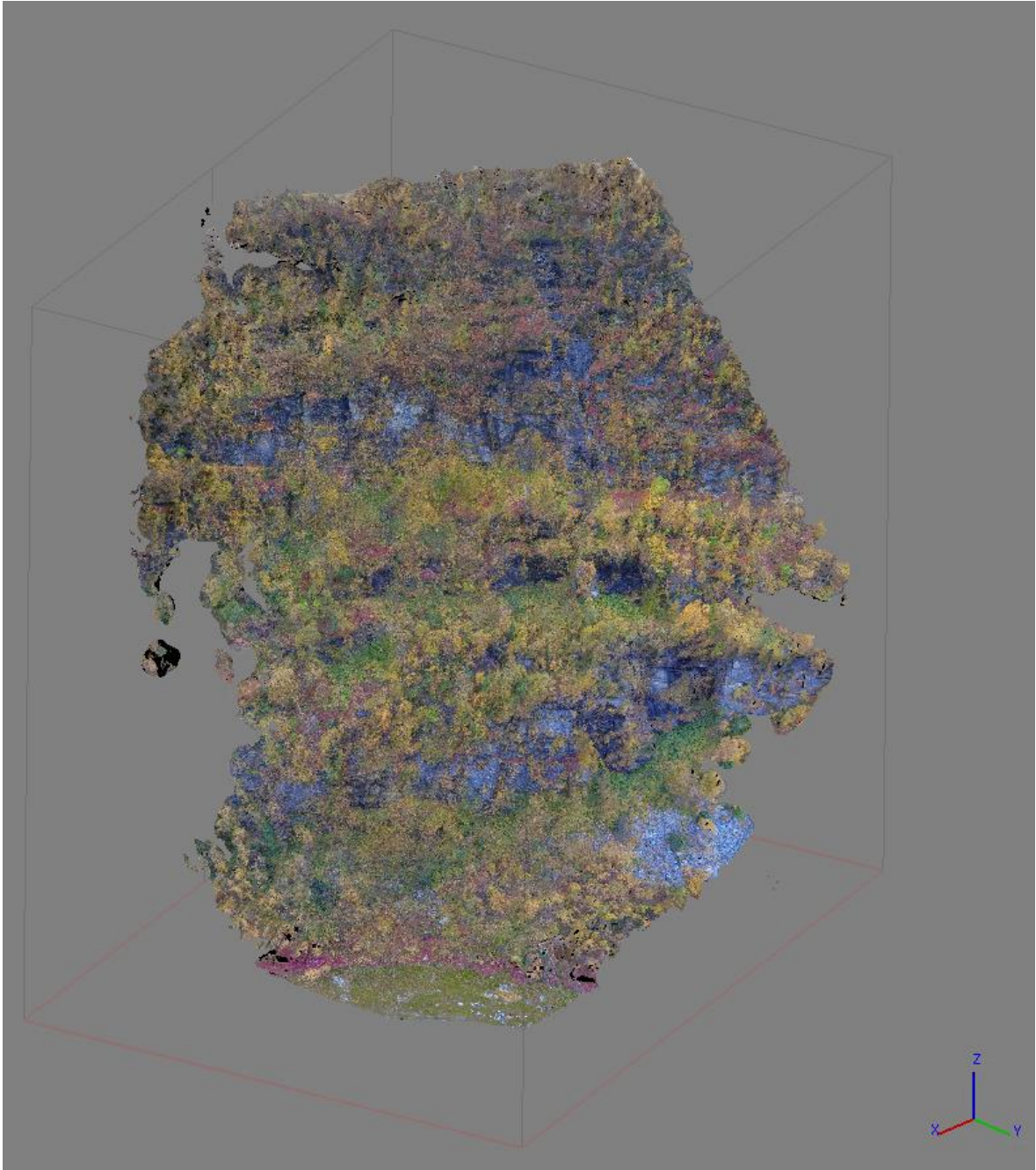


Figure 30: Rakkenes East case area 3D model. Model produced by photogrammetry.



*Figure 31: Rakkenes east upper slope. Picture is taken by drone towards south.*



*Figure 32: Rakkenes East talus. Picture is taken by drone towards south west. Notice people for scale.*

### 3.3.2 Case rockfalls

#### *Rakkenes west*

The area was the location of a June 18<sup>th</sup> 2014 rockfall that settled on a 50 – 100 m stretch of road. A SVV worker identified the source area and reported the event (Vegvesenet, 2014b) (see figure 33 and 34). The rockfall involved two source areas and several blocks with volumes of several m<sup>3</sup> (see figure 35). The report stated that the lower source area was a consequence of material being dislodged by falling material from above. A boulder as identified in pictures and report will be used for back calculation on this case area.

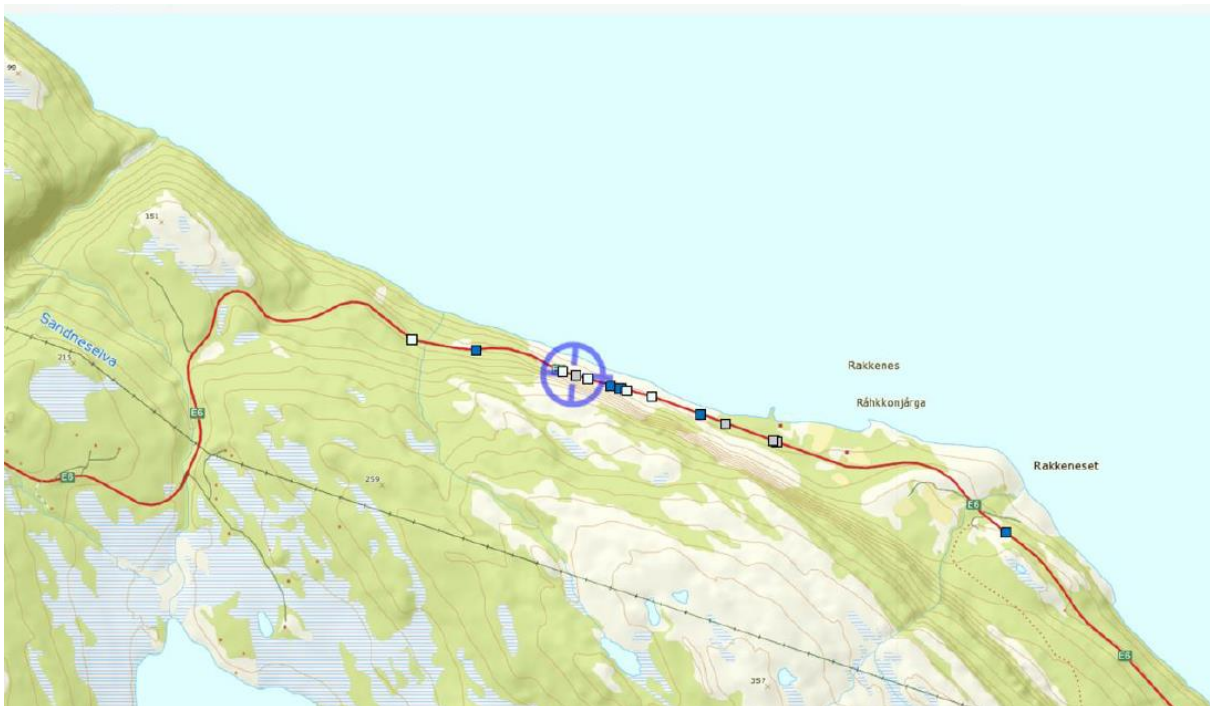


Figure 33: Location of 2014 rockfall as presented in SVV report. From (Vegvesenet, 2014b).

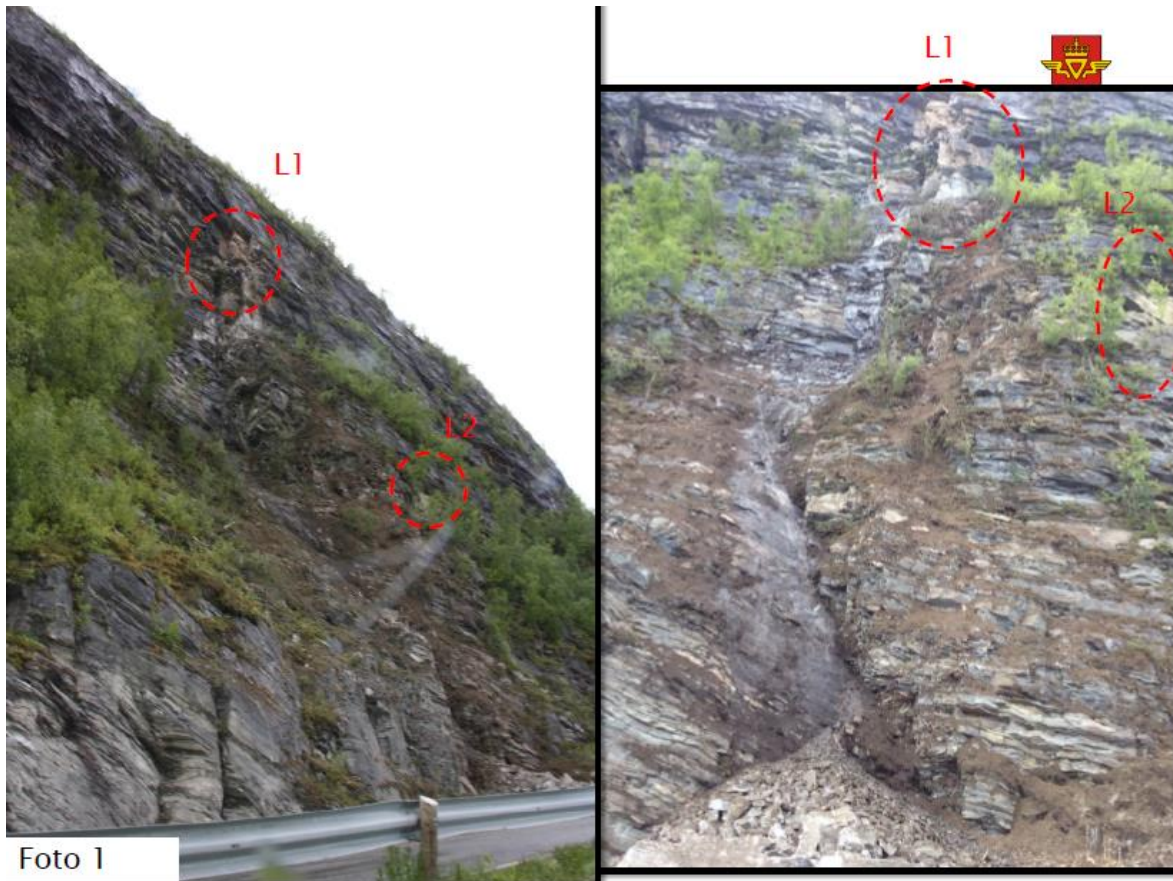


Figure 34: 2014 rockfall source areas L1 and L2 as identified in report. From (Vegvesenet, 2014b).



Figure 35: Boulders on the road after the 2014 rockfall. From (Vegvesenet, 2014b).

*Rakkenes central*

A boulder from the talus was described and treated as a historical case. Potential source areas were also attempted identified in field (see figure 37). It was deposited close to the road and had a flat angular geometry (see figure 36).



*Figure 36: Case boulder just above road. The folding ruler is 2 m long.*

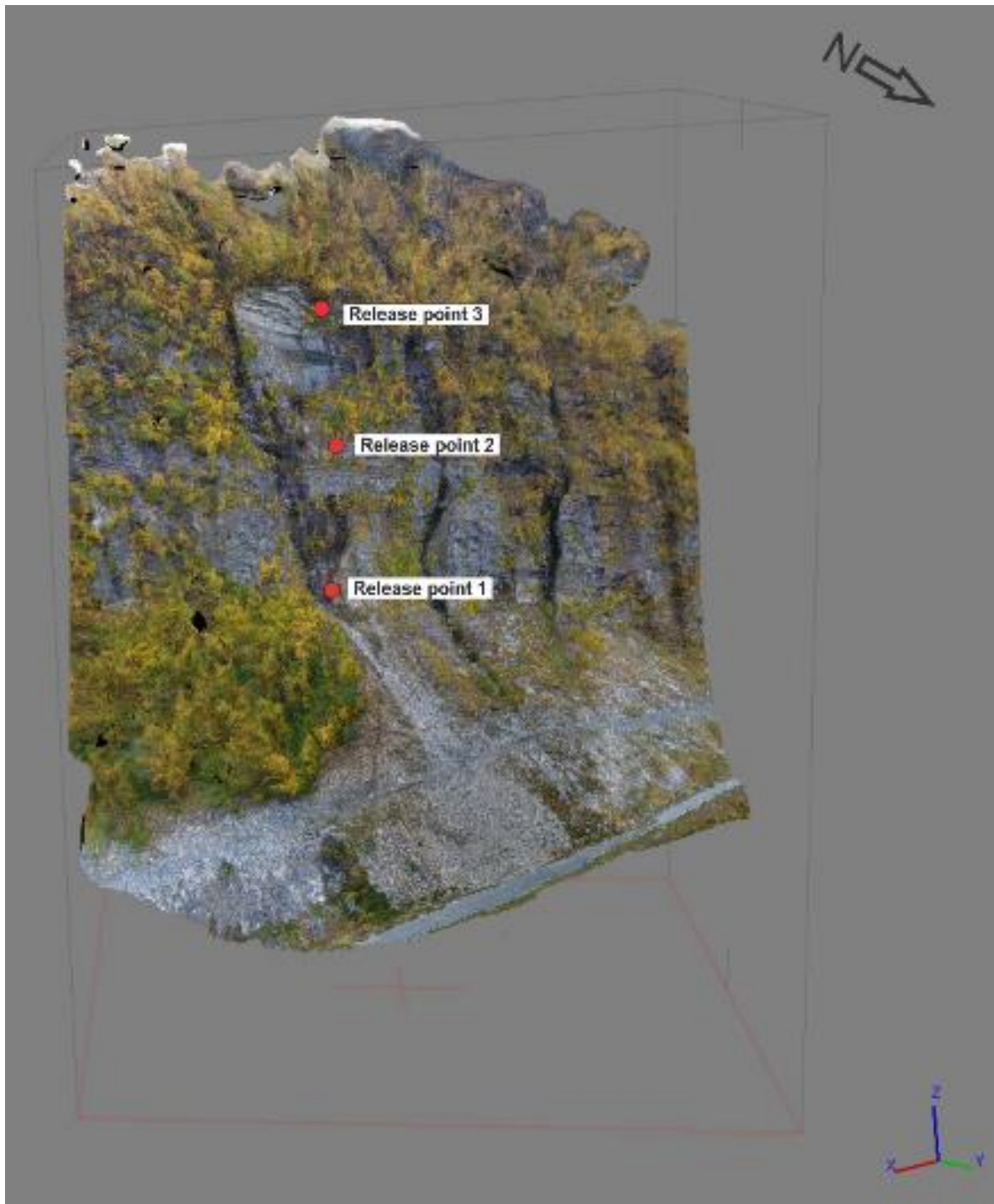


*Figure 37: Potential release points for boulder discovered in talus. 3D model was produced by photogrammetry.*

## 4. Method

### 4.1 Rockfall model descriptions

#### 4.1.1 Rocfall

Rocfall was submitted as a masters degree to the University of Toronto by (Stevens, 1998).

The software simulates the motion of lumped mass objects (rigid body mechanics has later been added in Rocfall version 6.0 (Rocscience)) on a two-dimensional slope interpolated between user defined vertices. Objects of user defined mass can be released from points of any coordinates and are subsequently accelerated as if subject to acceleration of gravity in vacuum conditions (see equation 1 and 2).

$$V_x = V_0 \quad \text{Eq. 1}$$

$$V_y = V_0 + gt \quad \text{Eq. 2}$$

Where  $V_x$  is velocity in the x-plane and  $V_y$  the velocity in the y-plane at any time in calculation. The subscript '0' refers to initial values before calculation.  $g$  is the acceleration of gravity ( $-9.81 \text{ ms}^{-2}$ ) and  $t$  is the time evolution.

Preceding impact, the velocity is transformed to its components normal and tangential to slope. Post impact velocities are calculated using these values and user defined normal and tangential coefficients of restitution for the impacted slope section (see equation 3 and 4).

$$V_{na} = V_{nb}R_n \quad \text{Eq. 3}$$

$$V_{ta} = V_{tb}R_t \quad \text{Eq. 4}$$

Where  $V$  and  $R$  are velocity and restitution coefficient respectively. The subscript  $n$  and  $t$  refers to slope normal and tangential values respectively and the subscript  $b$  and  $a$  refers to values before and after impact respectively.

If the object is in contact with surface and velocity is directed downslope or 0 the object motion will be governed by user defined friction angle.

If slope inclination is equal to friction angle, the object will continue to slide at its initial velocity. If it is steeper, the object will accelerate as a function of the slope and friction angle difference. If slope is gentler than friction angle the object will stop at a distance dependent on initial velocity and slope and friction angle difference.

Initial object velocity and position, slope vertex coordinates, restitution coefficients, friction angle and object mass may all be sampled from normal distribution with user defined standard deviation.

#### **4.1.2 RAMMS: Rockfall**

Software description of RAMMS:Rockfall can be found in its manual (Bartelt et al., 2016). Subchapter statements cite this manual.

The software simulates the motion of rigid body objects on a 3D surface. The objects are released from user defined source areas, points or lines. The surface geometry is a georeferenced raster DEM that may be divided into sections of equal terrain properties by using ESRI shapefiles. The simulated objects are programmed as polygons generated by using a convex hull function on a cloud of points. The objects volume/mass and density is user defined, and shape can be chosen from a in-program library or modelled in field by means of remote sensing techniques like laser or photogrammetry. The modelled object has three translational and three rotational degrees of freedom that allows it to move freely in 3D space. Upon release it is subject to a user defined number of random orientations, adding probabilistic elements to the simulation.

Initial movement is freefall and early movement may involve angular velocity due to uneven distribution of mass around the object center. When zero distance between surface and a point at the object is registered, the point is acted upon by contact forces that assures no penetration of surface. This can cause torque and rotation due to offset between this point and the center of mass. Whenever the object is in contact with surface it is subject to coulomb friction. This friction is quantified by a friction coefficient  $\mu$  that increases from a minimum ( $\mu_{\min}$ ) to a maximum value ( $\mu_{\max}$ ) at a rate depending on a constant  $\kappa$ . This time dependent friction is implemented to account for the progressive deformation of substrate that may occur during actual-conditions boulder sliding motion and is sensitive to material type. After rebound, friction remains for a duration quantified by the constant  $\beta$ . This is implemented to account for the obstacle constituted by material accumulated in front of sliding boulders in actual conditions. Again, friction and center of mass offset cause torque and rotation of object.

Whenever in contact with surface, in addition to friction, a drag force acting opposite to object velocity is implemented to account for actual-conditions viscoplastic deformation of substrate. The drag is a function of the square of the velocity and a drag coefficient. The value of the mentioned constants according to surface type is provided in table 1. Another type of drag can be implemented by user in the form of forest. Forest are modelled as layers of user defined height above surface where traversing objects are subject to drag. This drag force acts in opposite direction to object velocity and is proportional to the velocity and a drag constant based on user defined forest density (see table 2). The boulders continue downslope until some threshold minimum velocity or computing time is encountered, and the simulation ends.

Table 1: Respective ground parameters for material types. Modified from (Bartelt et al., 2016).

Terrain	$\mu_{\min}$	$\mu_{\max}$	$\beta$	$\kappa$	Drag
Extra soft	0.2	2	50	1	0.9
Soft	0.25	2	100	1.25	0.8
Medium soft	0.3	2	125	1.5	0.7
Medium	0.35	2	150	2	0.6
Medium hard	0.4	2	175	2.5	0.5
Hard	0.55	2	185	3	0.4
Extra hard	0.8	2	200	4	0.3
Snow	0.1	0.35	150	2	0.7

Table 2: Forest definitions and respective drag. Ha: Hectare ( $1ha=10\ 000\ m^2$ ). From (Bartelt et al., 2016).

	Density ( $m^2/ha$ )	Drag constant (kg/s)
Open forest	20	250
Medium forest	35	500
Dense forest	50	750

## 4.2 On-site work

The thesis work involved three field trips. The first to Aunfjellet and Revsnestinden on the 11<sup>th</sup> of July 2017. The second to Rakkenes the 14<sup>th</sup> of September 2017. A third field trip to Revsnestinden was carried out on the 14<sup>th</sup> of October 2017.

Boulders selected for back calculation were described in terms of size and geometry. Some were taken pictures of for the production of point clouds by photogrammetry.

Their settling locations were measured in with handheld GPS to provide historical reference when back calculating rockfalls. The substrate qualities in run out area were described to aid the selection of terrain parameters during back calculation. Descriptions included estimates of overall grain size, presence of large rock fragments, presence of vegetation and depth of soil. Forest was described by height and width estimates and a qualitative description of density. Data was also sampled for photogrammetry of slope and case boulders (historical rockfalls). A DJI Phantom 4 pro drone with 20 mega pixel camera was used to acquire photos of the slope (see figure 39). A Leica GPS 1200 Base RTK Smart Rover Station was used to geo-reference ground points that were marked with orange mace for identifications in photogrammetry software (see figure 38). A folding ruler was placed on boulder for scale if photos were taken of it for photogrammetry.



*Figure 38: Geo-referencing ground control points in field.*



*Figure 39: Collecting aerial photos with drone.*

### **4.3 Production of DEMs and boulder point clouds by photogrammetry**

Photogrammetry was done with Agisoft Photoscan by Agisoft LLC using drone photography of slopes. First the camera positions were aligned spatially using surface tie points present in two or more photographs. Then a point cloud was generated from photogrammetric triangulation. The ground control points highlighted in field were then identified in the photos and assigned field sampled GPS coordinates to geo-reference the model. If necessary, vegetation was removed manually from point cloud. A polygon mesh was then constructed based on the dense point cloud and used for the production of a digital elevation model. The model was then textured with orthophoto before the DEM and orthophoto were exported as 10 cm resolution ASCII grids and GeoTIFF respectively (see figure 40). For scanned-in boulders only a sparse point cloud was made (camera tie points) and assigned spatial coordinates using a folding ruler present in the pictures (see figure 41).

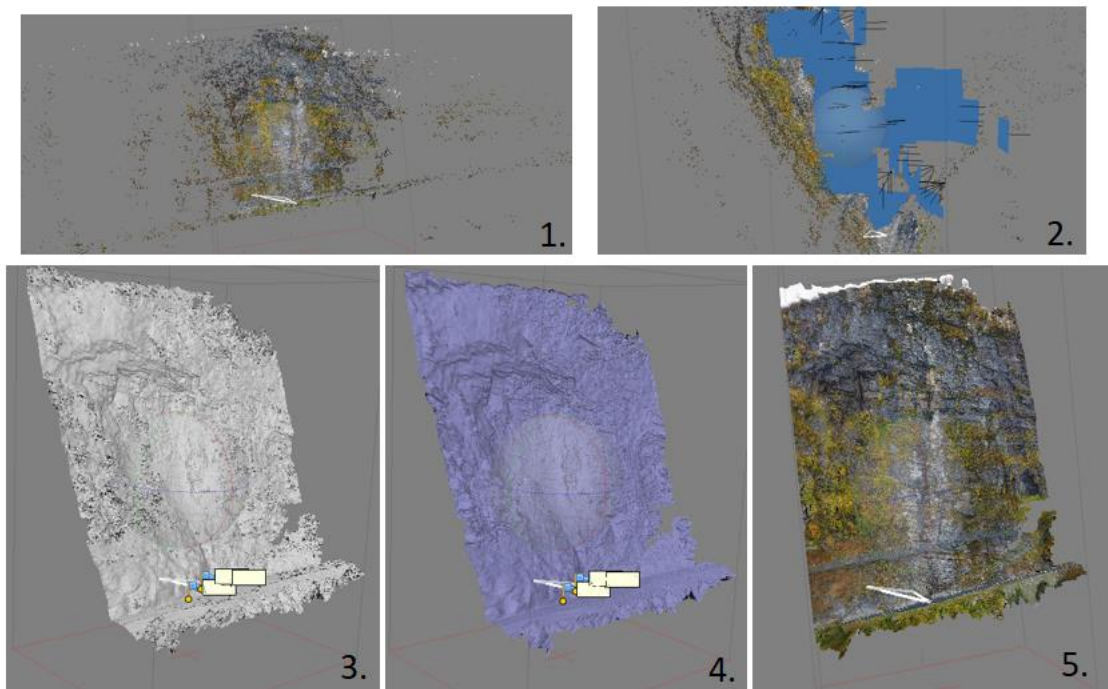


Figure 40: Slope photogrammetry workflow. 1) Sparse point cloud of tie points used to align cameras. 2) Aligned cameras. 3) Dense point cloud. 4) Mesh. 5) Mesh textured with orthophoto. Blue flags are locations of ground control points.

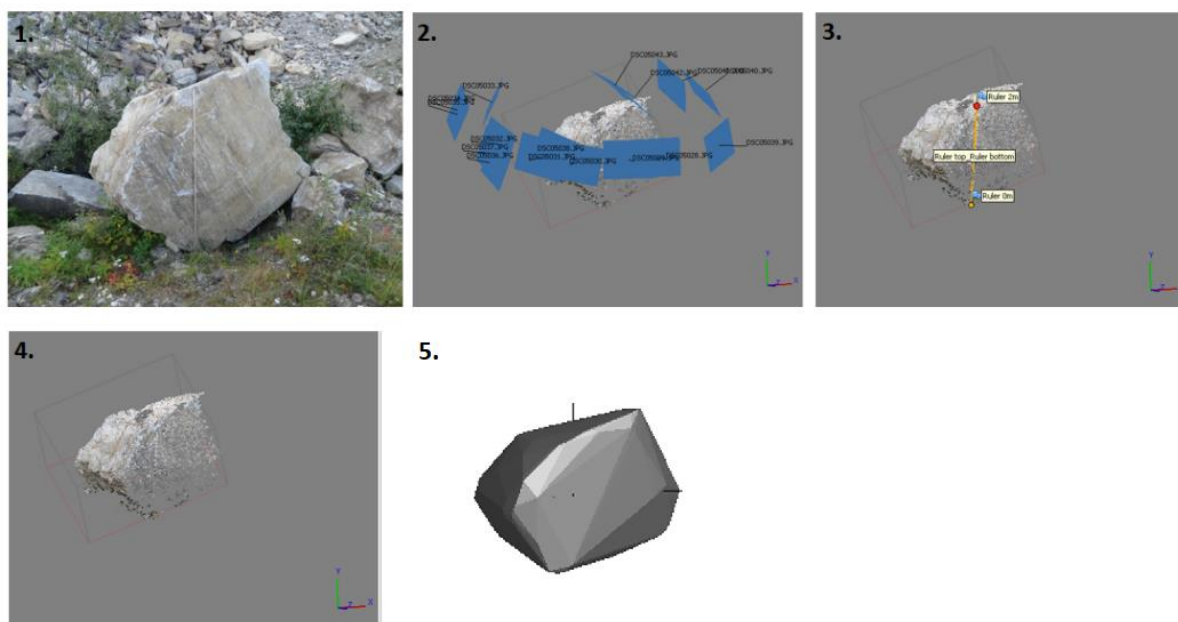


Figure 41: Boulder point cloud production. 1) Original boulder. 2) Aligned cameras. 3) Applying spatial reference. 4) Finished point cloud. 5) Visualization in RAMMS:Rockfall

#### **4.4 Preparing digital elevation models and 2D slope sections**

One meter resolution models for all case areas except Revsnestinden and 10 m resolution models for all case areas were obtained from the Norwegian Mapping Authority (Kartverket) (NMA) (Kartverket). The 1 m resolution models are currently being produced by NMA using airborne laser scans from helicopter and airplane, and nationwide coverage is expected only in 2021 (Kartverket) hence the absence of higher resolution in one of the case areas. The new 1 m resolution models largely have accuracies of 10 cm standard deviation, whilst the older 10 m resolution models have accuracies of 2-6 m standard deviation depending on the data age and terrain in the area (Steiwer, 2017).

The NMA model were resampled to 3 m resolution models using the nearest neighbor algorithm. Ten cm resolution models produced from photogrammetry were also resampled to 1- and 3 m resolutions using the same algorithm. In the end, 6 digital elevation models were produced for Aunfjellet, Rakkenes West, Rakkenes Central and Rakkenes East. One digital elevation model for Revsnestinden was also acquired (see figure 42). The 1 m resolution NMA LIDAR models and the 1 m resolution models produced by photogrammetry were later compared by raster subtraction. This aimed to highlight any elevation offset stemming from the two remote sensing techniques.

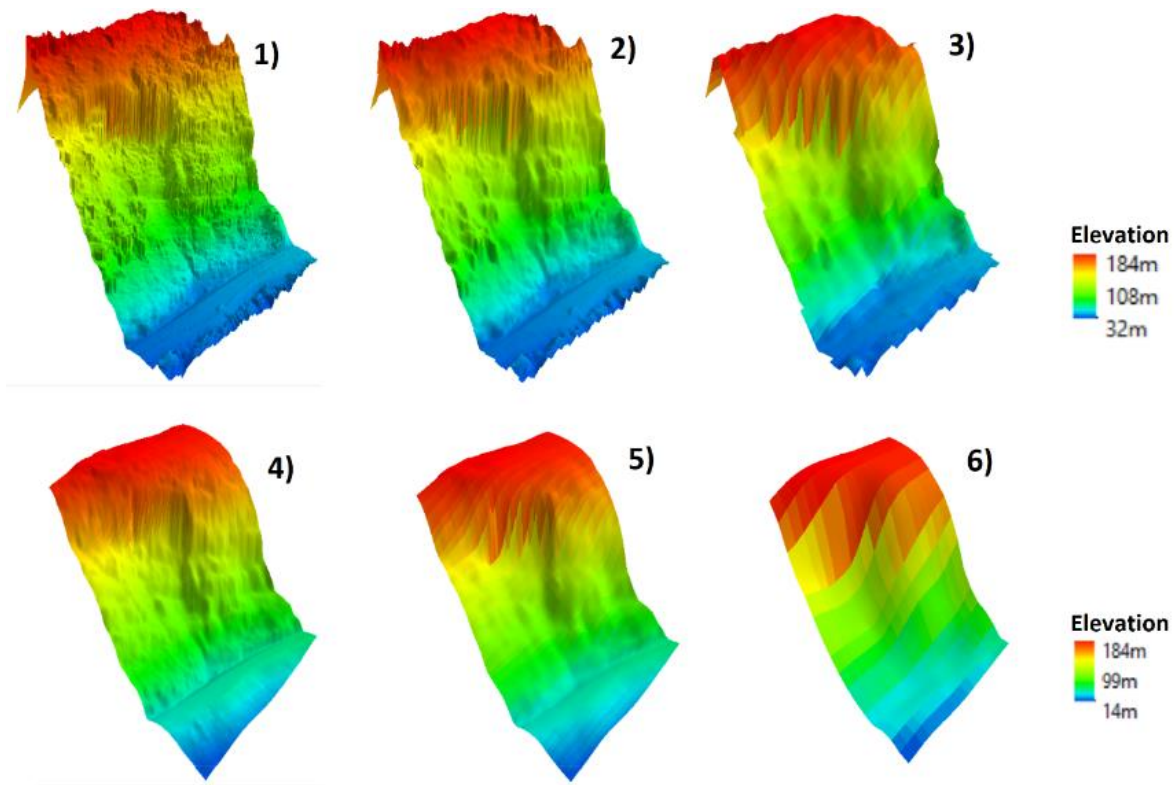


Figure 42: Example of digital elevation model line-up. Rakkenes West 3D rendered digital elevation models. 1) 10 cm resolution model from photogrammetry 2) 1 m resolution model from photogrammetry 3) 3 m resolution model from photogrammetry 4) 1 m resolution model from LIDAR 5) 3 m resolution model from LIDAR 6) 10 m resolution model from LIDAR.

Vertices for use in Rocfall were produced by making stack profiles along polylines in ArcMap. The polylines were fitted along converging steepest path lines produced by an ArcMap function (see figure 43). Only one polyline was produced for each case area. This was based on the steepest path from case source area on the 1 m resolution LIDAR derived digital elevation model (10 m resolution model for Revsnestinden). The LIDAR derived elevation models from NMA will from here on be referred to as “Aerial survey models” or “(resolution)A” whilst the photogrammetry derived elevation models will be referred to as “Terrestrial survey models” or “(resolution)T” for convenience.

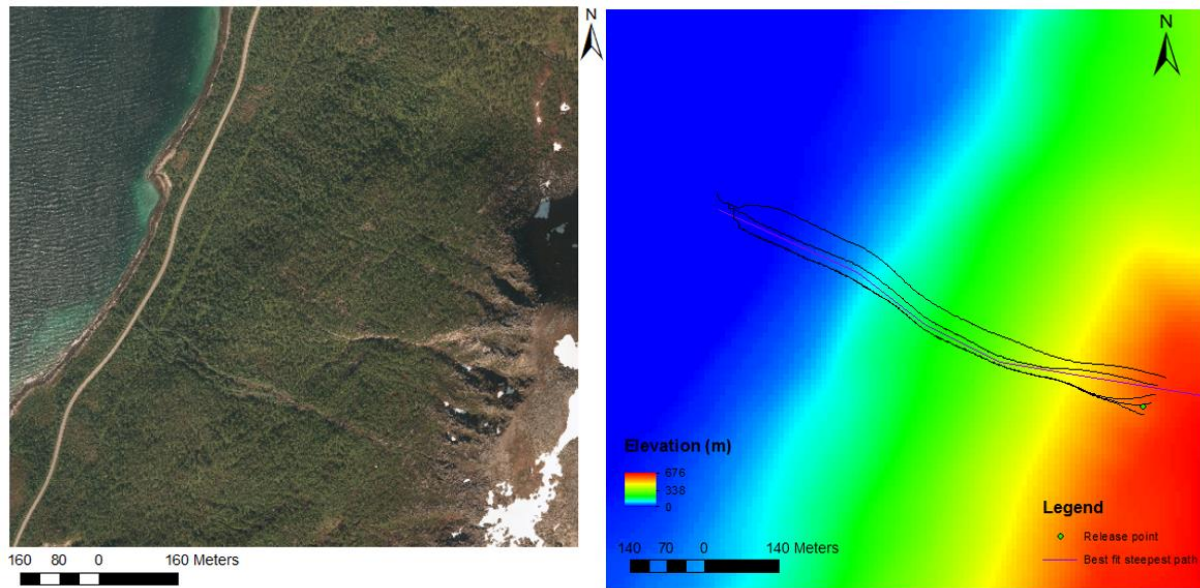


Figure 43: Example of procedure for producing the steepest line used to acquire the profile used in 2D modelling. The left picture is a orthophoto of Revsnestinden. The right figure show a number of steepest paths from locations around case source area, and a best fit polyline used for the export of stack profiles.

## 4.5 Setting up simulations

### 4.5.1 RAMMS:Rockfall

#### *Aunfjellet*

The source area was identified based on analysis of the digital elevation model and orthophoto. A georeferenced shapefile illustrating the source area was then produced for use in the simulations. A elongate wedge shaped boulder consistent with source was selected from the RAMMS:Rockfall library to be used for modelling. A density of  $2640 \text{ kg/m}^3$  was assigned this boulder corresponding to a suggested mean density for granite as stated in (Tenzer et al., 2011) (see table 3). The slope was divided into four material domains with respective shapefiles used in simulation. Material domain 1 is the upper slope and outcrops, material domain 2 is the talus section, material domain 3 is the ditch and area below road and material domain 4 is the road. Additionally, forest (enhanced drag) was added to selected areas. The shapefiles used are presented in figure 44 along with historical settling location.

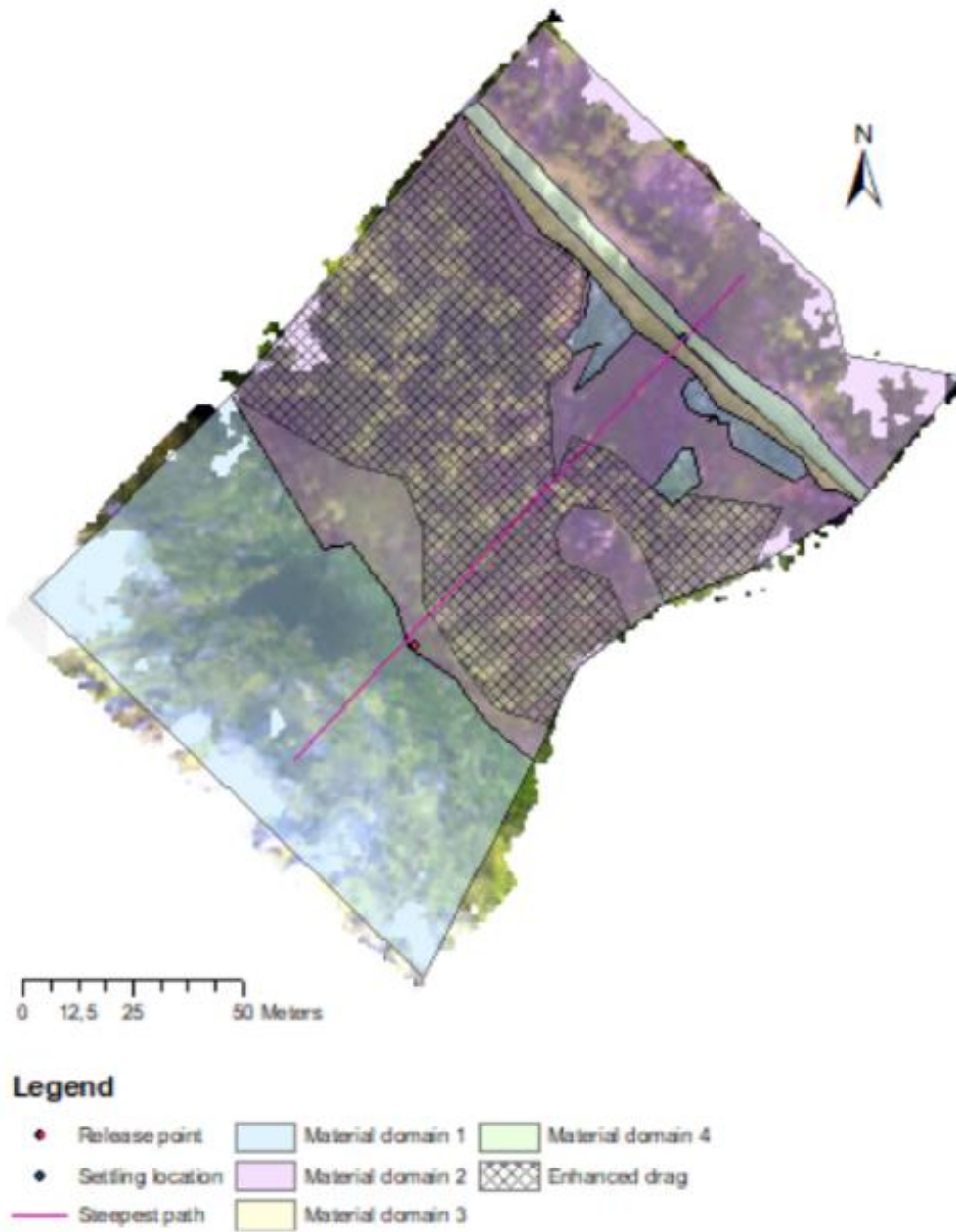


Figure 44: Shapefiles used for simulations on the Aunfjellet case area.

Table 3: Properties of boulder used in simulation.

X / Y / Z (m)	Density (kg/m <sup>3</sup> )	Volume (m <sup>3</sup> )	Mass (kg)	Name in RAMMS:Rockfall library	Figure
1.24/1.50/1.26	2640	1.00	2641.2	Real_long_1.2	

### *Revsnestinden*

The reported source area was identified in a georeferenced orthophoto and a shapefile was produced for use in simulation. The boulder geometry was derived from an imported point cloud produced with photogrammetry. A density of 2750 kg/m<sup>3</sup> was assigned the boulder corresponding to the density of quartzite and granite gneiss as stated in (Dorren and Seijmonsbergen, 2003) (see table 4). The slope was divided into two material domains. Material domain 1 is the bedrock in the upper slope and material domain 2 is the talus beneath. The shapefiles used, are presented in figure 45 along with historical settling location.

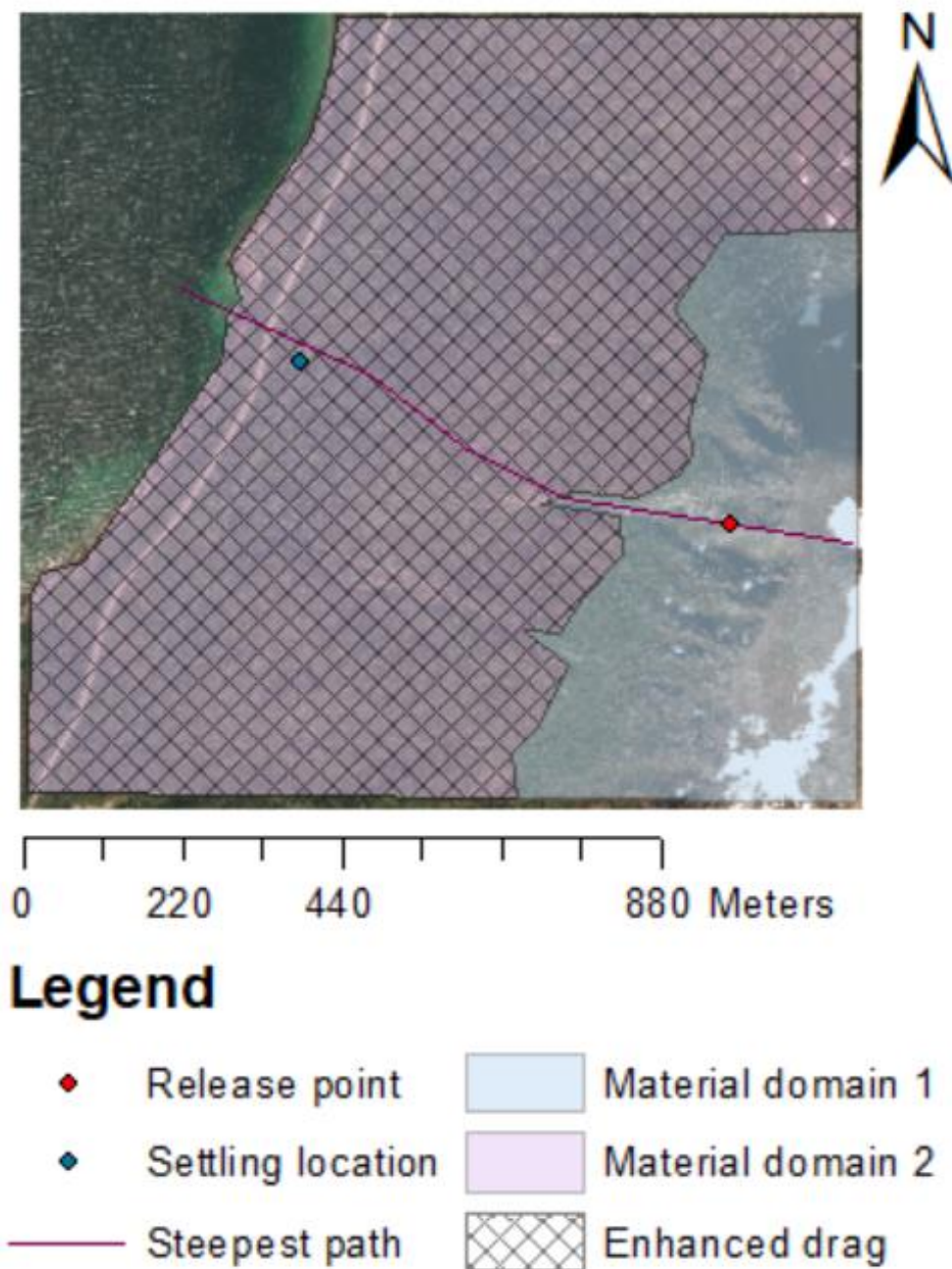


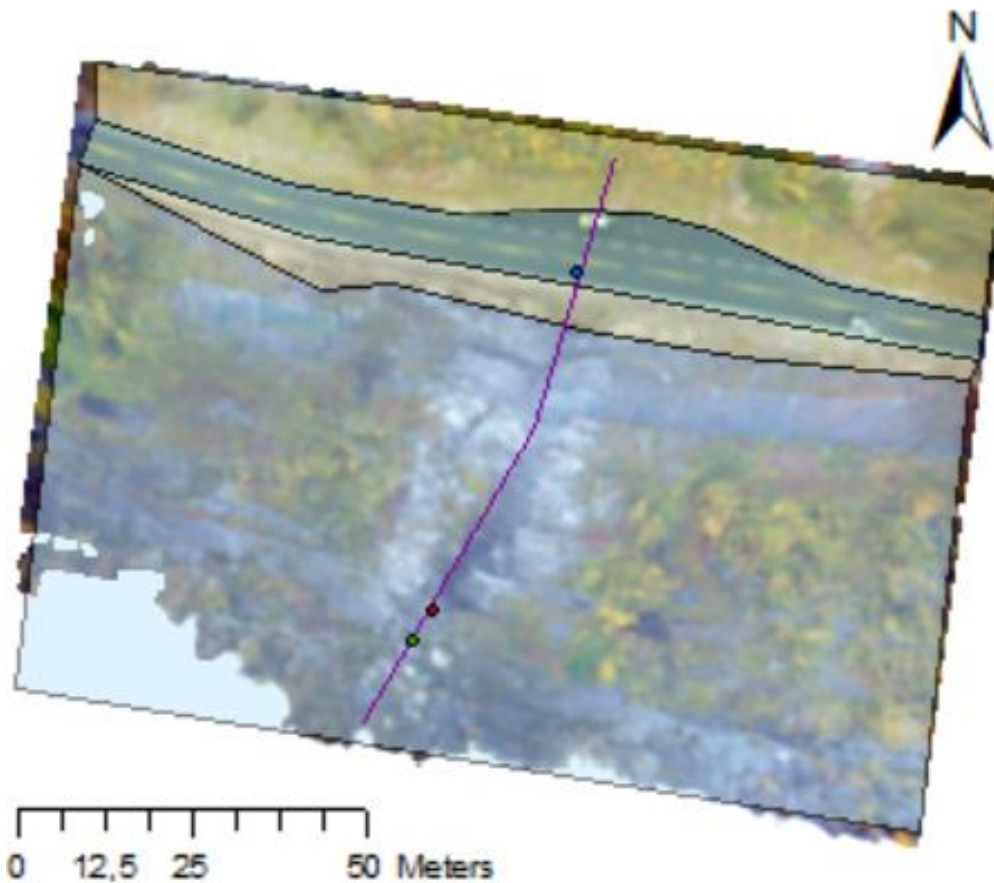
Figure 45: Revsnestinden shapefiles used in simulation. Orthophoto from NMA (Kartverket).

Table 4: Properties of boulder used in simulation.

X / Y / Z (m)	Density (kg/m <sup>3</sup> )	Volume (m <sup>3</sup> )	Mass (kg)	Name in RAMMS:Rockfall library	Figure
2.25/1.44/2.21	2750	2.54	6996.2	NA (Point cloud)	

### *Rakkenes West*

Source areas were identified based on report. Only the tallest release point was used as report concluded that lower release point was material that was simply dislodged by rockfalls from above. Measurements in Agisoft Photoscan places the source area at a height of 138 m. This corresponds to two different horizontal coordinates for the aerial survey and terrestrial survey model respectively, as there is some vertical displacement between the two. The terrestrial survey model release point was termed release point 1 while the aerial survey model release point was termed release point 2. Respective shapefiles for these locations were generated for use in simulation. The boulder shape most consistent with report in the RAMMS: Rockfall rock builder database was selected; a flat angular shape. A density of 2750 kg/m<sup>3</sup> was assigned the boulder corresponding to mean density of quartzite and granite gneiss as stated in (Dorren and Seijmonsbergen, 2003). The volume of a 1.2 m × 1.2 m × 1 m perfect cuboid, 1.44 m<sup>3</sup>, was also assigned to the boulder (see table 5). This geometry is consistent with report photos of the rockfall event. The slope was divided into three material domains consistent with field observations. Material domain 1 is the upper solid rock slope, material domain 2 is the ditch and area below road, mostly soil, and material domain 3 is the road. The shapefiles used are presented in figure 46 along with historical settling location.

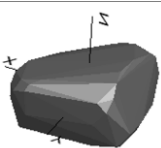


### Legend

- Release point 1  Material domain 1
- Release point 2  Material domain 2
- Settling location  Material domain 3
- Steepest path

Figure 46: Rakkenes west shapefiles used for simulation.

Table 5: Properties of boulder used in simulation.

X / Y / Z (m)	Density (kg/m <sup>3</sup> )	Volume (m <sup>3</sup> )	Mass (kg)	Name in RAMMS:Rockfall library	Figure
1.53/1.73/0.97	2750	1.42	3742.8	(4)_Real_Flat_1.77	

### *Rakkenes Central*

Three potential release point were identified in field. They were named release point 1, 2 and 3 in order of altitude. Release point 2 and 3 have equal horizontal coordinates and are referred colloquially to as release point 2 in figure. The geometry of the boulder is based on a point cloud generated using photogrammetry. A density of  $2750 \text{ kg/m}^3$  was assigned the boulder corresponding to the density of quartzite and granite gneiss as stated in (Dorren and Seijmonsbergen, 2003) (see table 6). The slope was divided into three material domains based on field observations. Material domain 1 is the upper slope bedrock, material domain 2 is the talus beneath, material domain 3 is the ditch above the road and material domain 4 is the road. The shapefiles used are presented in figure 47 along with historical settling location.

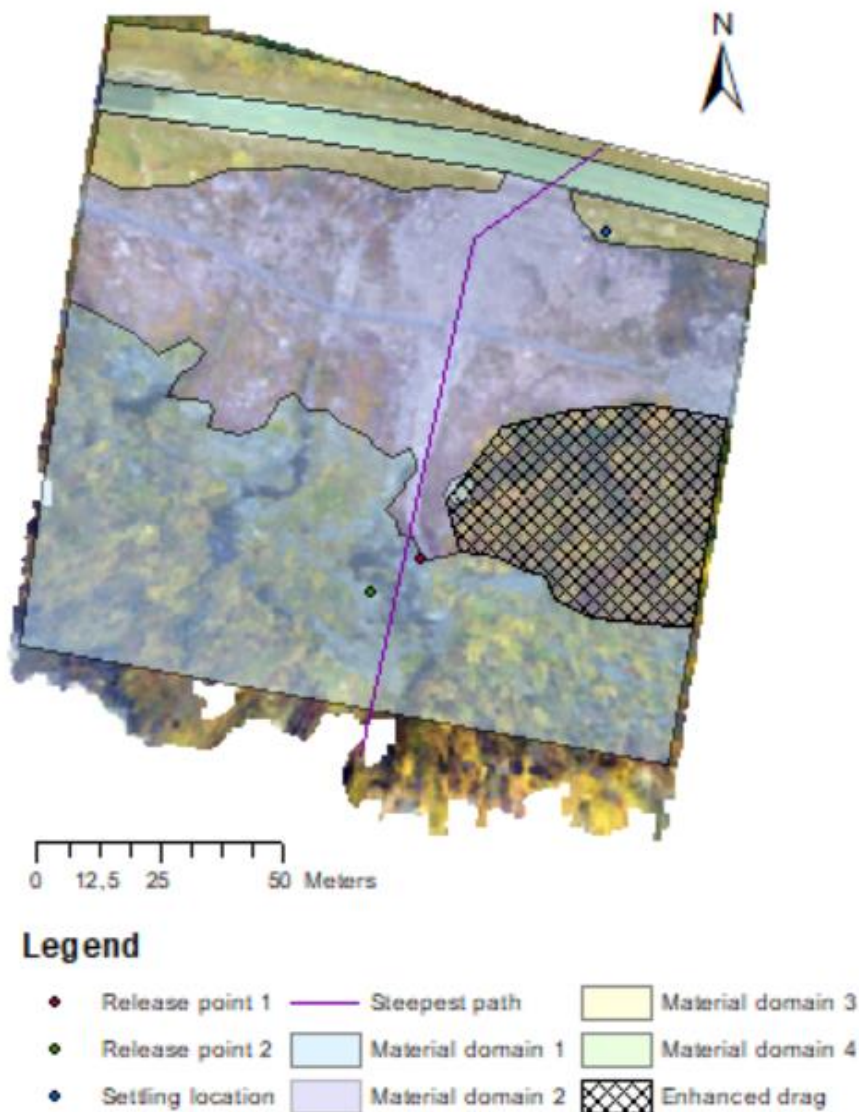


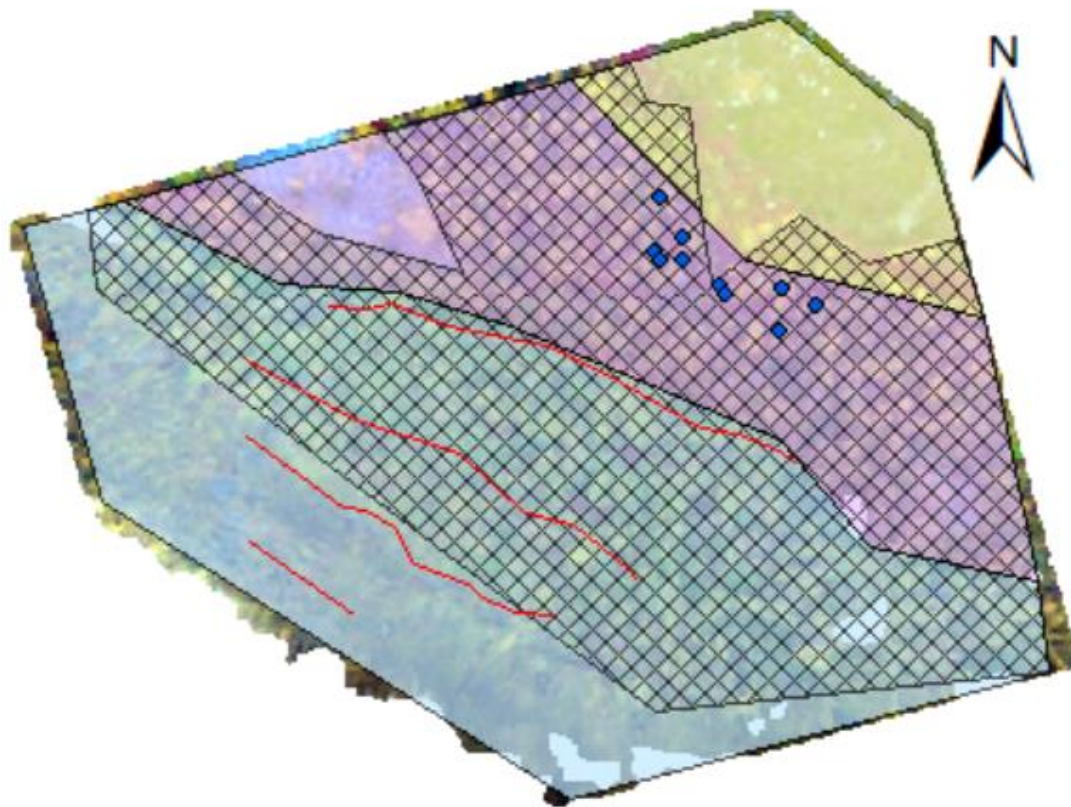
Figure 47: Rakkenes central shapefiles used for simulation.

Table 6: Properties of boulder used in simulation.

X / Y / Z (m)	Density (kg/m <sup>3</sup> )	Volume (m <sup>3</sup> )	Mass (kg)	Name in RAMMS:Rockfall library	Figure
3.35/2.64/2.36	2750	7.27	19 991.5	NA (Point cloud)	

### *Rakkenes East*

There was no calibration of input parameters on this case area. Literature values and values that had been successful during back calculation was used for this simulation. Boulders were released from lines fixed along the bottom of four distinct cliff sections on the rockface. A 20 m initial vertical offset was assigned corresponding to upper parts of the tallest cliffs. A total of 28 release points were spread out across these polylines by the RAMMS:Rockfall software. Each release point released 10 different boulders with 2 random orientations, allowing a total of 560 trajectories. The geometry of the boulders used in simulation are consistent with field measurements, generally, flat or elongated shapes were assigned corresponding to the axes lengths (see table 7). Densities of 2750 kg/m<sup>3</sup> were assigned these boulders corresponding to the density of quartzite and granite gneiss as stated in (Dorren and Seijmonsbergen, 2003). The slope was divided into three material domains; Material domain 1 is the cliff section, material domain 2 is the talus beneath the cliff and material domain 3 is the flat section beneath talus consisting mostly of soil. Forest (Enhanced drag) was added to select areas. A terrestrial survey model with 1 m resolution was used as elevation input. The shapefiles used are presented in figure 48 along with field established historical settling locations.

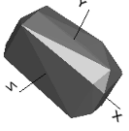
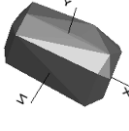
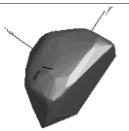
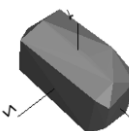
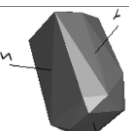
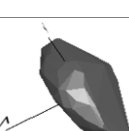
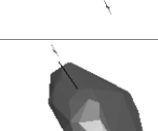


**Legend**

- Release lines
- Historical settling locations
- Material domain 1
- Material domain 2
- Material domain 3
- Enhanced drag

*Figure 48: Rakkenes East shapefiles used for simulation.*

Table 7: Properties of boulder used in simulation.

Name	X / Y / Z (m)	Density (kg/m <sup>3</sup> )	Volume (m <sup>3</sup> )	Mass (kg)	Name in RAMMS:Rockfall library	Figure
E1	2.43/1.46/1.21	2750	3.297	9066.4	(3)-long_2.0	
E2	2.16/1.30/1.08	2750	2.315	6367.6	(3)-long_2.0	
E3	1.17/0.97/0.50	2750	0.261	717.2	(4)-Real_Flat_2.35	
E4	3.08/1.54/2.12	2750	4.534	12468.5	(4)-Real_Long_2.0	
E5	1.72/2.31/1.56	2750	2.848	7833.2	(4)-Real_Long_1.5	
E6	1.51/0.91/0.76	2750	0.799	2197.1	(3)-long_2.0	
E7	1.96/1.18/0.98	2750	1.743	4794.0	(3)-long_2.0	
E8	0.89/0.53/0.44	2750	0.159	438.0	(3)-long_2.0	
E9	1.65/1.36/0.7	2750	0.731	2011.5	(4)-Real_Flat_2.35	
E10	2.48/2.31/2.64	2750	4.04	11118.4	NA (Pointcloud)	

## 4.5.2 Rocfall 6.0

### *Aunfjellet*

The release point was placed to correspond to the 3D simulation. A smooth triangular shape from the Rocfall 6.0 shape library was used to approximate wedge like boulder, mass was set about equal to the value used in 3D simulation (see table 8). Material domains were also sectioned like in the 3D simulation (see figure 49).

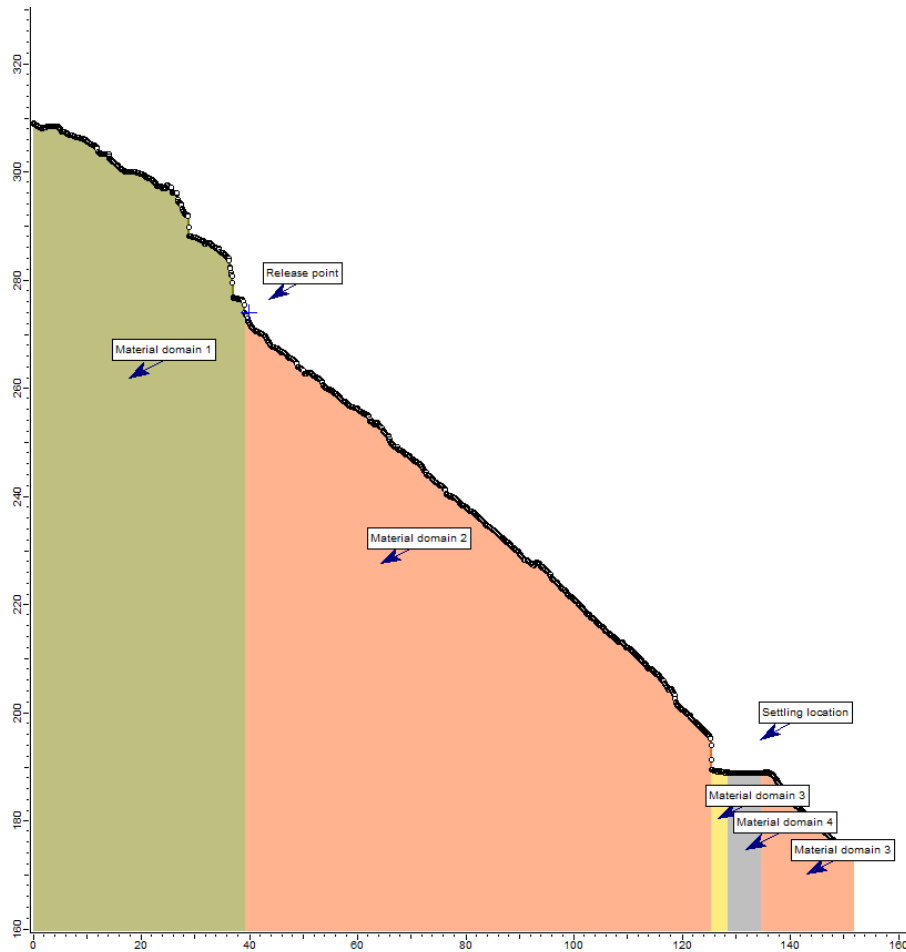
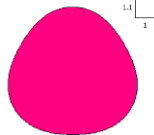


Figure 49: Aunfjellet material domains, source area and historical settling location.

Table 8: Properties of boulder used in simulation.

X:Y ratio	Density (kg/m <sup>3</sup> )	Mass (kg)	Name in Rocfall 6.0 library	Figure
11:10	2640	2641	Smooth triangle	

## Revsnestinden

The release point was placed to correspond to the 3D simulation. Lumped mass analysis was used due to difficulty in translating the oblong geometry of the boulder to 2D, mass was set about equal to the value used in 3D simulation (see table 9). The slope was sectioned like in 3D simulation with the addition of road and ocean for esthetic purposes (see figure 50). Their material properties did not intervene with any trajectory and will be omitted from further description.

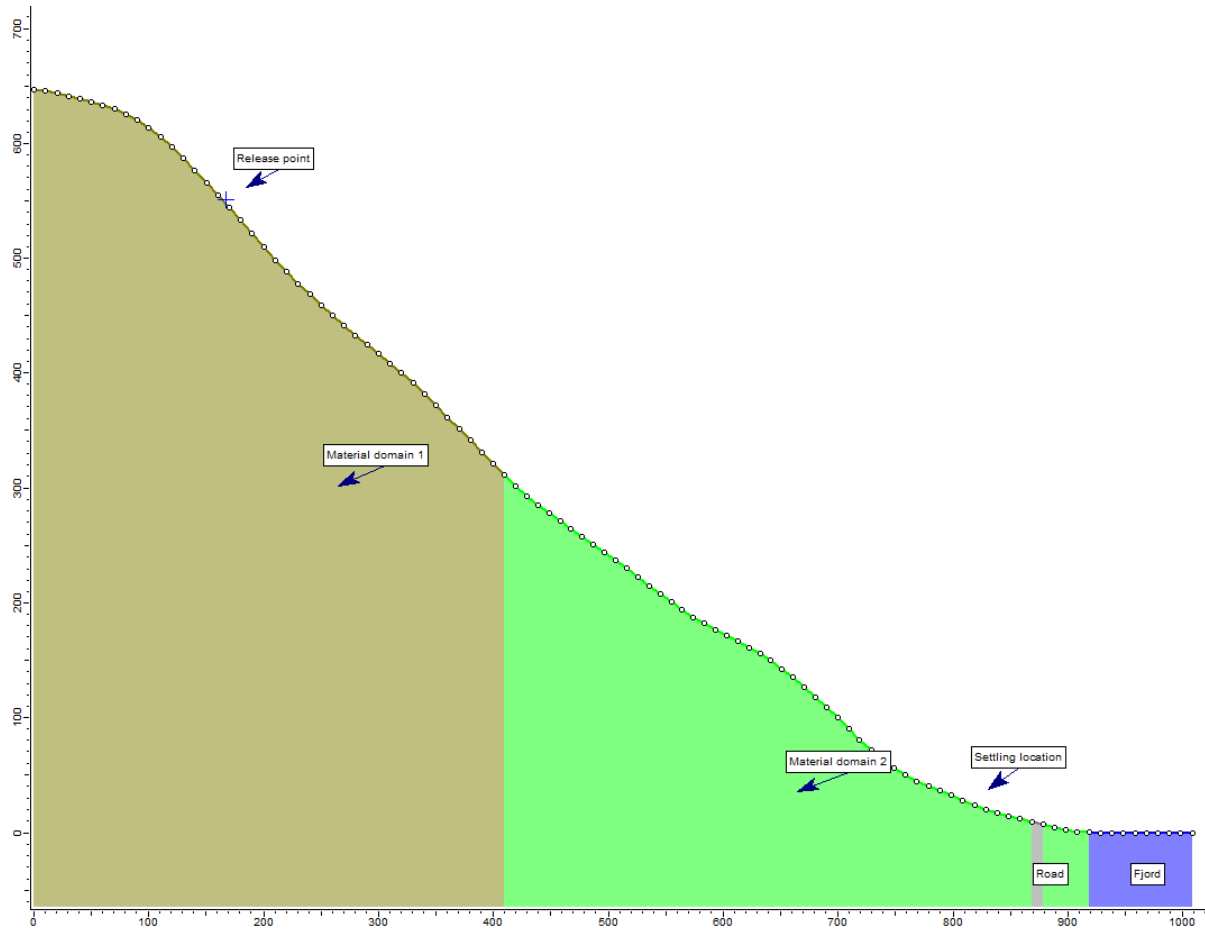


Figure 50: Revsnestinden material domains, source area and historical settling location.

Table 9: Properties of boulder used in simulation.

X:Y ratio	Density (kg/m <sup>3</sup> )	Mass (kg)	Name in Rocfall 6.0 library	Figure
n/a	2750	6996	NA (Lumped mass)	NA

### Rakkenes West

The release point was placed to correspond to the 3D simulation. The geometry that best corresponded with the described boulder for this area was selected from the Rocfall rock shape library, a flat rectangular shape (see table 10). Mass was set about equal to the value used in 3D simulation. The slope was sectioned like in 3D simulation (see figure 51).

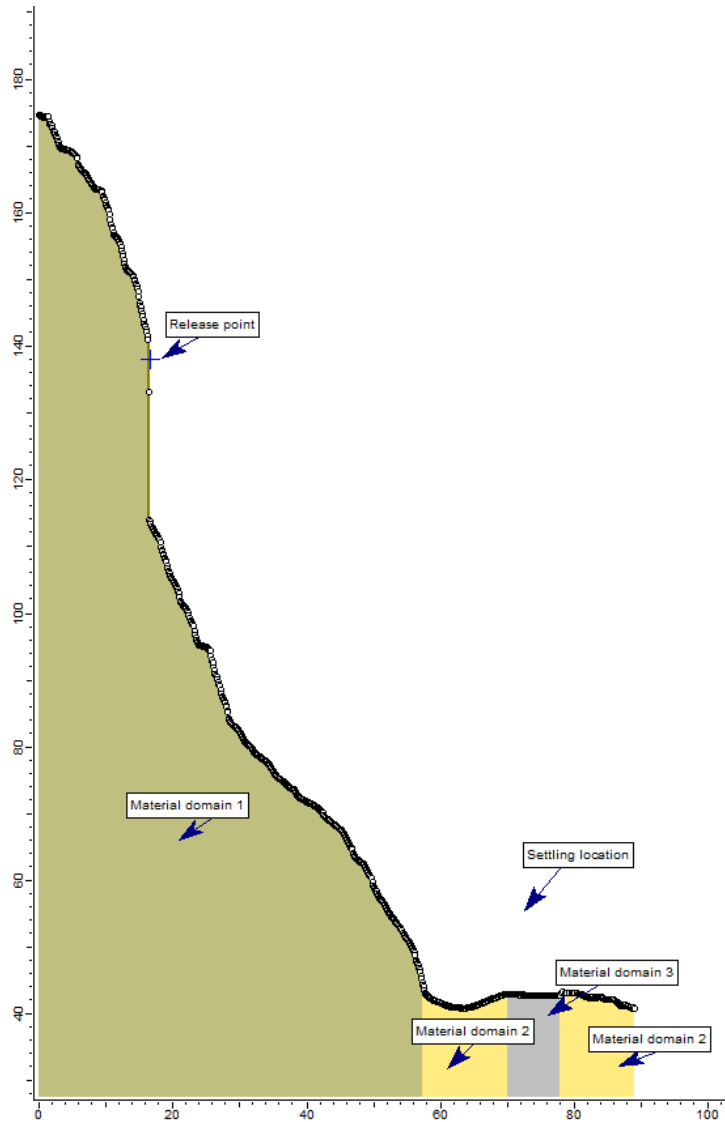
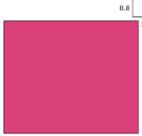


Figure 51: Rakkenes West material domains, source area and historical settling location.

Table 10: Properties of boulder used in simulation.

X:Y ratio	Density (kg/m <sup>3</sup> )	Mass (kg)	Name in Rocfall 6.0 library	Figure
5:4	2750	3899	Polygon 5:6	

### *Rakkenes Central*

The release point was placed to correspond to the 3D simulation. Its altitude was approximated to 104 m by back calculation in 3D simulation. Lumped mass analysis was used due to difficulty translating the flat disk-shaped geometry of boulder to a 2D. Mass was set about equal to the value used in 3D simulation (see table 11). The slope was sectioned like in 3D simulation but excluding the ditch above road (see figure 52).

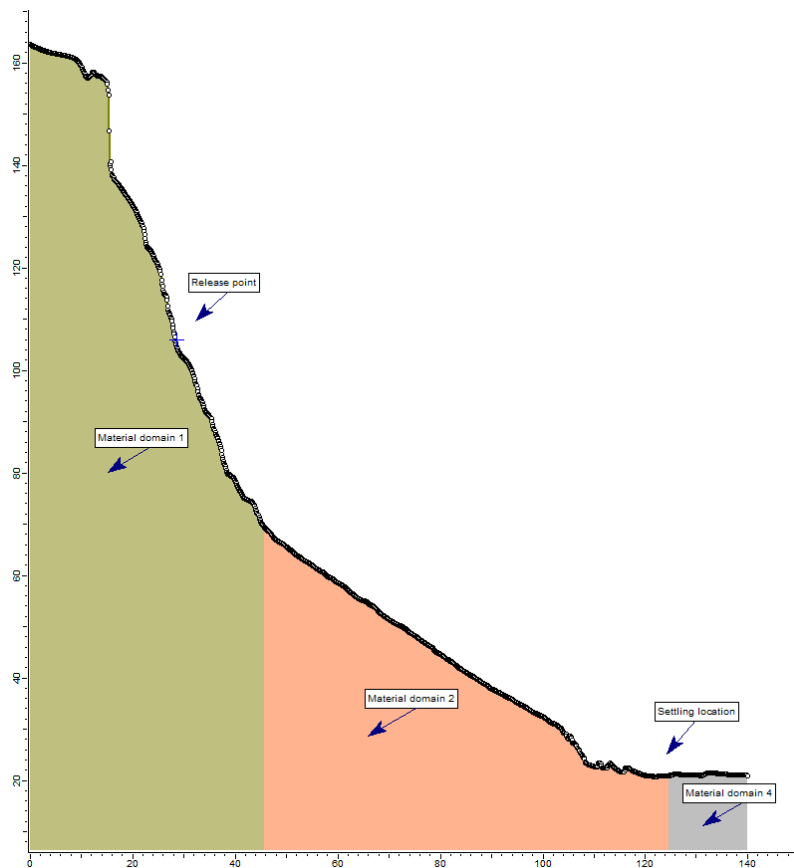


Figure 52: Rakkenes Central material domains, source area and historical settling location.

Table 11: Properties of boulder used in simulation.

X:Y ratio	Density (kg/m <sup>3</sup> )	Mass (kg)	Name in Rocfall 6.0 library	Figure
n/a	2750	19992	NA (Lumped mass)	NA

### **4.6 Material input calibration and final simulation**

For each case area expect Rakkenes East back calculations were performed to produce most realistic material input. Boulder properties and material subdivision were kept equal in all intra-case simulations.

For each case and each DEM (up to six per case), terrain parameters were varied to produce output most similar with field/reported observations. 100 boulders were for each terrain model on each case released from locations consistent with historical source zones. For RAMMS:Rockfall this corresponds to 100 random initial orientations of boulder before release.

Initial material values were set based on suggested values in literature, and then varied if needed to produce output settling location in accordance with historical case. For Rocfall, the selection of initial restitution coefficients were based on the values obtained by (Hau et al., 1996), (Pfeiffer and Bowen, 1989) and (Robotham et al., 1995). The terrain type guidelines in (Bartelt et al., 2016) were used when selecting initial terrain types in RAMMS:Rockfall (see table 12)

Table 12: RAMMS:Rockfall material types. From (Bartelt et al., 2016).

Category	Picture	Description	Example
Extra soft		Very wet ground. Cannot cross without deep sink-in. No high vegetation	Moor, turf, gley
Soft		Soft ground with many deep soil layers. Ground contains no large rock fragments. Often very moist. Foot inudations remains and are visible. Wet and deep surface soil	Moist meadow

Medium soft		Rocks penetrate meadow surface leaving impact scars. Soil is deep, few rock fragments. Rank vegetation.	Meadow
Medium		Meadow is deep, but contains rock fragments. The meadow can be covered with vegetation. Soil structure of a medium deepness. Rank vegetation.	Meadow
Medium hard		Penetration depths are small. Ground is flat. Rocky debris is present. Shallow surface soil. Usually little (initial) vegetation.	Non-paved mountain roads, mountain meadow, pebble
Hard		Rocks jump over ground. Mixture of large and small rocks. Usually without any vegetation.	Rock scree, pebble, coarse rock, paved roads

---

Extra  
hard



Ground is very hard and is marginally deformed by rocks. No vegetation and no surface soil.

Bedrock, cliff

---

Snow



Rocks slide on snow surface.

Snow

---

## **5 Results**

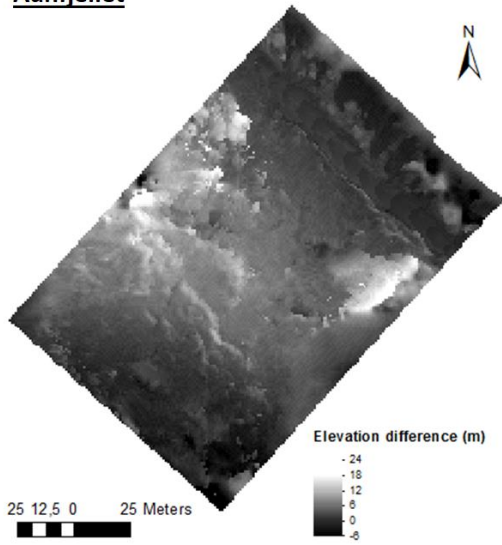
### **5.1 Back calculation findings**

Back calculation was not successful on Aunfjellet using 10 m and 10 cm resolution models. The 10 m resolution model did not include the roadcut and settling on historical location could not be achieved. The 10 cm models could cause extreme run outs and early settling with close to equal input. On Aunfjellet this resolution caused boulders to either halt prematurely or exceed desired run out.

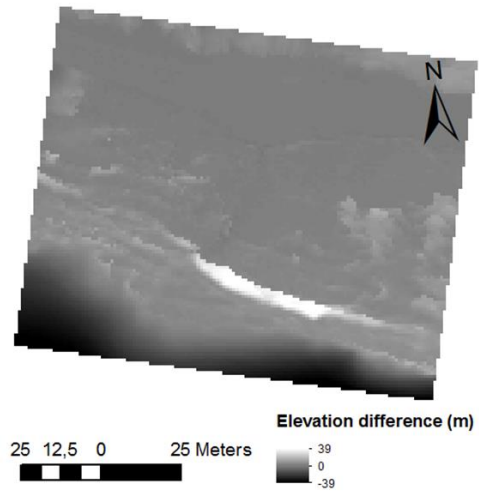
### **5.2 Raster math findings**

The 1 m resolution aerial survey model raster was subtracted from the 1 m resolution terrestrial survey model raster. The resulting rasters are presented in figure. They all show increased elevation in steep areas and consequently steeper slopes for the terrestrial survey model (produced by photogrammetry) relative to existing LIDAR data. See figure 53.

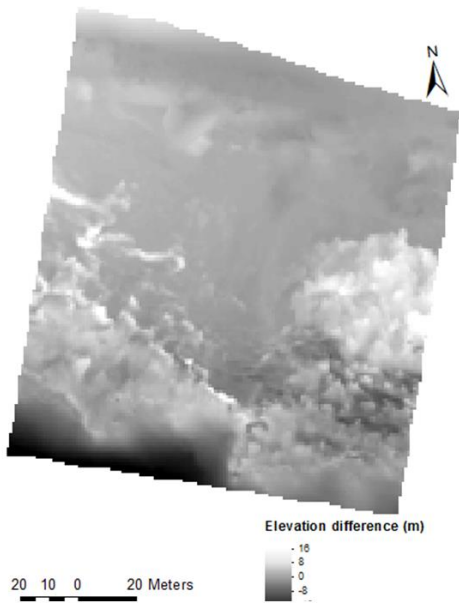
**Aunfjellet**



**Rakkenes West**



**Rakkenes Central**



**Rakkenes East**

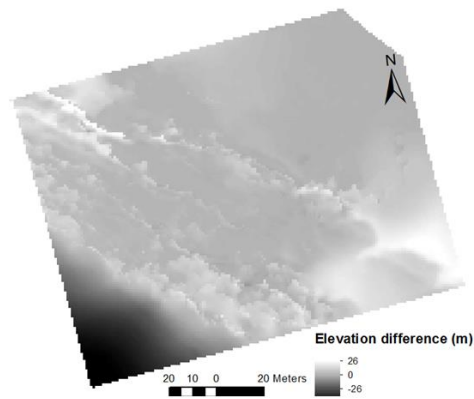


*Figure 53: Rasters created by subtracting the 1 m resolution aerial survey model from the 1m resolution terrestrial survey model. Bright fringes are areas where terrestrial survey model have higher elevation values than LIDAR data.*

## 5.3 Simulation output

### 5.3.1 RAMMS: Rockfall simulations

#### 5.3.1.1 Aunfjellet

##### *Terrestrial survey model - 1m resolution (1T)*

Results from this simulation are presented in figure 54. Trajectories are spread out laterally early in the simulation and initially moves north east. Trajectories are then deflected northwards and onto the road. Total kinetic energy ranges from 0 to 761 kJ, passing heights ranges from 0 to 15 m. Highest values for both total kinetic energy and passing height are calculated just above the road. Passing heights are low close to source area, suggesting a primarily rolling or sliding motion.

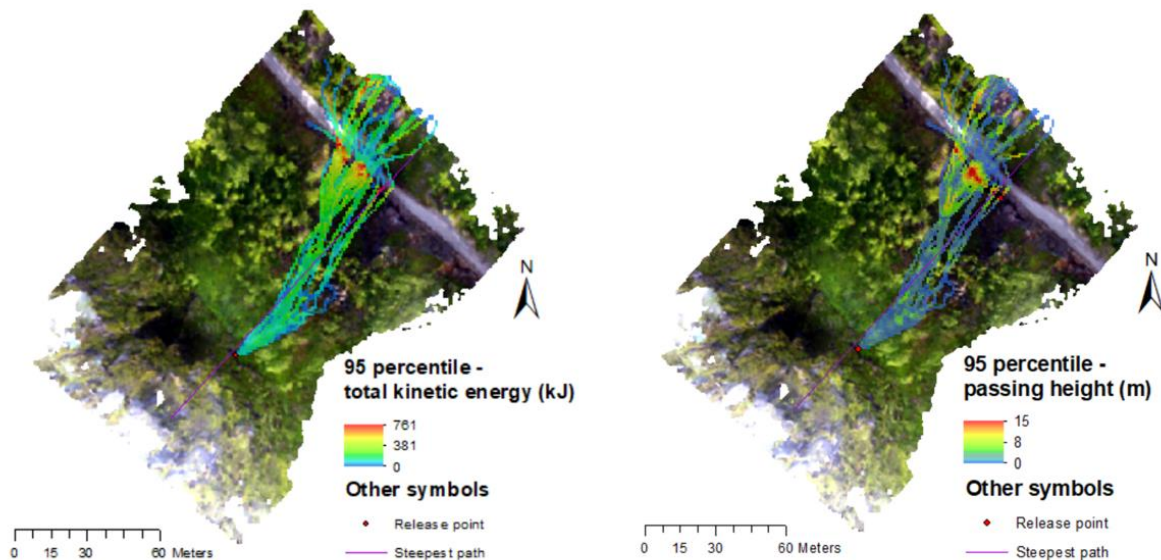


Figure 54: Output total kinetic energy (left) and bounce height (right) for simulation.

##### *Aerial survey model - 1m resolution (1A)*

Results from this simulation are presented in figure 55. Trajectories are spread out laterally early in the simulation and initially move north east. They are then deflected northwards and onto the road. Total kinetic energy ranges from 0 to 797 kJ, passing height ranges from 0 to 11 m. Highest values for both total kinetic energy and passing height are calculated just above the road. Passing heights are generally low close to source area, suggesting a primarily rolling or sliding motion however bounces can be inferred everywhere in run out.

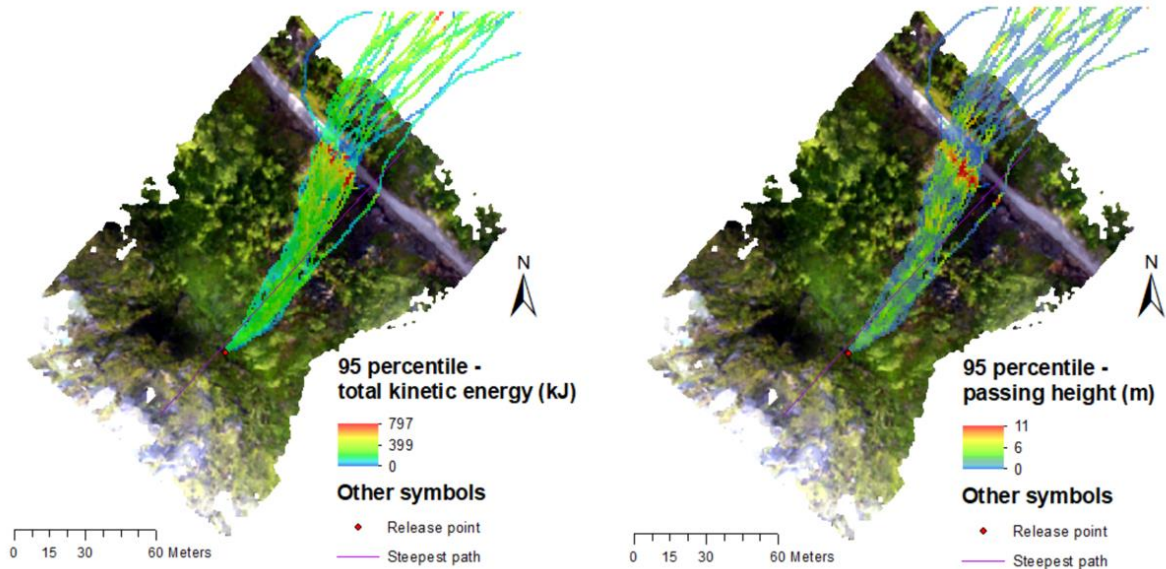


Figure 55: Output total kinetic energy (left) and bounce height (right) for simulation.

### Terrestrial survey model - 3m resolution (3T)

Results from this simulation are presented in figure 56. Trajectories are spread out laterally early in the simulation and initially move north east. Trajectories are then deflected northwards and onto the road. Total kinetic energy ranges from 0 to 691 kJ, passing heights ranges from 0 to 8 m. Highest values for both total kinetic energy and passing height are calculated just above the road. Passing heights are generally low close to source area, suggesting a primarily rolling or sliding motion. Bouncing occurs mainly in western sections of trajectory spread, slightly above road.

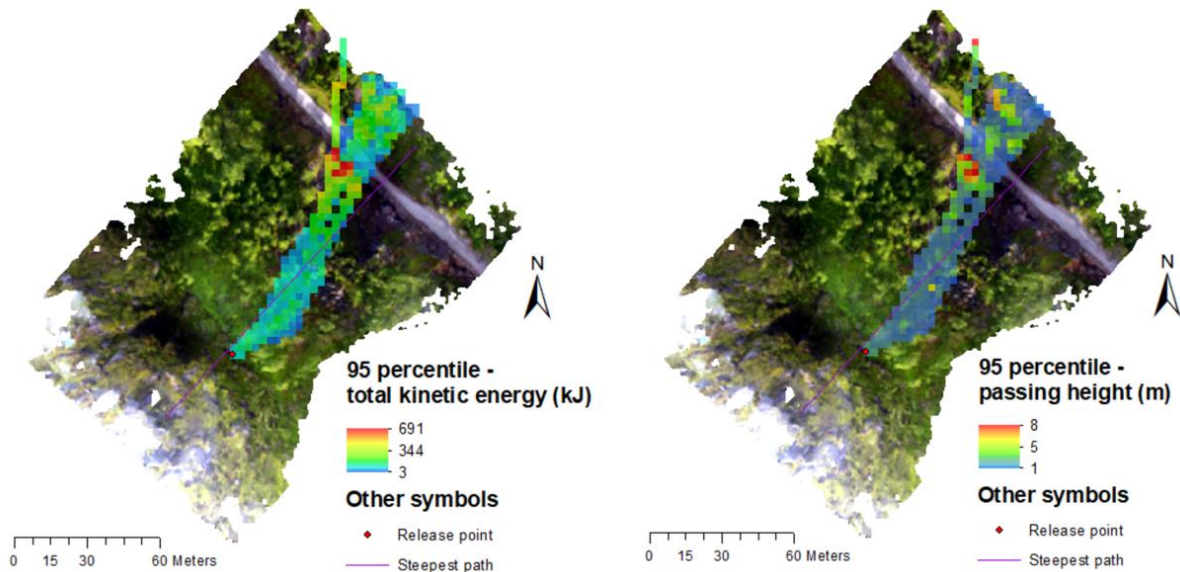


Figure 56: Output total kinetic energy (left) and bounce height (right) for simulation.

### *Aerial survey model - 3m resolution (3A)*

Results from this simulation are presented in figure 57. Trajectories remains fairly constrained laterally. Early movement is directed northeast and is later deflected northwards and onto the road. Total kinetic energy ranges from 0 to 534 kJ, passing height ranges from 0 to 4 m. Highest values for both total kinetic energy and passing height are calculated just above the road in eastern sections of trajectory. Passing heights are generally low close to source area, suggesting a primarily rolling or sliding motion.

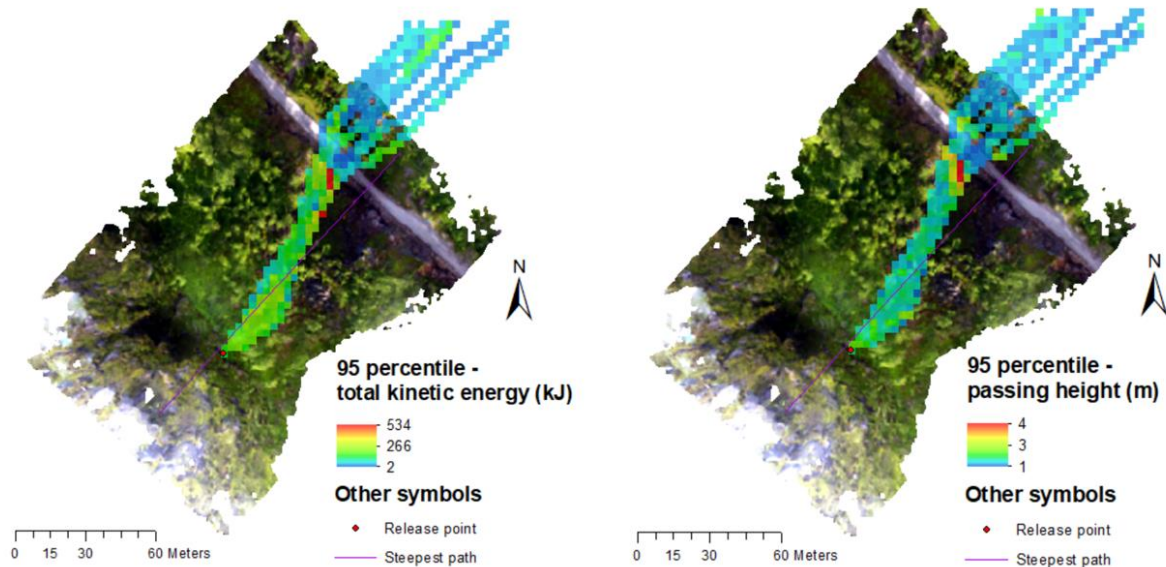


Figure 57: Output total kinetic energy (left) and bounce height (right) for simulation.

### *Terrestrial survey model - 10cm resolution (0.1T)*

Results from this simulation are presented in figure 58. Trajectories become steadily more spread out laterally throughout run out, resulting in a significantly wide, potential run out area. Early trajectory movement is directed northeast and is later deflected northwards and onto the road. Total kinetic energy ranges from 0 to 1568 kJ, passing heights ranges from 0 to 19 m. Highest values for both total kinetic energy and passing heights are calculated just above the road. Passing heights increase quickly and boulders appear to mostly bounce downslope.

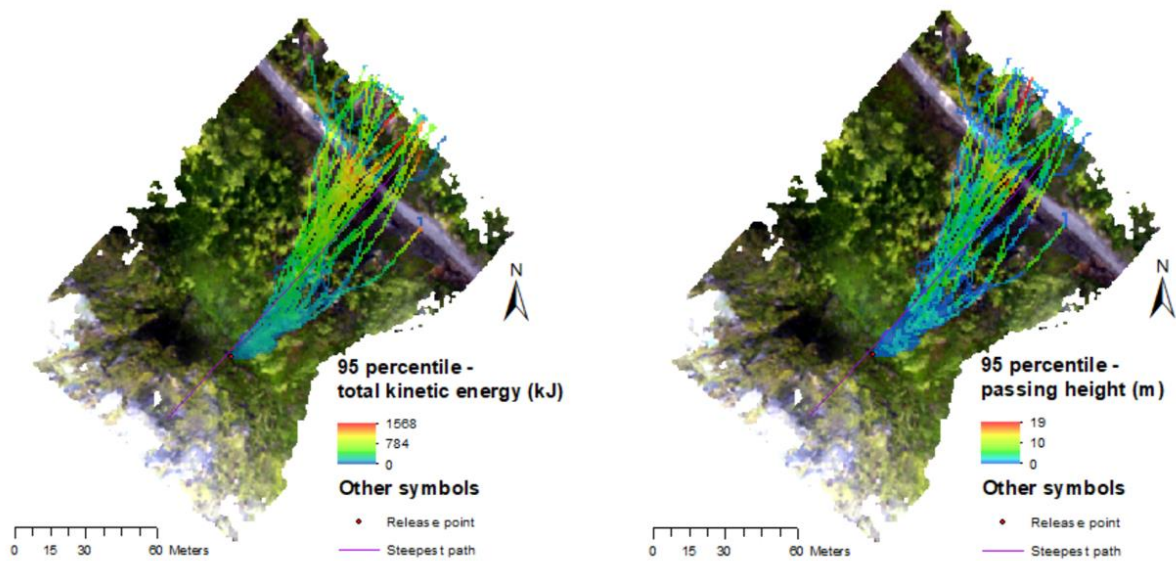


Figure 58: Output total kinetic energy (left) and bounce height (right) for simulation.

#### Aerial survey model - 10m resolution (10A)

Results from this simulation are presented in figure 59. Trajectories remains fairly constrained laterally and confined to steepest path. Total kinetic energy ranges from 39 to 671 kJ, passing heights ranges from 0 to 3 m. Highest values for total kinetic energy are calculated just above the road in eastern sections of trajectory. Passing heights are generally low throughout run out, suggesting a primarily rolling or sliding motion.

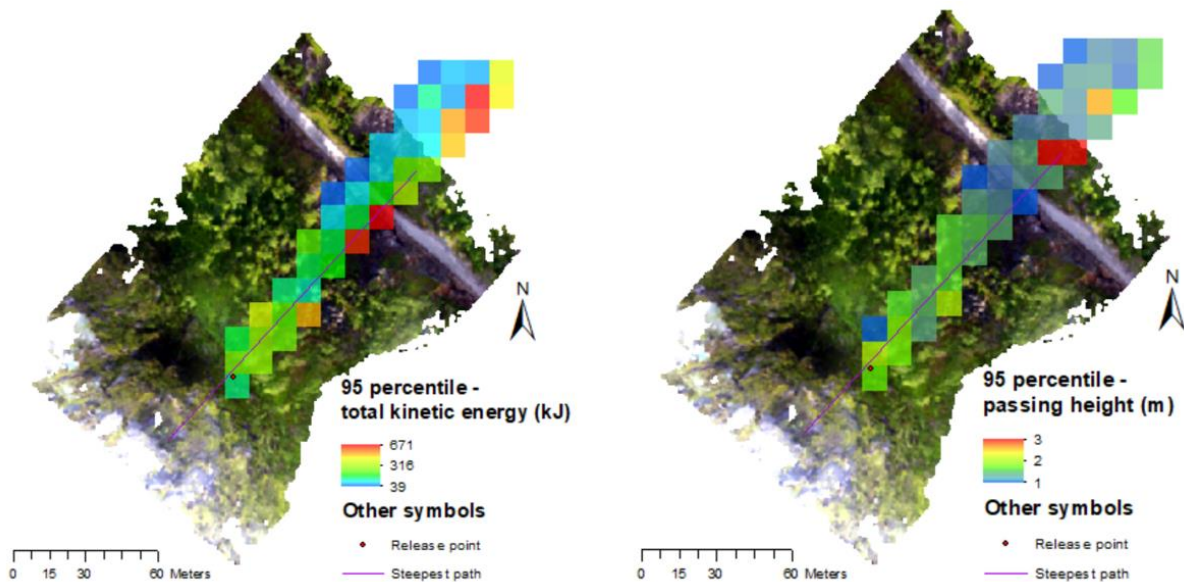


Figure 59: Output total kinetic energy (left) and bounce height (right) for simulation.

### Summary

Select summarizing statistics for Aunfjellet 3D rockfall simulations output total kinetic energy and passing height are presented in table 13 and table 14 respectively.

Table 13: Aunfjellet 3D rockfall simulations output total kinetic energy summarizing statistics.

	1T	1A	3T	3A	0.1T	10A
Mean (kJ)	121.7	165.2	85.5	57.3	218.2	114.6
95 percentile maximum (kJ)	760.7	797.5	691.3	533.6	1568.3	671.3

Table 14: Aunfjellet 3D rockfall simulations output passing height summarizing statistics.

	1T	1A	3T	3A	0.1T	10A
Mean (m)	1.41	1.56	1.01	0.89	2.21	0.91
95 percentile maximum (m)	15.23	11.10	8.48	4	19.04	2.99

#### 5.3.1.2 Revsnestinden

##### *Aerial survey model - 10m resolution.*

Results from this simulation are presented in figure 60. Trajectories becomes steadily more spread out laterally but concentric around steepest path. Total kinetic energy ranges from 0 to 10064 kJ, passing height ranges from 0 to 32 m. Highest values for total kinetic energy and passing height are calculated at distances about 1/3 of total run out. Passing height increase early but becomes lower downslope, particularly in southern sections of trajectory spread. The highest passing height and total kinetic energy values are generally observed along steepest path. Select summarizing statistic for this case areas simulations are presented in table 15 and table 16.

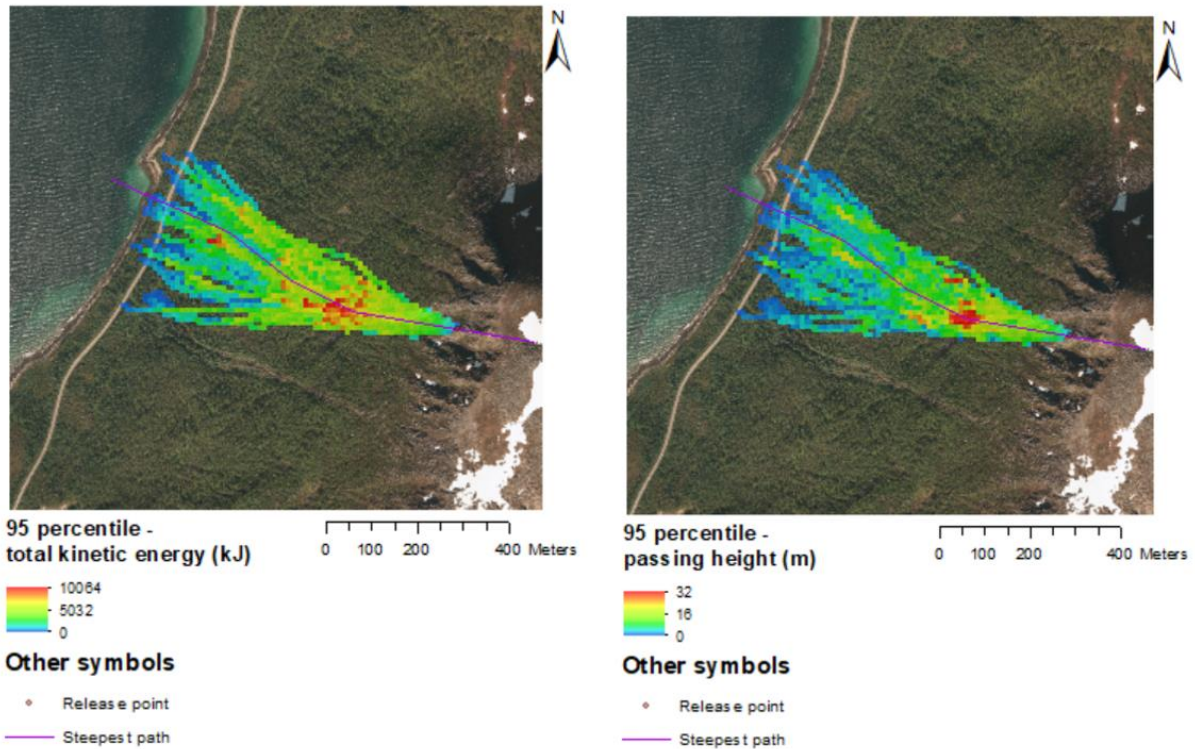


Figure 60: Output total kinetic energy (left) and bounce height (right) from Revsnestinden rockfall simulation.

Table 15: Revsnestinden 3D rockfall simulation output total kinetic energy summarizing statistics.

Mean (kJ)	1897.8
95 percentile maximum (kJ)	10064.0

Table 16: Revsnestinden 3D rockfall simulation output passing height summarizing statistics

Mean (m)	3.94
95 percentile maximum (m)	31.74

### 5.3.1.3 Rakkenes West

#### *Terrestrial survey model - 1m resolution (1T)*

Results from this simulation are presented in figure 61. Trajectories becomes steadily more spread out downslope and is concentric around early steepest path. Total kinetic energy ranges from 0 to 2366 kJ, passing height ranges from 0 to 25 m. Highest values for total kinetic energy and passing height are calculated just above road. Bouncing height max values seem confined to steepest path (western sections of trajectory spread).

Passing height and total kinetic energy increase early but is immediately lowered on impact with sub horizontal substrate (road).

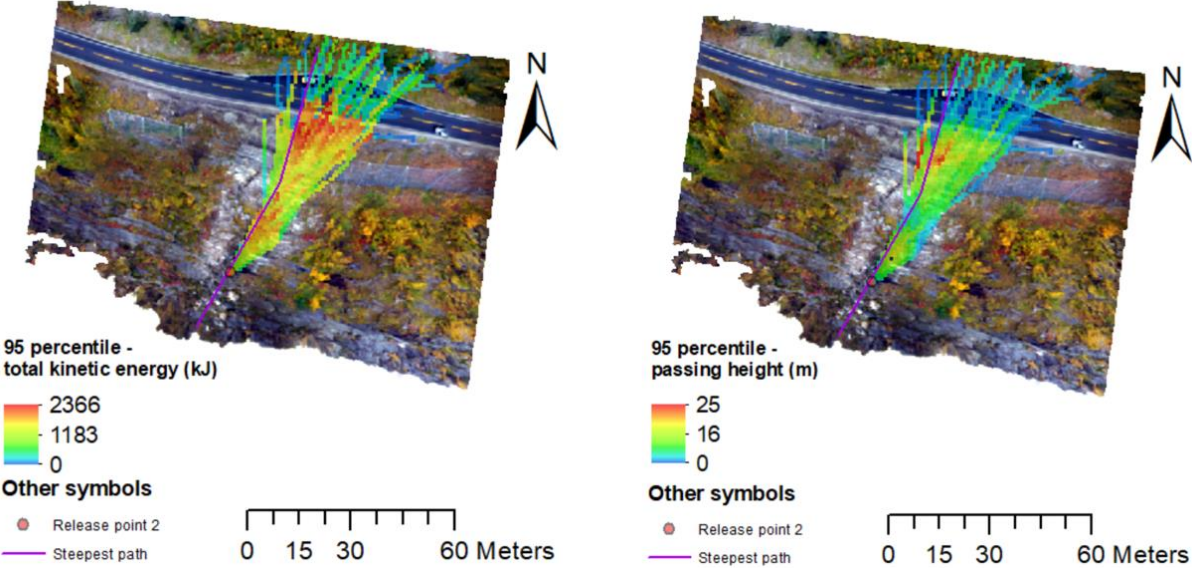


Figure 61: Output total kinetic energy (left) and bounce height (right) for simulation.

*Aerial survey model - 1m resolution (1A)*

Results from this simulation are presented in figure 62. Trajectories becomes steadily more spread out downslope, but are concentric around early steepest path. Total kinetic energy ranges from 0 to 2513 kJ, passing heights ranges from 0 to 23 m. Highest values for total kinetic energy and passing height are calculated just above road. Bouncing height max values seem confined to steepest path (western sections of trajectory spread). Passing height and total kinetic energy increase early but is immediately lowered on impact with sub horizontal substrate (road).

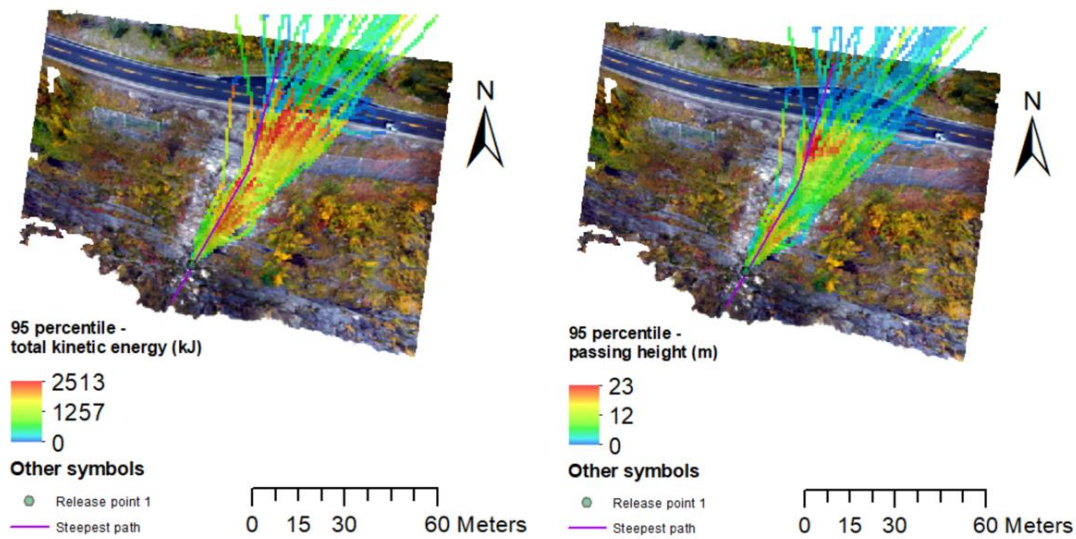


Figure 62: Output total kinetic energy (left) and bounce height (right) for simulation.

*Terrestrial survey model - 3m resolution (3T)*

Results from this simulation are presented in figure 63. Trajectories becomes steadily more spread out downslope but are concentric around early steepest path. Total kinetic energy ranges from 0 to 2838 kJ, passing height ranges from 0 to 21 m. Highest values for total kinetic energy and passing height are calculated just above road. Bouncing height value seem elevated along steepest path (western sections of trajectory spread). Passing height and total kinetic energy increase early but is immediately lowered on impact with sub horizontal substrate (road).

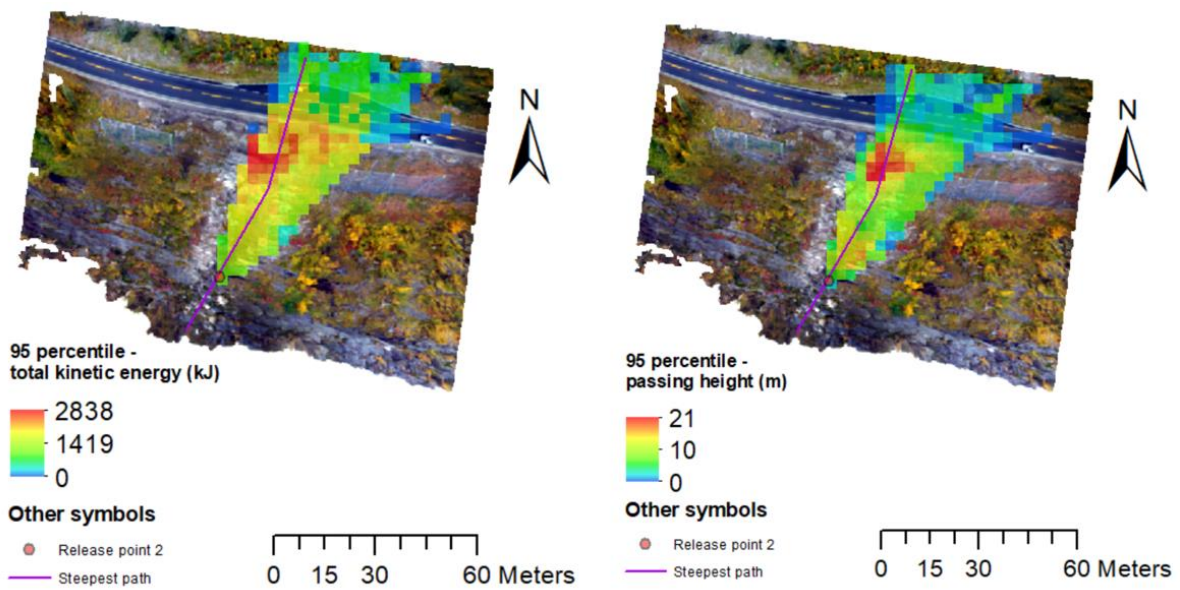


Figure 63: Output total kinetic energy (left) and bounce height (right) for simulation.

*Aerial survey model - 3m resolution (3A)*

Results from this simulation are presented in figure 64. Trajectories becomes steadily more spread out downslope but are concentric around early steepest path. Total kinetic energy ranges from 16 to 2545 kJ, passing height ranges from 0 to 19 m. Highest values for total kinetic energy and passing height are calculated just above road. Bouncing height value seem elevated along steepest path. Passing height and total kinetic energy increase early but is immediately lowered on impact with sub horizontal substrate (road).

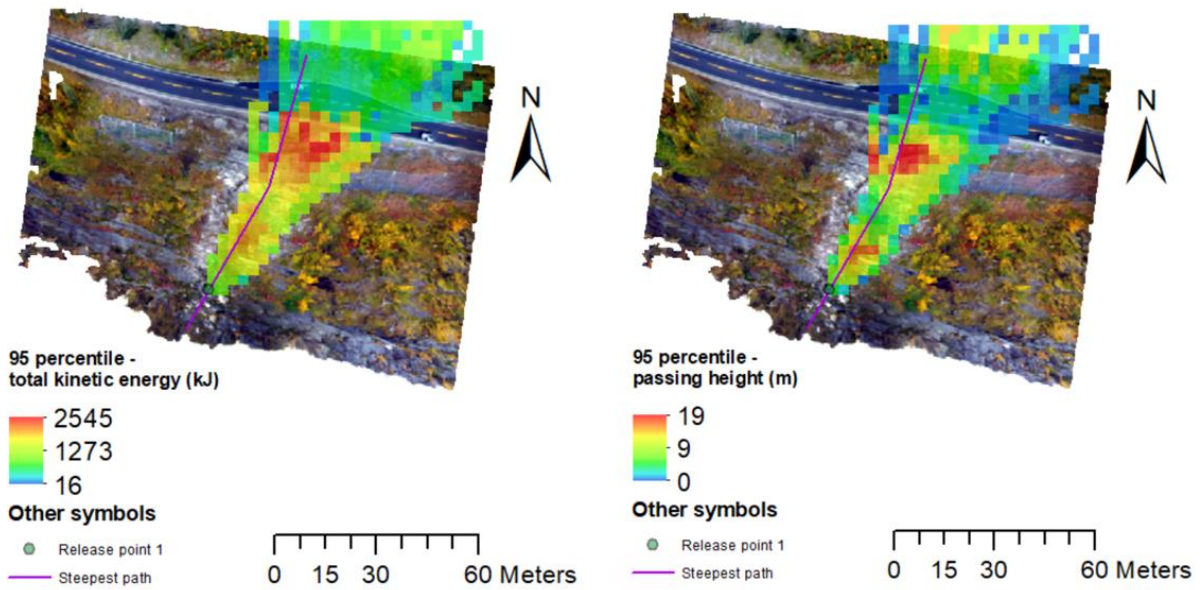


Figure 64: Output total kinetic energy (left) and bounce height (right) for simulation

*Terrestrial survey model - 10cm resolution (0.1T)*

Results from this simulation are presented in figure 65. Trajectories becomes steadily more spread out downslope but are concentric around early steepest path. Total kinetic energy ranges from 0 to 2324 kJ, passing heights ranges from 0 to 25 m. Highest values for total kinetic energy and passing height were calculated just above road. Passing heights are generally higher in western section of trajectory spread, along steepest path. Passing heights and total kinetic energy increase rapidly on release but is immediately lowered on impact with sub-horizontal substrate (road).

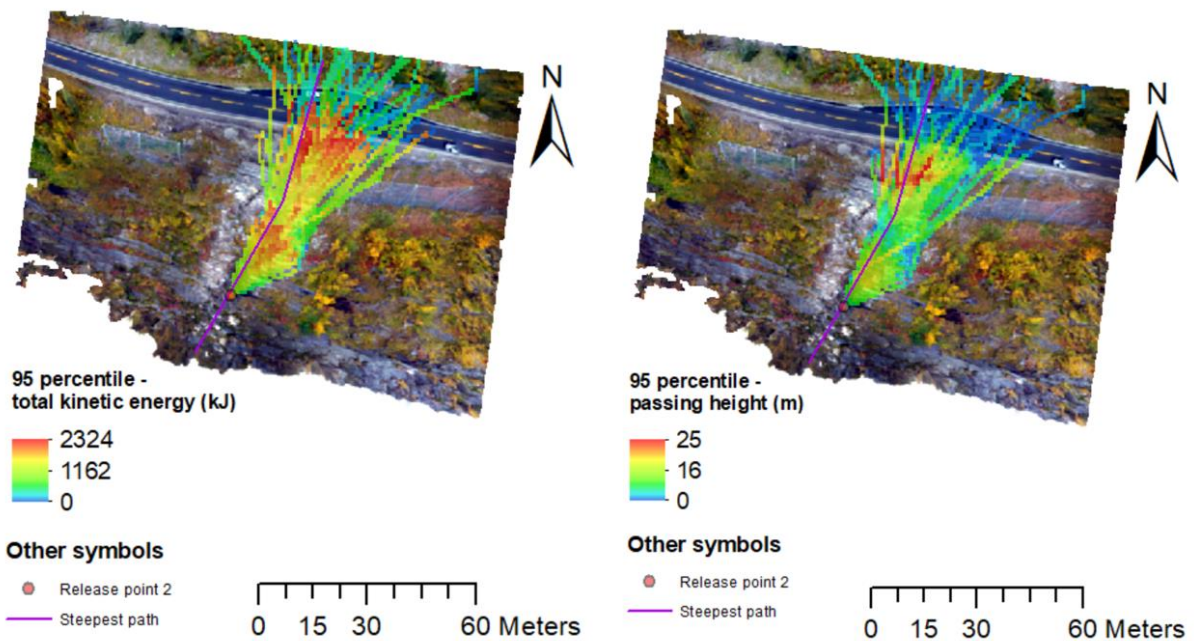


Figure 65: Output total kinetic energy (left) and bounce height (right) for simulation.

*Aerial survey model - 10m resolution (10A)*

Results from this simulation are presented in figure 66. Trajectories becomes steadily more spread out downslope but is concentric around early steepest path. Total kinetic energy ranges from 568 to 2338 kJ, passing height ranges from 2 to 12 m. Highest values for total kinetic energy and passing height are calculated just above road. Passing height and total kinetic energy increase early but is immediately lowered on impact with sub horizontal substrate (road).

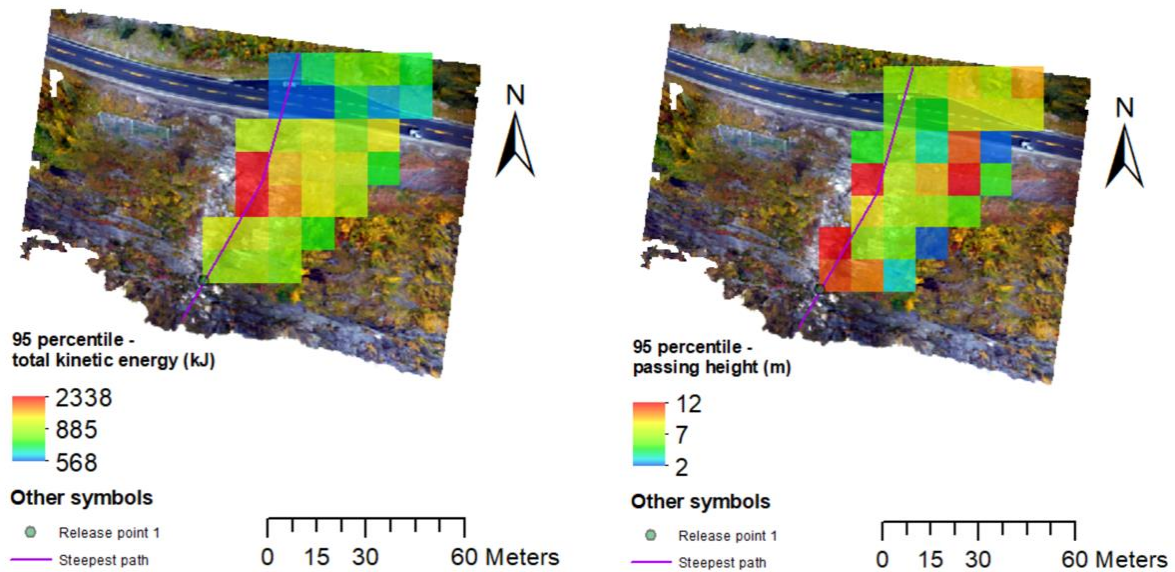


Figure 66: Output total kinetic energy (left) and bounce height (right) for simulation.

**Summary**

Select summarizing statistic for Rakkenes West 3D rockfall simulations output total kinetic energy and passing height are presented in table 17 and table 18 respectively.

Table 17: Rakkenes West 3D rockfall simulations output total kinetic energy summarizing statistics.

	1T	1A	3T	3A	0.1T	10A
Mean (kJ)	737.1	724.5	775.1	663.7	744.4	802.4
95 percentile maximum (kJ)	2366.0	2513.0	2837.8	2544.8	2324.8	2337.9

Table 18: Rakkenes West 3D rockfall simulations output passing height summarizing statistics.

	1T	1A	3T	3A	0.1T	10A
Mean (m)	3.87	3.83	3.57	3.22	4.99	2.88
95 percentile maximum (m)	24.55	23.05	21.37	18.81	25.00	11.99

### 5.3.1.4 Rakkenes Central

#### *Terrestrial survey model - 1m resolution (1T)*

Results from this simulation are presented in figure 67. Trajectories becomes steadily more spread out downslope but are concentric around steepest path. Total kinetic energy ranges from 0 to 8342 kJ, passing heights ranges from 0 to 14 m. Highest values of passing height are calculated near cliff face. Total kinetic energy remains fairly constant throughout run out but passing heights decrease immediately after reaching talus. Total kinetic decrease suddenly before reaching the road. Both passing heights and total kinetic energies seem fairly similar laterally.

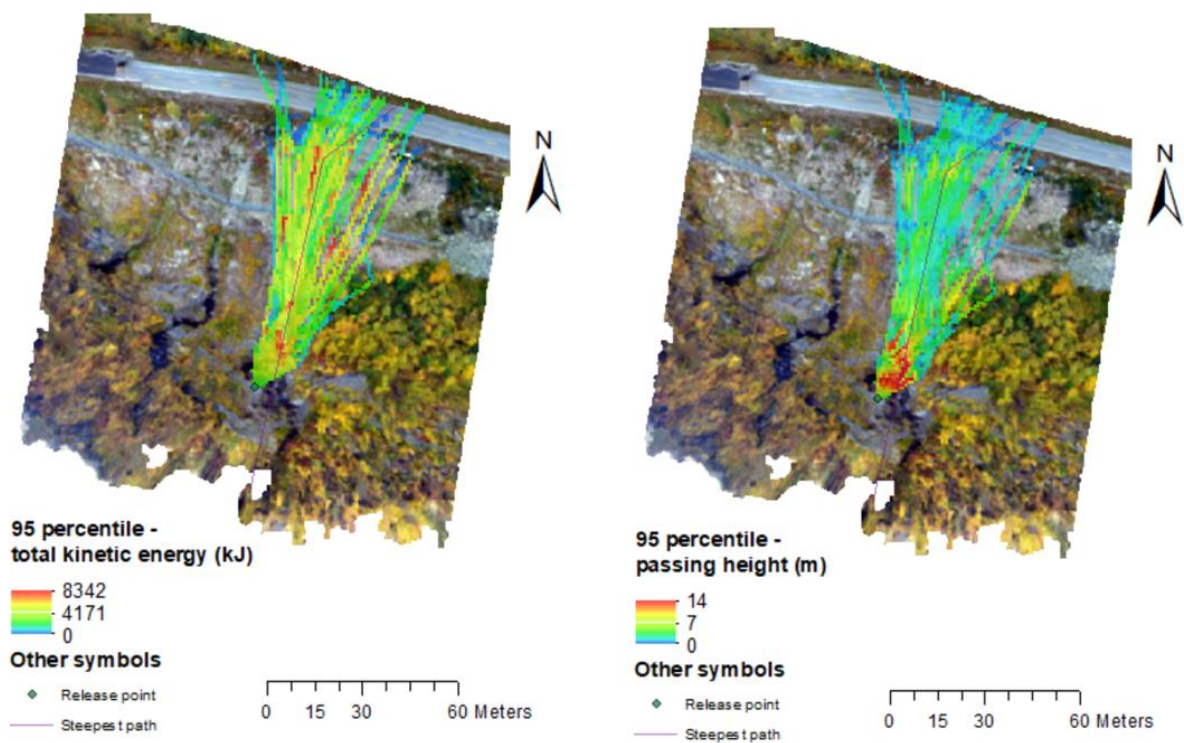


Figure 67: Output total kinetic energy (left) and bounce height (right) for simulation.

*Aerial survey model - 1m resolution (1A)*

Results from this simulation are presented in figure 68. Trajectories become steadily more spread out downslope but are concentric around steepest path. Total kinetic energy ranges from 0 to 9475 kJ, passing heights range from 1 to 14 m. Highest values for passing height are calculated near cliff face. Total kinetic energy remains fairly constant throughout run out (although effectively lowered near ditch above road) but passing heights decrease immediately after reaching talus. Passing height does however remain somewhat elevated along steepest path profile.

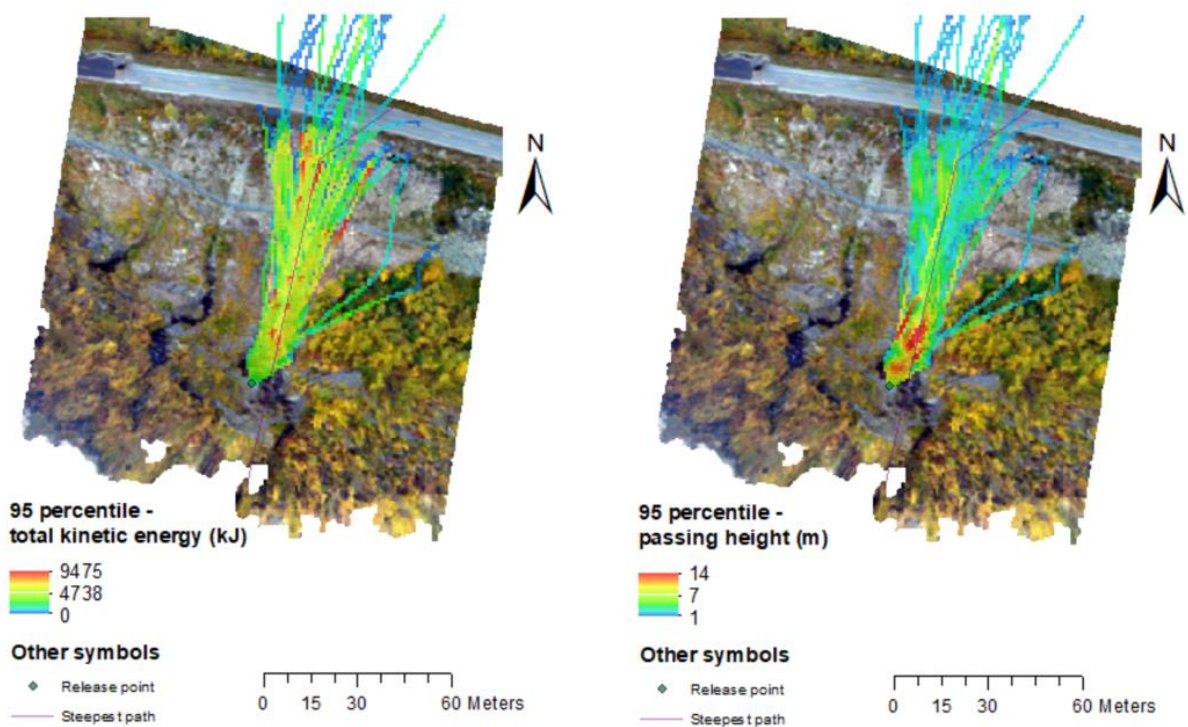


Figure 68: Output total kinetic energy (left) and bounce height (right) for simulation.

*Terrestrial survey model - 3m resolution (3T)*

Results from this simulation are presented in figure 69. Trajectories steadily spread out laterally throughout run out but are largely concentric around steepest path. Total kinetic energy values ranges from 0 to 9241 kJ, passing height ranges from 1 to 14 m. Highest values for passing height are calculated near cliff face and just before reaching talus in eastern sections of trajectory spread. Total kinetic energy remains fairly constant throughout run out (although effectively lowered near ditch above road) but passing heights decrease immediately after reaching talus.

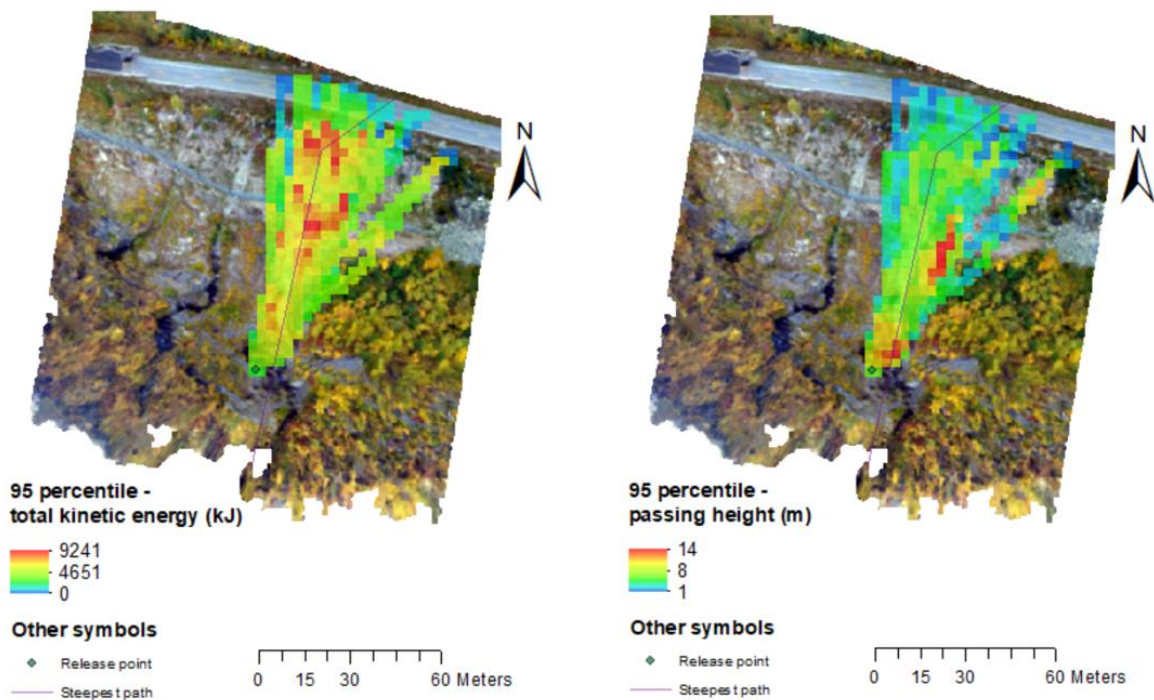


Figure 69: Output total kinetic energy (left) and bounce height (right) for simulation

### Aerial survey model - 3m resolution (3A)

Results from this simulation are presented in figure 70. Trajectories steadily spreads out laterally throughout run out but are concentric around steepest path. Total kinetic energy ranges from 0 to 8049 kJ, passing height ranges from 1 to 13 m. Highest values for passing height are calculated near cliff face. Total kinetic energy remains fairly constant throughout run out (although effectively lowered near ditch above road) but passing heights decrease immediately after reaching talus. Total kinetic energies are highest along steepest path.

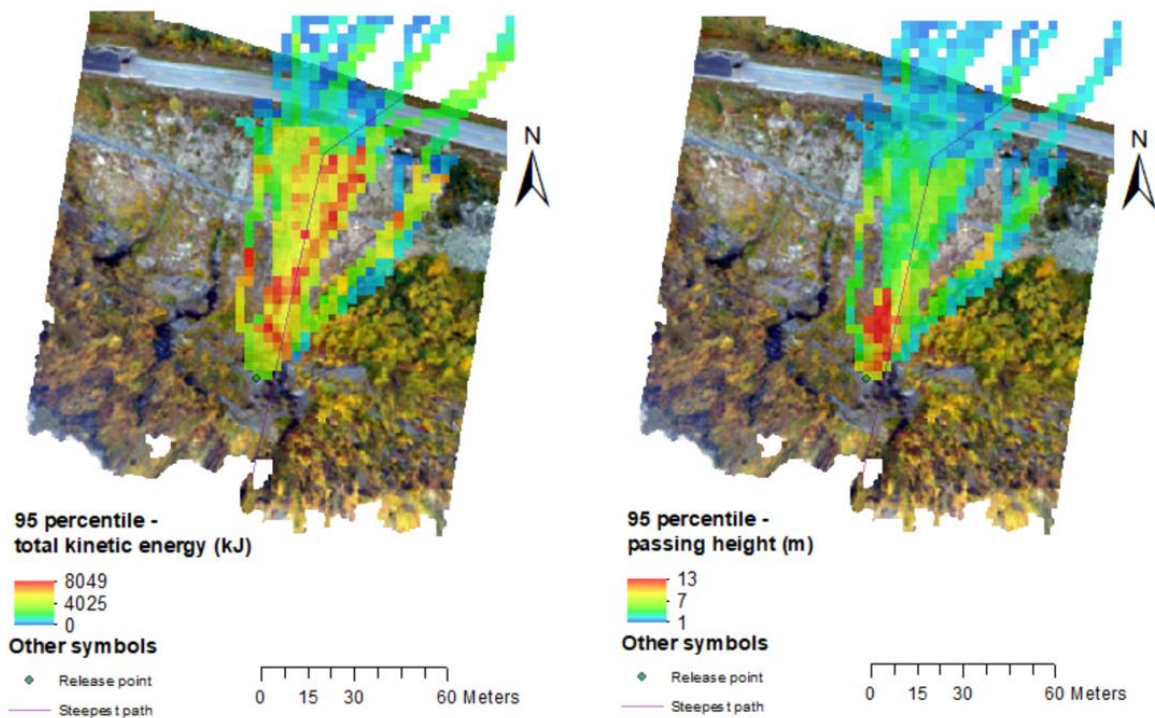


Figure 70: Output total kinetic energy (left) and bounce height (right) for simulation.

*Terrestrial survey model - 10cm resolution (0.1T)*

Results from this simulation are presented in figure 71. Trajectories remains confined to steepest path, deviation from it appear to result in settling. Total kinetic energy ranges from 0 to 7033 kJ, passing heights ranges from 4 to 12 m. Highest values for passing height are calculated near cliff face. Total kinetic energy remains fairly constant throughout run out (although effectively lowered near ditch above road) but passing heights decrease immediately after reaching talus. Both kinetic energy and passing heights remains somewhat elevated along steepest path profile.

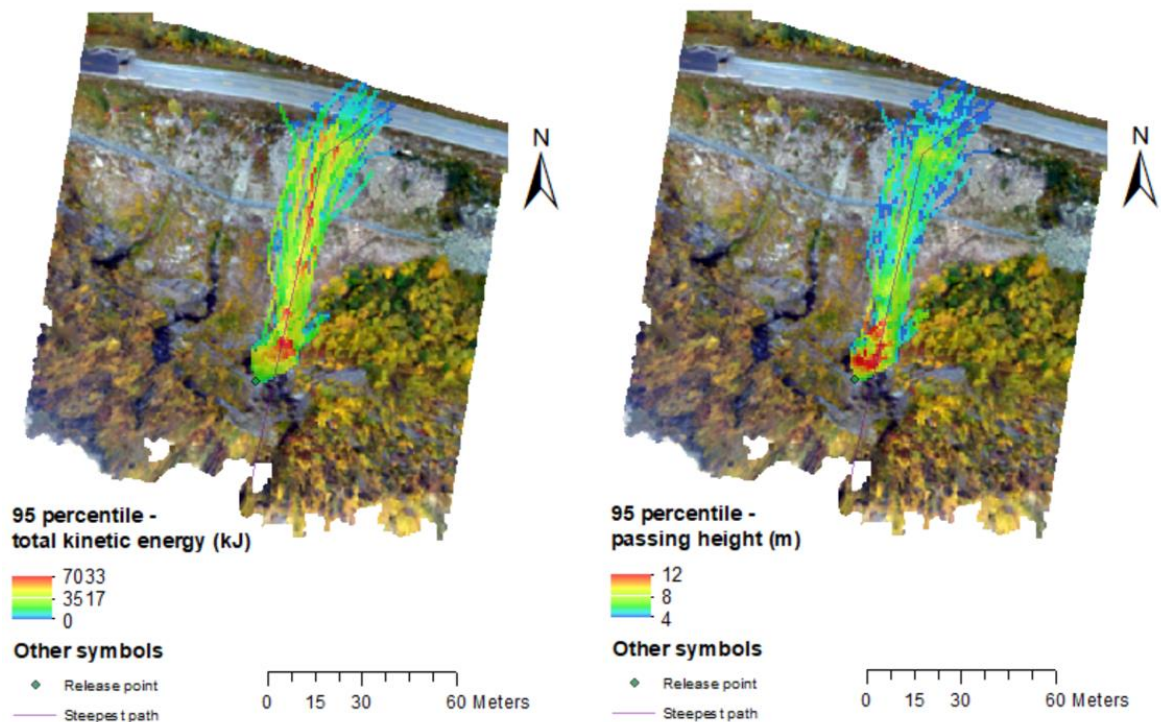


Figure 71: Output total kinetic energy (left) and bounce height (right) for simulation.

*Aerial survey model - 10m resolution (10A)*

Results from this simulation are presented in figure 72. Trajectory spread increase downslope but remain concentric around steepest path. Total kinetic energy ranges from 16 to 8757 kJ, passing height ranges from 1 to 9 m. Highest values for total kinetic energy are calculated along talus slope in eastern sections of trajectory spread. Highest passing height is calculated just below cliff and below road.

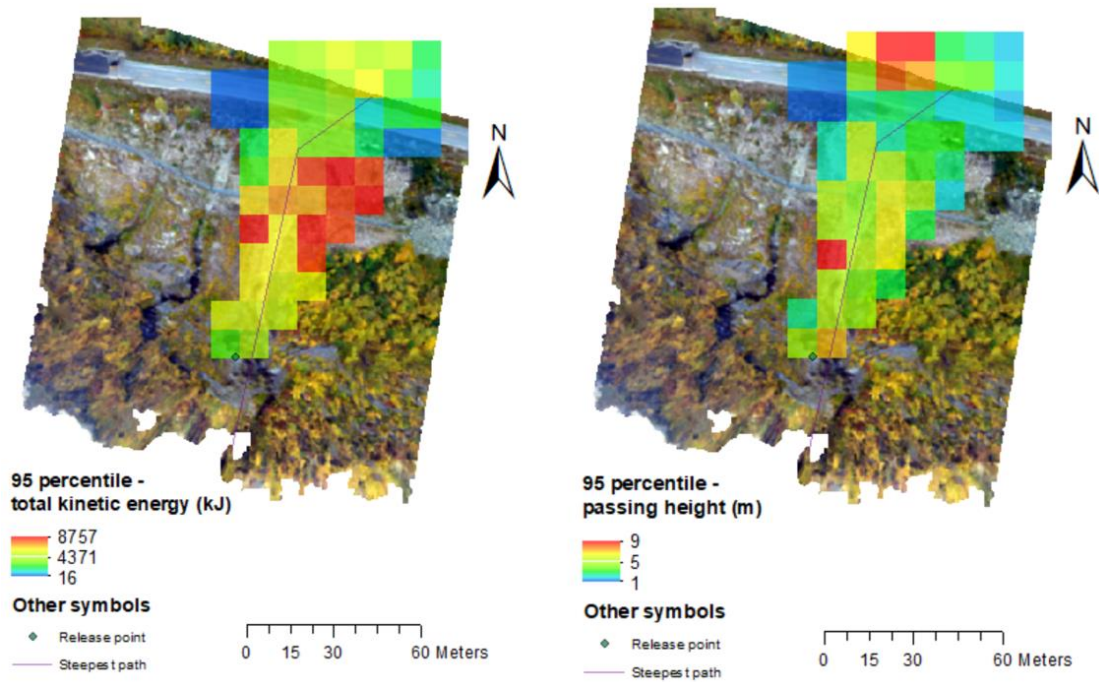


Figure 72: Output total kinetic energy (left) and bounce height (right) for simulation.

**Summary**

Select summarizing statistic for Rakkenes Central 3D rockfall simulations output total kinetic energy and passing height are presented in table 19 and table 20 respectively.

Table 19: Rakkenes Central 3D rockfall simulations output total kinetic energy summarizing statistics.

	1T	1A	3T	3A	0.1T	10A
Mean (kJ)	2420.6	2132.9	2873.5	1984.5	1381.3	2455.9
95 percentile maximum (kJ)	8342.5	9474.7	9240.9	8049.3	7033.7	8757.0

Table 20: Rakkenes Central 3D rockfall simulations output passing height summarizing statistics.

	1T	1A	3T	3A	0.1T	10A
Mean (m)	3.91	2.57	3.01	2.47	2.82	2.30
95 percentile maximum (m)	14.14	14.12	13.67	13.09	12.81	9.39

### 5.3.1.5 Rakkenes East

Simulation results are presented in figure 73 and figure 74. It shows energetic trajectories that settle mostly in talus near field observed settling locations. Most have velocities parallel to slope normal but some low energy boulders roll into settling location from the east.

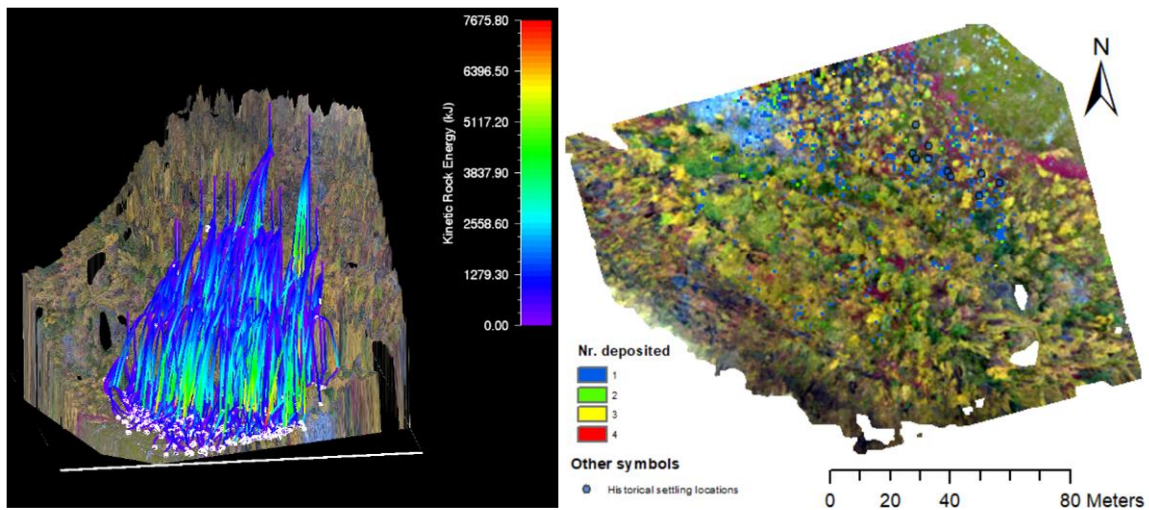


Figure 73: Trajectories and total kinetic energy (left) and simulation settling locations (right).

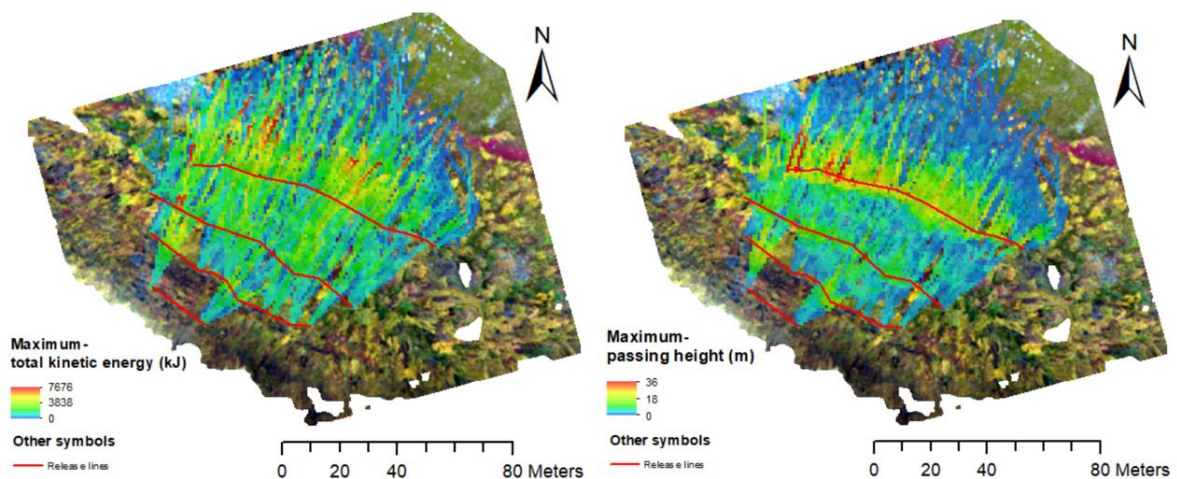


Figure 74: Output total kinetic energy (left) and passing height (right) from simulation.

### 5.3.2 Rocfall 6.0 simulations

#### 5.3.2.1 Aunfjellet

##### *Terrestrial survey model - 1m resolution (1T)*

Results from this simulation are presented in figure 75. Total kinetic energies ranges from under 50 kJ to almost 300 kJ. Passing height values ranges from about 1 to up to nearly 7 m. Total kinetic energy and jump heights remain fairly constant downslope although distinctly increased just upslope of road. A mid-slope decrease in total kinetic energy can also be observed. Overall passing heights are just in excess of a meter, suggesting a primarily rolling or sliding motion.

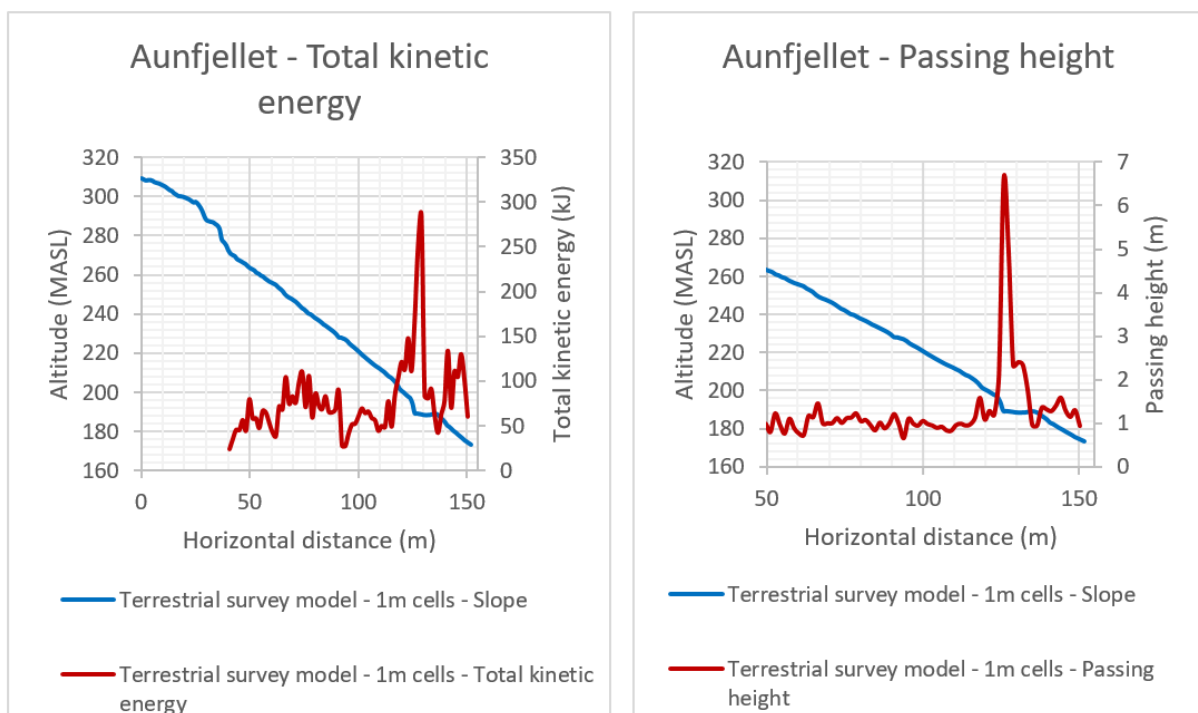


Figure 75: Output total kinetic energy (left) and bounce height (right) for simulation.

##### *Aerial survey model - 1m resolution (1A)*

Results from this simulation are presented in figure 76. Total kinetic energies ranges from under 50 kJ to almost 350 kJ. Passing height values ranges from about 1 m to up to slightly above 5 m. Total kinetic energy and passing heights remain fairly constant throughout run out although distinctly increased just upslope of road. A mid-slope decrease in total kinetic energy and passing height can also be observed. Overall passing heights are just in excess of a meter, suggesting a primarily rolling or sliding motion.

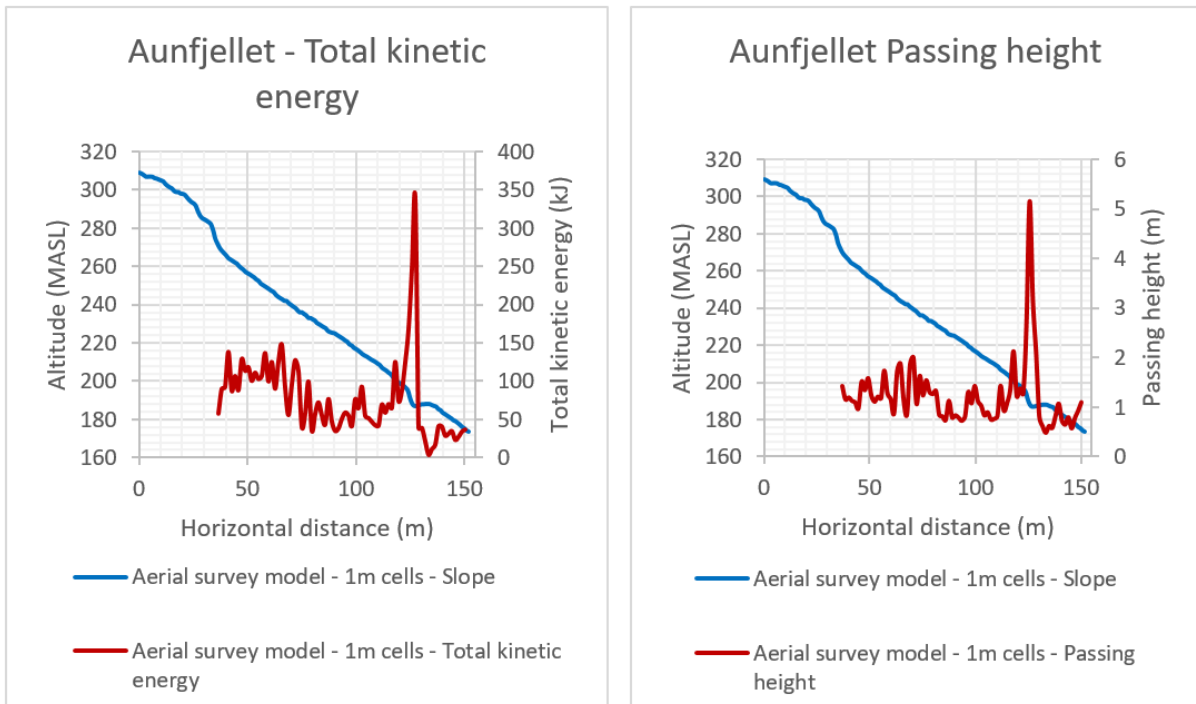


Figure 76: Output total kinetic energy (left) and bounce height (right) for simulation.

**Terrestrial survey model - 10cm resolution (0.1T)**

Results from this simulation are presented in figure 77. Total kinetic energies ranges from about 160 kJ to almost 1400 kJ. Passing height values ranges from about a meter to up to nearly 18 meters. Total kinetic energy and passing heights increase progressively downslope and peaks can be seen just above road. A drastic increase in passing height can also be seen just below a sub-horizontal slope section mid-slope. Passing height values quickly increase to values of up to 4 meters, indicating that boulders are primarily bouncing downslope.

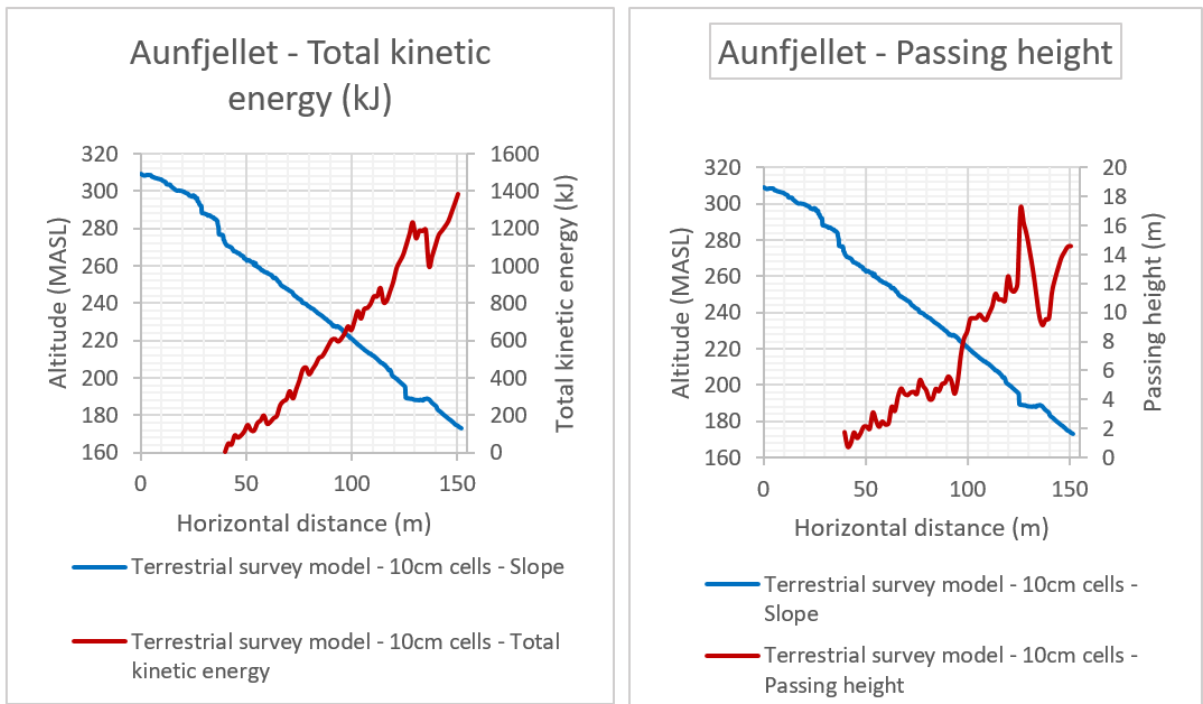


Figure 77: Output total kinetic energy (left) and bounce height (right) for simulation.

**Aerial survey model - 10m resolution (10A)**

Results from this simulation are presented in figure 78. Total kinetic energy varies rapidly between 0 to about 60 kJ. Passing heights are overall low, under a meter.

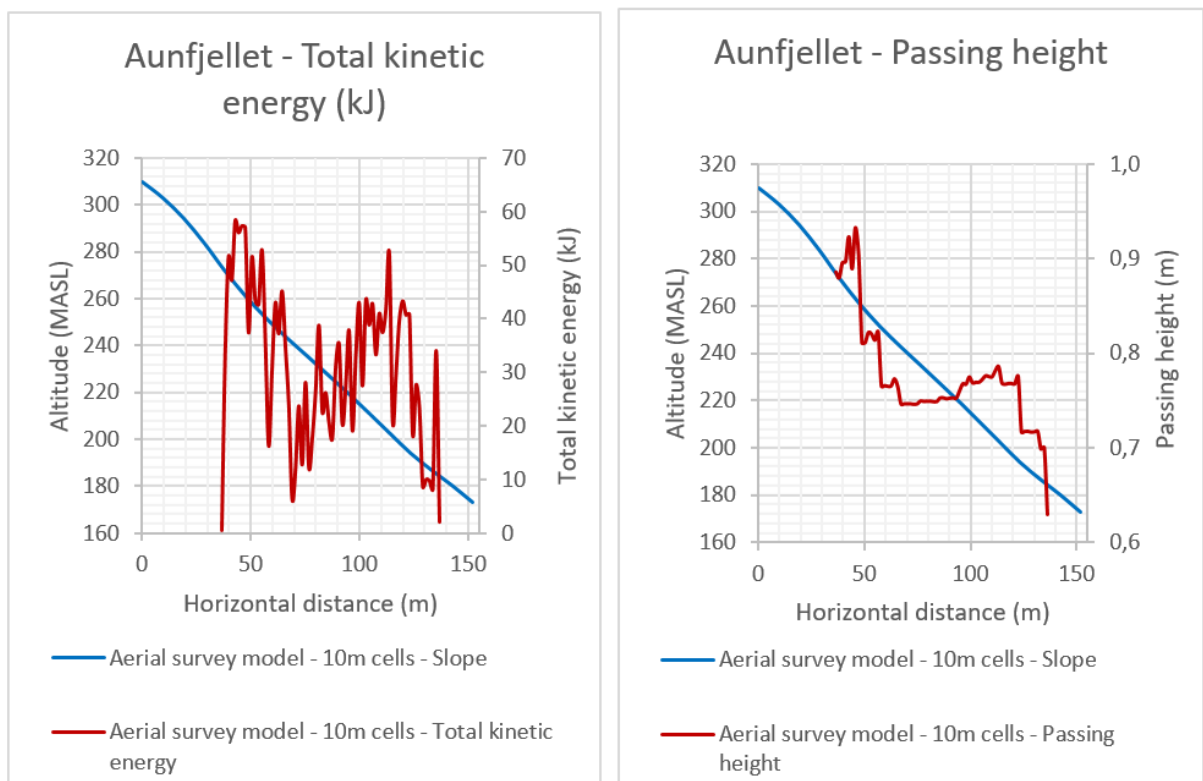


Figure 78: Output total kinetic energy (left) and bounce height (right) for simulation.

### *Summary*

Select summarizing statistic for Aunfjellet 2D rockfall simulations output total kinetic energy and passing height are presented in table 21 and table 22 respectively.

*Table 21: Aunfjellet 2D rockfall simulations output total kinetic energy summarizing statistics.*

	1T	1A	0.1T	10A
Mean (kJ)	47.0	46.9	317.5	8.4
95 percentile maximum (kJ)	285.1	339.0	1382.9	58.3

*Table 22: Aunfjellet 2D rockfall simulations output passing height summarizing statistics.*

	1T	1A	0.1T	10A
Mean (m)	0.99	0.93	3.42	0.73
95 percentile maximum (m)	6.61	5.15	17.19	0.93

### **5.3.2.2 Revsnestinden**

#### *Aerial survey model 10m resolution (10A)*

Results from this simulation are presented in figure 79. Total kinetic energies ranges from about 500 kJ to over 2000 kJ. Total kinetic energy and jump heights initially increase gradually downslope, primarily in two iterations separated by an area of fairly constant kinetic energy. Kinetic energy then decreases downslope before a peak can be observed corresponding to a steep profile section. Passing heights are negligible, suggesting a primarily rolling or sliding motion. Select summarizing statistics for the output are provided in table 23 and table 24.

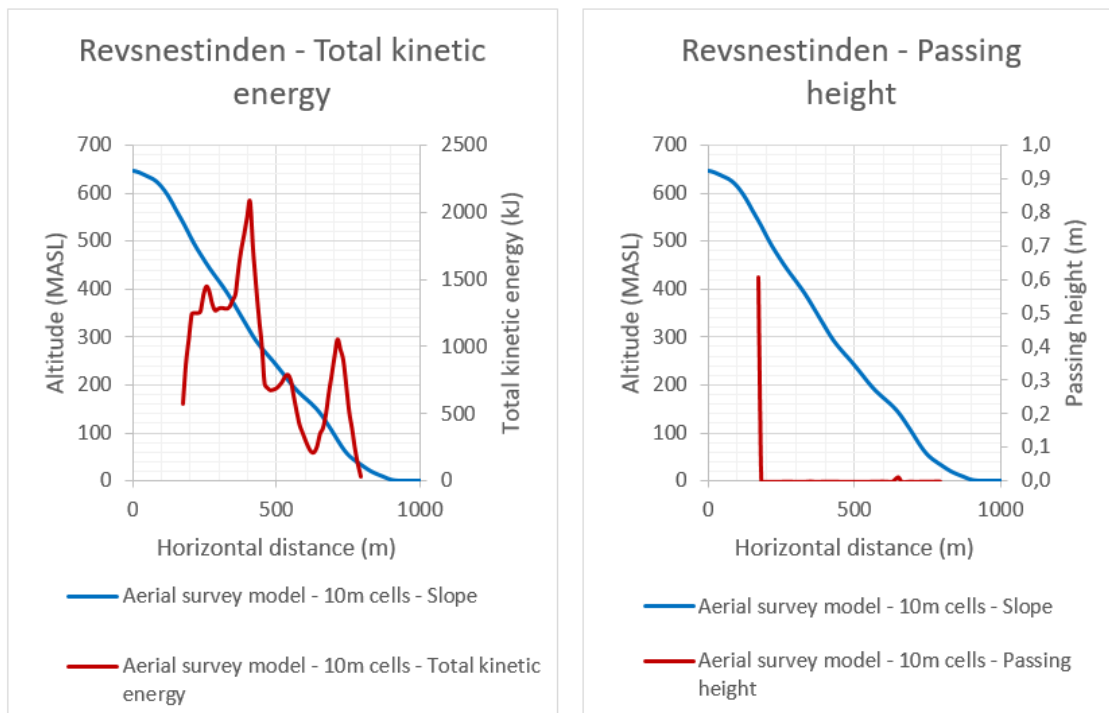


Figure 79: Revsnestinden 2D rockfall simulation output total kinetic energy (left) and passing height (right)

Table 23: Revsnestinden 2D rockfall simulations output total kinetic energy summarizing statistics.

Mean (kJ)	837.3
95 percentile maximum (kJ)	2077.9

Table 24: Revsnestinden 2D rockfall simulations output passing height summarizing statistics.

Mean (m)	0.00
95 percentile maximum (m)	0.61

### 5.3.2.3 Rakkenes West

#### *Terrestrial survey model - 1m resolution (1T)*

Results from this simulation are presented in figure 80. Total kinetic energies ranges from about 500 kJ to about 2000 kJ. The highest calculated passing height is slightly below 23 m. Total kinetic energy and jump heights initially increase gradually downslope, primarily in two iterations separated by an mid-slope section of decreasing total kinetic energy and passing height corresponding to a gentle section of the slope. The second increase in total kinetic energy and passing height terminates in a peak value for both that can be observed just above the road followed by a swift decrease where the road encountered.

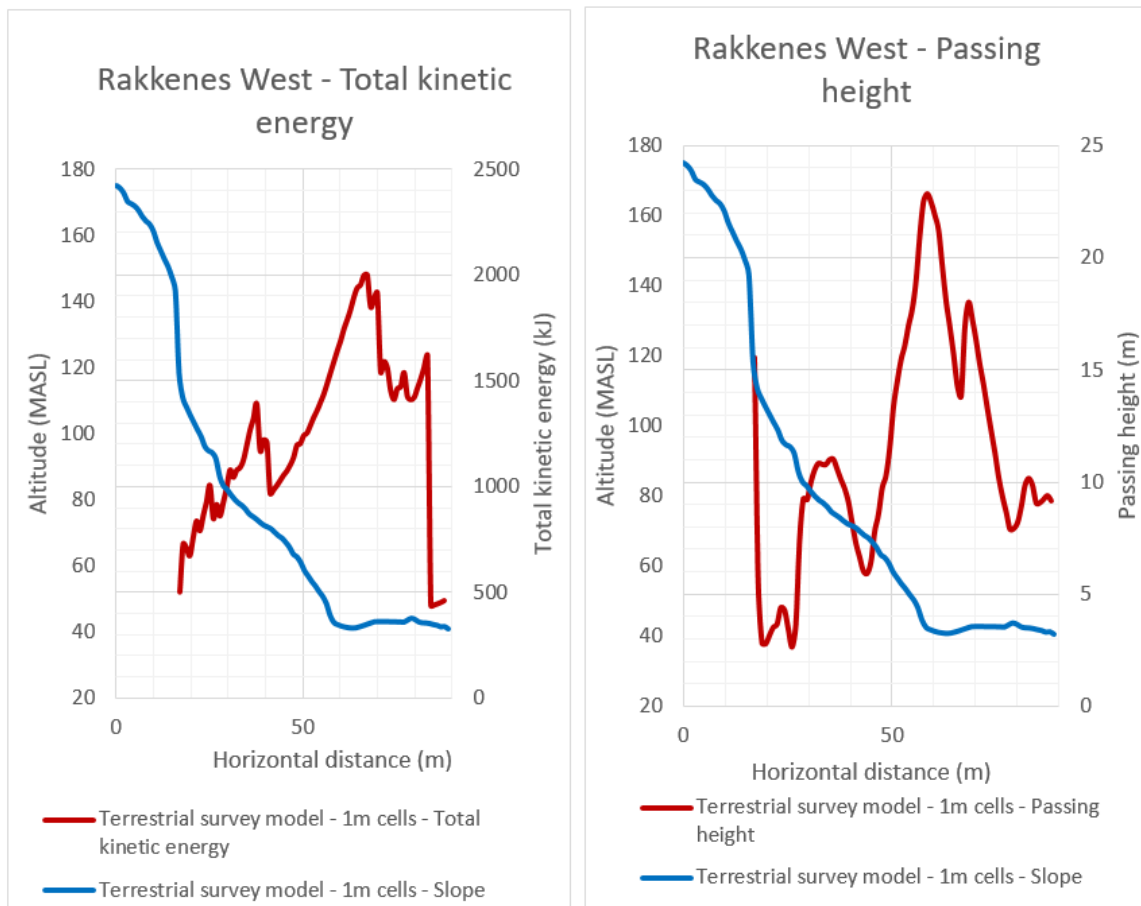


Figure 80: Output total kinetic energy (left) and bounce height (right) for simulation.

**Aerial survey model - 1m resolution (1A)**

Results from this simulation are presented in figure 81. Total kinetic energies ranges from about 300 kJ to slightly 2000 kJ. The highest calculated passing height is slightly above 20 m. Total kinetic energy and jump heights initially increase gradually downslope, primarily in two iterations separated by a mid-slope section of decreasing total kinetic energy and passing height corresponding to a gentle section of the slope. The second increase in total kinetic energy and passing height terminates in a peak value for both that can be observed just above the road followed by a swift where the road is encountered.

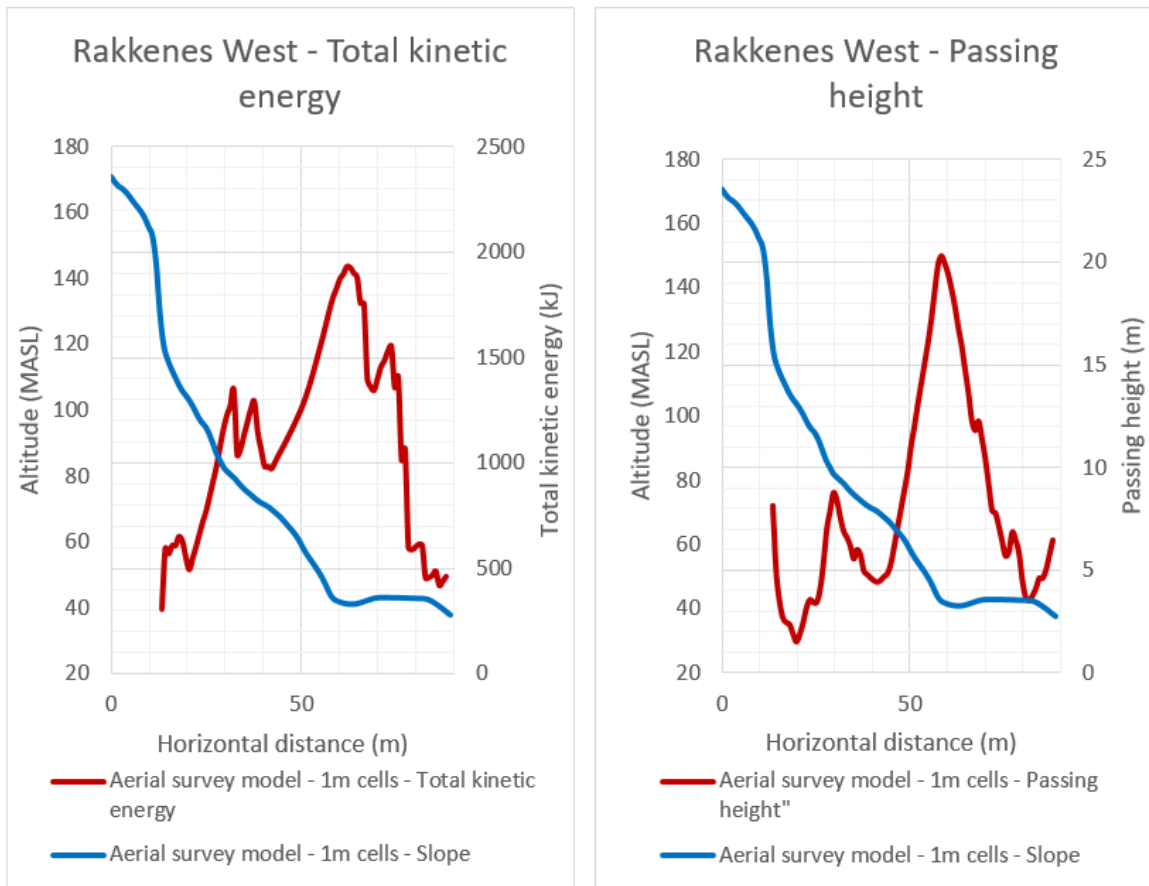


Figure 81: Output total kinetic energy (left) and bounce height (right) from simulation.

### ***Terrestrial survey model - 10cm resolution***

Results from this simulation is presented in figure 82. Total kinetic energies ranges from below 400 kJ to almost 1900 kJ. The highest calculated passing height is about 23 m. Total kinetic energy and jump heights initially increase to two similar peak values separated by a mid-slope section of decreasing total kinetic energy and passing height corresponding to a gentle section of the slope. The second increase in total kinetic energy and passing height terminates with a swift decrease in both parameter values where the road is situated.

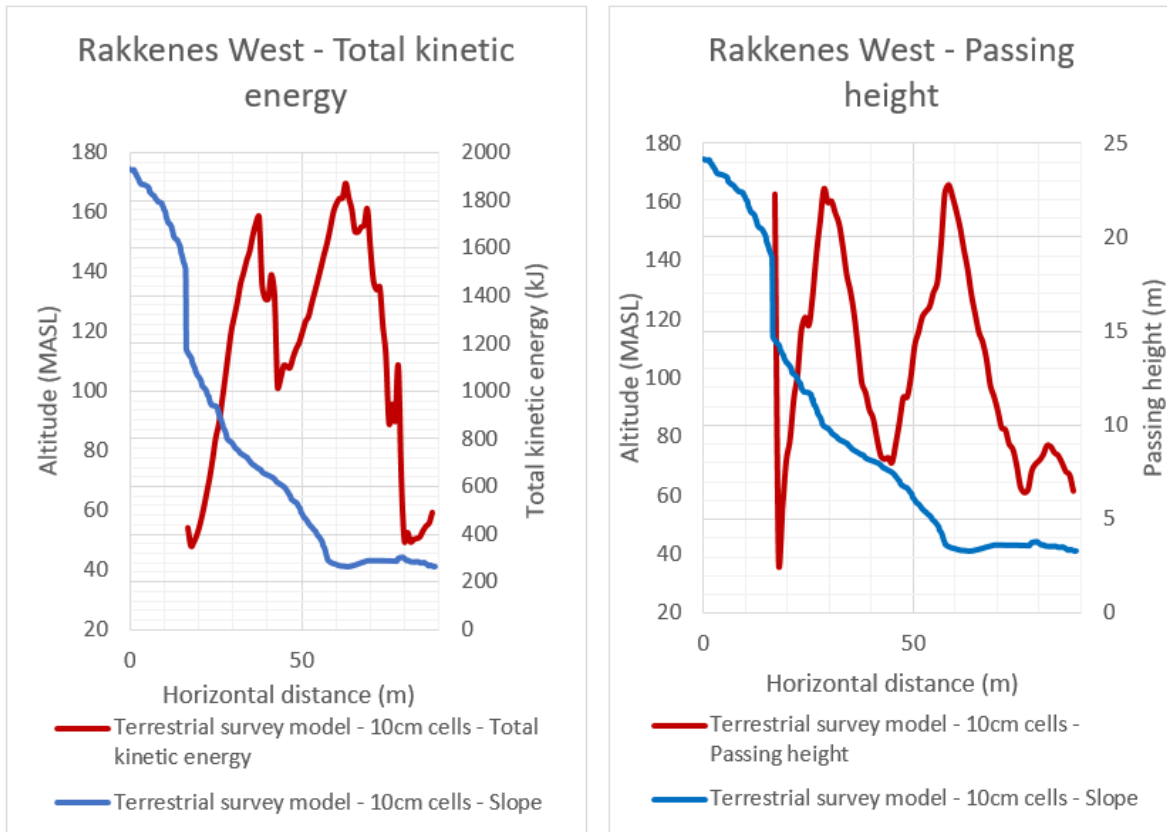


Figure 82: Output total kinetic energy (left) and bounce height (right) from simulation.

**Aerial survey model - 10m resolution**

Results from this simulation are presented in figure 83. The total kinetic energy has a quite simple evolution of gradual increase downslope before reaching a peak value just above road. Values subsequently remain constant around about 2000 kJ for about 15 m before swiftly decreasing when reaching the road. Passing height values also increase downslope but fluctuates around 7 m mid-slope before increasing to peak value of 11.66 m.

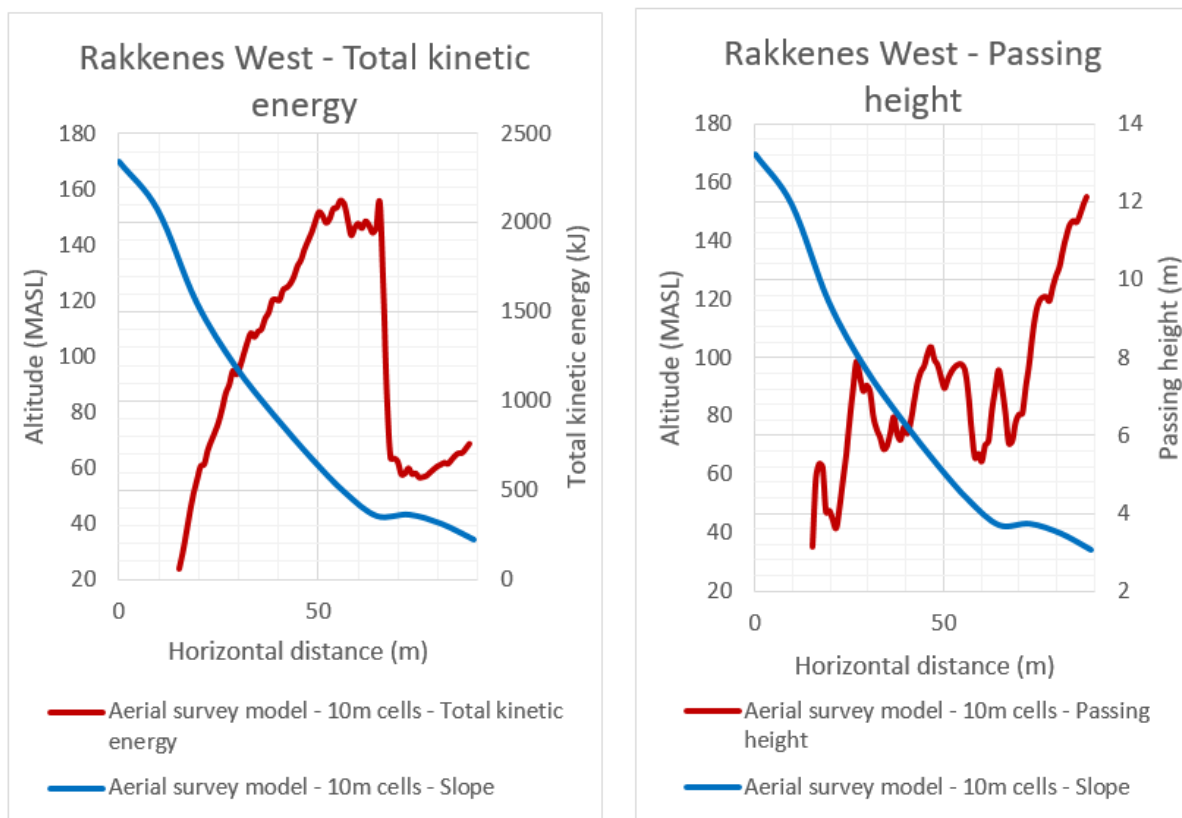


Figure 83: Output total kinetic energy (left) and bounce height (right) from simulation.

### Summary

Select summarizing statistic for Rakkenes West 2D rockfall simulations output total kinetic energy and passing height are presented in table 25 and table 26 respectively.

Table 25: Rakkenes West 2D rockfall simulations output total kinetic energy summarizing statistics.

	1T	1A	0.1T	10A
Mean (kJ)	749.2	619.6	587.7	541.6
95 percentile maximum (kJ)	2002.5	1927.4	1870.7	2128.4

Table 26: Rakkenes West 2D rockfall simulations output passing height summarizing statistics.

	1T	1A	0.1T	10A
Mean (m)	5.57	3.74	6.23	2.90
95 percentile maximum (m)	22.83	20.32	22.76	11.66

### 5.3.2.4 Rakkenes Central

#### *Terrestrial survey model - 1m resolution (1T)*

Results from this simulation is presented in figure 84. The total kinetic energy swiftly increase downslope over the course of the first 10 meters. The parameter values subsequently increase to a peak value of nearly 6000 kJ for the next 40 m. Total kinetic energy then decrease to values as low as almost 100 kJ before a last final increase. Passing heights have similar evolution but peaks earlier and decrease in value more swiftly after peak. The boulders appear to have a bouncing motion for the majority of the run out. Maximum calculated passing height is nearly 5 meters.

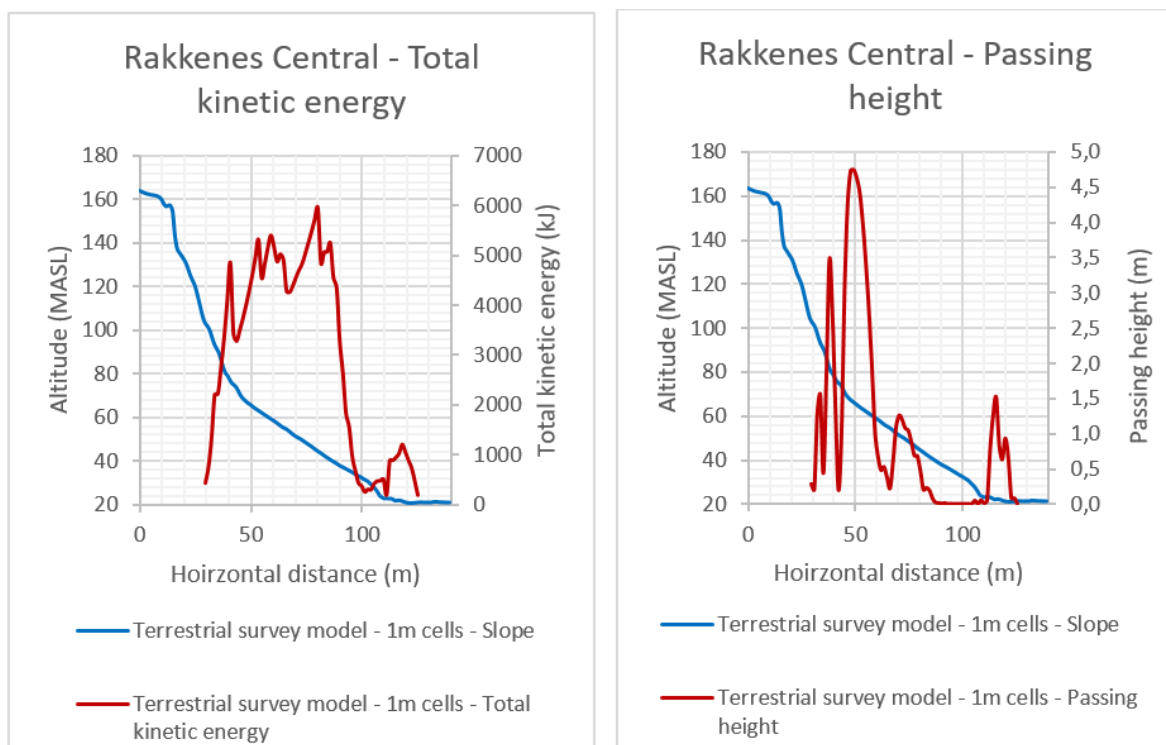


Figure 84: Output total kinetic energy (left) and bounce height (right) from simulation.

#### *Aerial survey model - 1m resolution (1A)*

Results from this simulation are presented in figure 85. The total kinetic energy swiftly increase downslope over the course of about 20 m to a peak value of about 4000 kJ. Values subsequently fluctuates around 3500 kJ for the next 30 m before rapidly decreasing to 200-300 kJ for the remainder of the trajectories. Passing heights have similar evolution but peaks earlier to about two and half meters and decrease in value more swiftly after peak. The last 30 m of run out shows negligible passing height, and a rolling or sliding motion can be inferred.

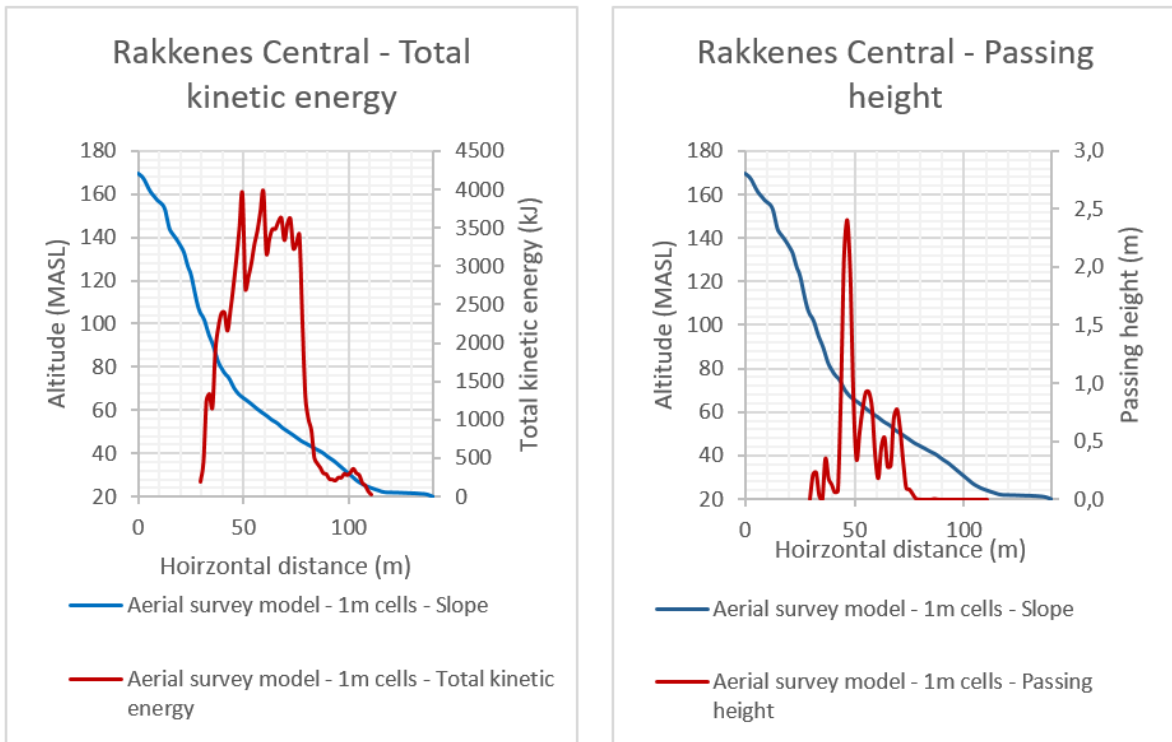


Figure 85: Output total kinetic energy (left) and bounce height (right) from simulation.

**Terrestrial survey model -10cm resolution (0.1T)**

Results from this simulation are presented in figure 86. The total kinetic energy increase downslope to a peak value of about 9000 kJ mid-slope. After peak total kinetic energy remains fairly constant around 5500 kJ for about 40 m before decreasing rapidly near road. Passing heights have nearly identical evolution although peak values are shifted about 30 m upslope. Passing height values remained elevated throughout slope indicating a primarily bouncing motion. Maximum passing height is over 12 m.

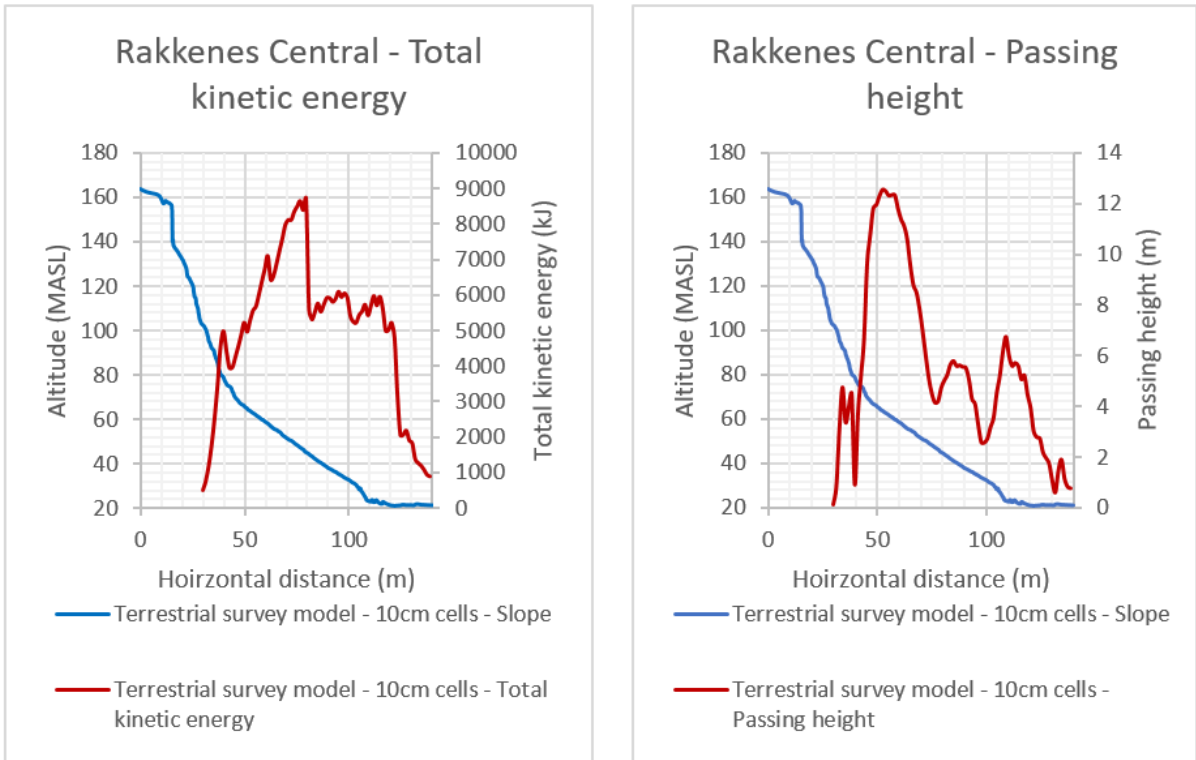


Figure 86: Output total kinetic energy (left) and bounce height (right) from simulation.

**Aerial survey model - 10m resolution (10A)**

Results from this simulation is presented in figure 87. The total kinetic energy increase downslope to a peak value of about 3000 kJ in the first 10 m. After peak total kinetic energy is reduced gradually over the next 120 m to about half this value. It then approaches close to zero value the last 10 m. Maximum passing height is under half a meter and occurs early in run out, the boulders appear to mostly roll or slide downslope.

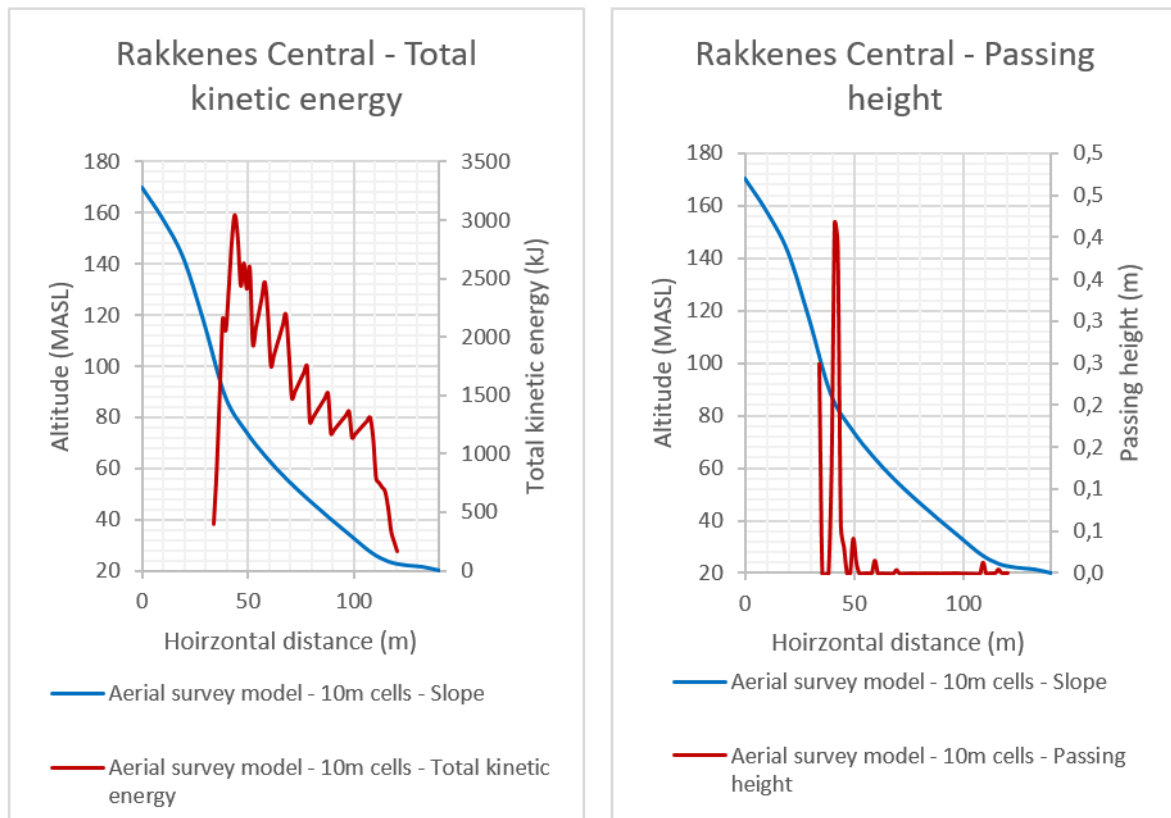


Figure 87: Output total kinetic energy (left) and bounce height (right) from simulation.

### Summary

Select summarizing statistic for Rakkenes Central 2D rockfall simulations output total kinetic energy and passing height are presented in table 27 and table 28 respectively.

Table 27: Rakkenes Central 2D rockfall simulations output total kinetic energy summarizing statistics.

	1T	1A	0.1T	10A
Mean (kJ)	2010.3	937.2	3160.3	1310.2
95 percentile maximum (kJ)	5949.0	3967.2	8697.3	3046.5

Table 28: Rakkenes Central 2D rockfall simulations output passing height summarizing statistics.

	1T	1A	0.1T	10A
Mean (m)	0.51	0.14	2.87	0.01
95 percentile maximum (m)	4.74	2.41	12.54	0.42

## 6 Summary and discussion

### 6.1 Resolution control on output

It should be noted that the material parameters are rarely kept equal across resolutions, in order to calibrate parameters to real world results. Any difference is therefore not solely due to the resolution itself. The output values are the output values congruent with a realistic run out distance. It should also be stressed that Aunfjellet back calculations using 10 cm and 10 m resolution models were largely unsuccessful and realistic run out was not achieved (exaggerated run out distance). Passing height and bounce height will be used synonymously in the text. This based on the assumption that difference in passing height (vertical distance to surface) chiefly to owe to difference in bounce heights (restitution direction away from slope).

#### *3D*

See figure 88 for overview of 3D simulation output. Bounce height values seem proportional to resolution. Higher resolution values usually result in higher passing height values. No deviation from this trend was observed in 3D simulations except when using the 10 cm resolution model in Rakkenes Central, where many boulders settled prematurely. The effect of resolution on bounce height is most apparent on Aunfjellet and Rakkenes West and only small deviations are seen on Rakkenes Central. The increased bounce height seem to stem from more effective trajectory deflection accompanying added surface detail. The Rakkenes Central talus cone largely consists of fine grained material and has a mostly smooth surface, so output was quite similar across resolutions on this case. On Aunfjellet added resolution adds much more detailed features that are anything from rocks, vegetations tree stumps etc. Simulations on this case area is therefore much more sensitive to resolution input. This show that the effect of high resolution elevation input is much more potent for detailed surfaces, particularly those that are gentle enough that surface contact is ample. In Rakkenes West the slope is so steep that boulder surface contact was minimal and the added detail therefore did little to deaccelerate boulders but rather acted as gentle surfaces on which more horizontally directed impact restitutions could take place.

Lower resolutions generally produced increased run out using the same material parameters as for higher relative resolutions. Additionally, trajectories are often more confined to steepest path and less spread out laterally when lower resolutions are used, effectively producing results more similar to 2D modelling. A similar result was obtained by (Agliardi and Crosta, 2003).

This is particularly apparent on Aunfjellet where trajectories on the 10 m resolution surface was effectively constrained to the steepest path. The increased run out and less spread out trajectories with lower resolutions are likely due to the removal of features that promotes high angle collisions that deaccelerate and/or deflect the boulder. Since the boulders are randomly varied in angle upon release, it follows that every subsequent collision results in an outrun that is more dissimilar to another. However, if the surface on which collision takes place is more similar, as is the case when using low resolution digital elevation models, this effect could be suppressed.

While 10 cm resolution models calculates the highest bounce height and total kinetic energy values, several issues with such high resolution was encountered during back calculation. Equal friction/restitution coefficients resulted in both extreme run out and arbitrary settling locations in even steep slope sections. As previously mentioned this effect was particularly debilitating on the rough terrain of Aunfjellet where a good back calculation could not be executed due to either exaggerated or underestimated run out distances with only minor variations in material input. For Aunfjellet many of these features were moss, tree stumps, small rock clasts and other substrates whose effect are already considered in RAMMS:Rockfall impact calculations (drag,  $\kappa$  and  $\beta$  coefficient). On the steep Rakkenes West this high resolution was unproblematic due to decreased surface contact. Here, the added detail may additionally be warranted due to added features being solid rock and perfectly capable of deflecting boulder trajectories. It follows that gentle slopes with much surface detail are particularly ill-fit for simulations with ultra-high (<1 m) resolution. Particularly if one can argue that the added detail, in fact, proves little actual obstacle for large falling boulders.

1 m and 3 m resolution model were generally assigned similar material properties for successful back calculation. The smoother surface of the latter always resulted in reduced output passing height, while kinetic energies were not noteworthyly changed between the two resolutions. They did well to show important terrain features such as road cuts, steep slopes and performed overall well.

Simulations using 10 m resolution models always output the lowest bounce height, but output kinetic energy was similar to simulations using other DEMs. Friction and restitution generally needed to be adjusted as to halt boulders in realistic settling positions when this resolution was applied. It would seem the removal of surface details allow further run out with literature material input.

The lowered bounce height is likely partly caused by the added friction/drag but also the non-existent slope angle variation that would otherwise deflect boulder trajectories. In other words, using a 10m resolution digital elevation model is problematic when accurate bounce heights must be calculated. It should be clear that such low resolutions cannot be used when it obscures important terrain features. On Aunfjellet the subhorizontal road section was not explicit in the 10 m resolution DEM and a realistic simulation could not be executed. On Rakkenes West this low resolution caused the interpolation of surfaces much gentler than what was observed and bounce heights were severely underestimated. Otherwise such low resolution arguably makes for a good, coarse run out and kinetic energy estimate on relatively smooth surfaces.

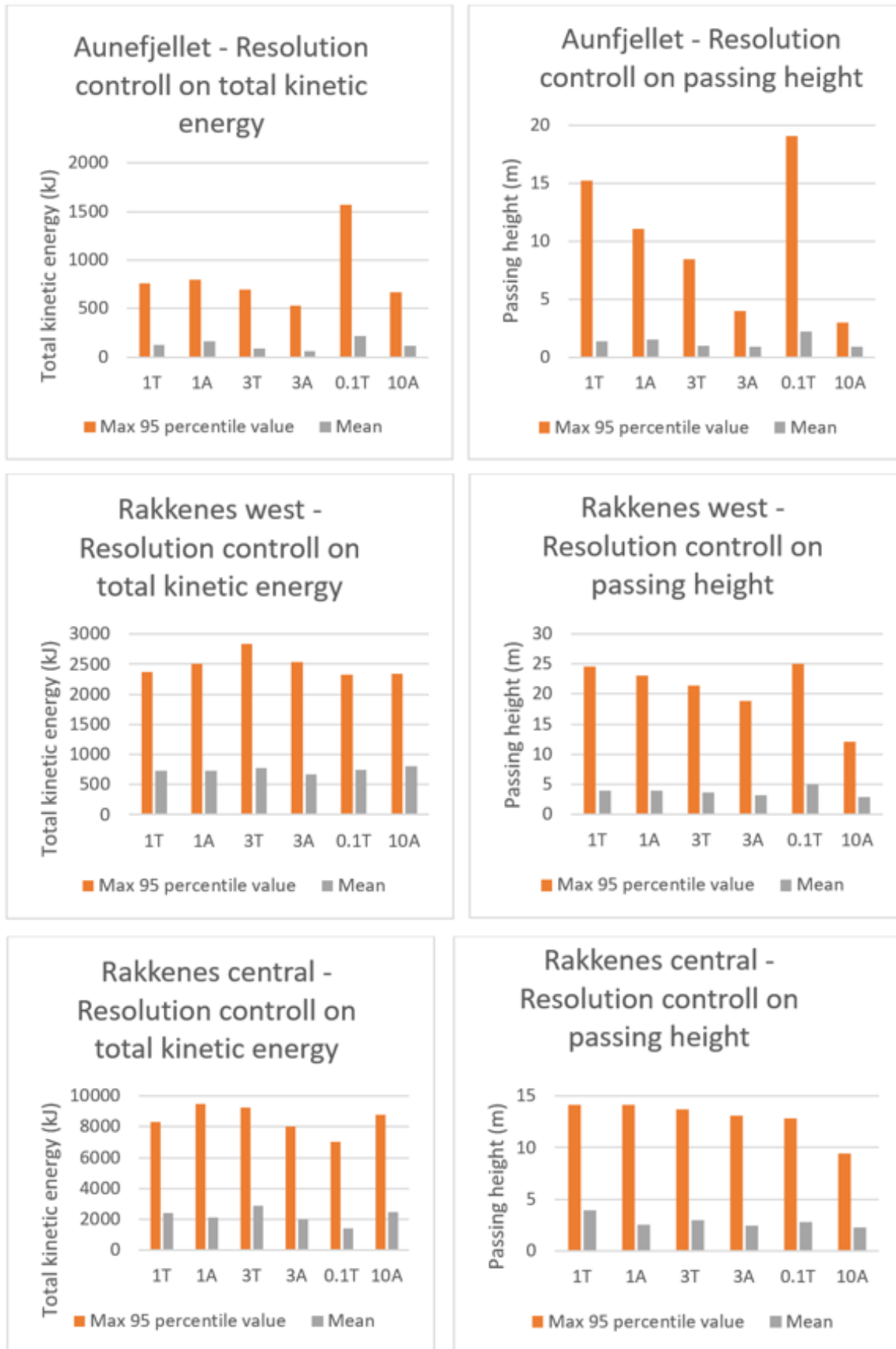


Figure 88: Summarizing statistics for all 3D rockfall simulations except the Revsnestinden simulation (only one resolution was used here).

## 2D

See figure 89 for overview of 2D simulation output. In 2D simulations the trend of increasing bounce heights and total kinetic energy with decreasing resolution is even more clear. 10 cm resolution models have by far the highest bounce height values throughout the slope. On the other end 10 m resolution generally show the lowest passing heights and total kinetic energy. This trend is particularly apparent on Rakkenes Central and Aunfjellet, but not very striking at Rakkenes West where output values across resolutions are largely similar. The difference between output across resolutions stands out on Aunfjellet. Here, total kinetic energies and passing heights increase much more explicitly when using high resolution elevation data. However, a accurate back calculation was not achieved with 10 m and 10 cm resolution slopes, which should be kept in mind. It still illustrates the erratic run outs associated with ultra-high resolution which was also observed in several 3D simulations. The only clear deviation from higher total kinetic energy and bounce height with higher resolution can be seen at Rakkenes West. Here the 10 m resolution model had the highest maximum total kinetic energy, however still the lowest bounce heights. The line interpolated between the spaced vertices is considerably gentler than when higher resolution is applied. This cause less high angle collisions with road that impairs kinetic energy, but also less minor slope angle deviations that would act to deflect boulder trajectories and cause elevated passing heights. That higher total kinetic energy is often seen congruent with higher bounce height could be rooted in causality. Less contact with substrate means less impairing of velocity (material coefficient of restitution is never set to 1, so collisions will never be entirely elastic), and a relation between the two is expected.



Figure 89: Summarizing statistics from all 2D simulations. Each row show results from a individual case area. Graphs are, from leftmost to rightmost column; ,max total kinetic energy as function of horizontal position, max passing height as function of horizontal position, summarizing statistics for total kinetic energy and summarizing statistics for passing height.

## 6.2 Remote sensing technique effect on output

### 3D

Steep sections of the terrestrial survey models (produced with photogrammetry) are consistently steeper than in the aerial survey model (see figure 53). Inaccuracies with LIDAR survey pertaining to parallel incident angles of laser beams and enhanced error with steeper slopes were touched on by (Jaboyedoff et al., 2012) and (Hodgson and Bresnahan, 2004) respectively, and one or both of these conditions is likely the cause of the offset. The aerial survey models also appear to have smoother features which could result from LIDAR sampling inaccuracy of about 10 cm as opposed to the local survey photogrammetry's cm scale accuracy. Generally speaking, aerial survey models produce lower output bounce heights and total kinetic energy than do terrestrial survey models in 3D rockfall simulations (see figure 90). Output passing heights are, in fact, without exception lower when applying aerial survey LIDAR derived models. The reason for this appears to be more explicit detail on terrestrial survey models that are more capable of deflecting boulders, and steeper slopes that cause higher vertical distances to surface during bounces. The difference between the models particularly sway bounce height output on Aunfjellet where a around 4 m difference can be observed. In Rakkenes West a subtler 1-2 m can be observed. One can appreciate the importance this difference might have if one were to construct a catching fence based on this output. As far as kinetic energy is concerned difference is very subtle, difference never exceeding about 500 kJ and mean values being largely similar.

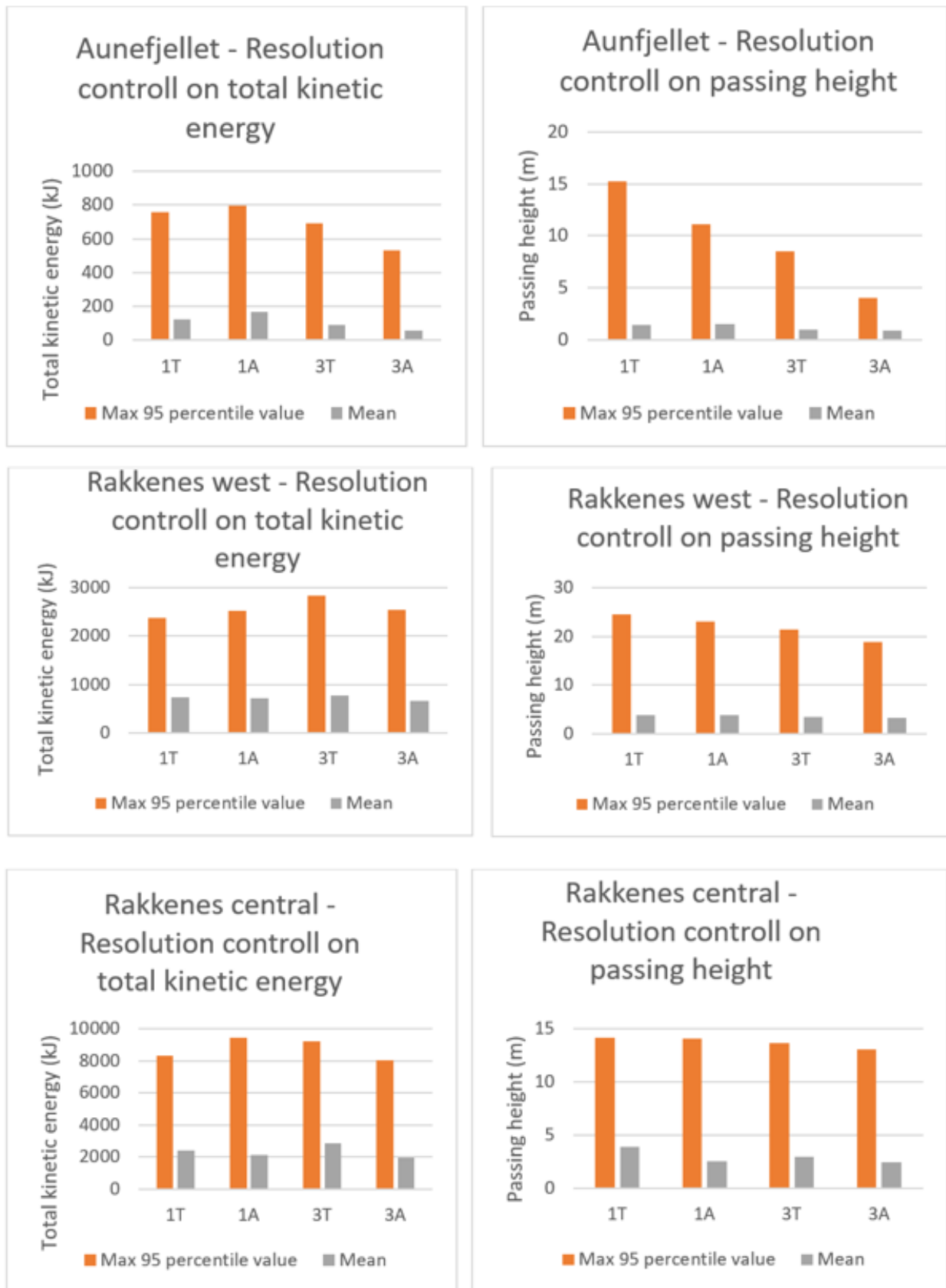


Figure 90: Summarizing statistics from all 3D simulations except the Revnestinden simulation where only LIDAR data was used. Each row show results from an individual case area. Graphs are, from leftmost to rightmost column; summarizing statistics for total kinetic energy and summarizing statistic for passing height.

## *2D*

Passing heights are consistently lower for 2D simulations where the slope is derived from an aerial survey model, as was the case for the 3D simulations (see figure 91). Bounce heights may vary as much as 2.5 m when a terrestrial remote sensing technique is used over aerial equivalents. Total kinetic energy output is also lower for all simulations when aerial survey models are used, although the difference is usually subtle.

By far the greatest difference between the two outputs was observed on Rakkenes Central where mean and max total kinetic energy is about 1000 and 2000 kJ higher respectively for the terrestrial survey model. Max bounce height is also increased about 2 m for the terrestrial survey model, but mean values are similarly low. The reason for this seems to be more explicit detail on the terrestrial survey model, allowing more effective deflection of objects. Also, a steeper slope that causes higher passing height.



Figure 91: Summarizing statistics from all 2D simulations except the Revnestinden simulation. Each row show results from a individual case area. Graphs are, from leftmost to rightmost column; Max total kinetic energy as function of horizontal position, max passing height as function of horizontal position, summarizing statistics for total kinetic energy and summarizing statistics for passing height.

### 6.3 2D vs 3D modelling

2D simulations generally show lower passing energy heights and total kinetic energy values (see figure 92). The largest differences can be seen on simulations on gentle taluses like Revsnestinden and Rakknes Central. It is not as striking on steep rock slopes where 2D and 3D simulation output are more similar. This steep (90-70 °) landform has so far been the most versatile in terms of resolution, sampling technique and simulation mode.

The simulations have shown that where rolling motions is observed in 2D simulations, 3D simulation will often return bouncing motions. For example, on Revsnestinden total kinetic energy and passing height is severely lowered in 2D simulations relative to 3D. A over 1000 kJ difference in mean kinetic energy and a about 8000 kJ difference in max kinetic energy can be observed. Mean passing height is increased from 0 to about 4 m when applying 3D software and maximum bounce height is over 30m higher in 3D simulations (relative to under a meter in 2D simulations). In Rakkenes central extreme differences are again seen with up to 5000 kJ kinetic energy value difference being observed on 1A models (1 m resolution aerial survey model). The difference in maximum bounce height is at least 8 meters and up to over 10 m. It follows that gentle talus slopes are very sensitive landforms in terms of simulation method (2D vs 3D). The reason for this is likely due to the difference in impact configuration. Rocfall calculates impact by using simple restitution coefficients. A sliding/rolling motion will never result in much bouncing on a gentle detail-less slope because slope normal velocity is close to zero and even a elastic collision will cause the boulder to maintain its rolling/sliding motion. The more complex surface interaction of 3D simulation likely gives rise to higher bounce heights. Primarily due to torque and rotation caused by impacts and sliding friction, which in turn can cause (in particular less compact rockforms) to deviate from rolling/sliding motion.

On Rakkenes West 2D and 3D results are more similar, 2D simulations actually returning higher bounce height on 1T. For 10A bounce height is still over 10 m higher for 3D simulations. The decreased sensitivity to input on this landform has been appreciated earlier. Again, the reason is likely that the impact mechanics and impact configuration affect results less due to less boulder-surface contact. Modelling parabolic arcs in freefall is on the other hand not affected by slope geometry or its assigned parameters.

For all locations 10 cm resolution model have higher or just about equal bounce heights and mean kinetic energy in 2D modelling with the sole exception of Rakkenes West where max difference between 2D and 3D output is fairly consistent. It seems that added detail may produce results that are more similar to 3D simulations. The problem with ultra-high resolution is that detail from, for example, vegetation and loose rocks are treated as unrealistic solid surfaces that have no probabilistic value. Using lower resolution (1 m for example) and sampling vertex coordinates from normal distribution will likely cause more variation in restitution angle, higher average bounce heights and results more similar to 3D. This will also account for slope angle uncertainties that undoubtedly is present.

Whilst seemingly unfit for kinetic energy (unless slope is steep) and bounce height estimates 2D has shown no shortcoming in producing a realistic run out with literature values when 1 m resolution height data is used. There has neither been observed large deviation from steepest path, or a concentric pattern around it (cone shape pattern around steepest path) in any of the 3D simulation. Furthermore, steepest path run-outs usually encompass simulation maximum in terms of kinetic energy and bounce height. It follows that cautiously extrapolating a 2D simulation run out distance, where slope is derived from steepest path elevation data, into a cone shape will produce a sound worst case run out estimate if there is no significant lateral variation downslope.

As previously touched on, results become more similar to 2D when lower resolution elevation models are used. Outrun becomes more confined to steepest path when low resolution elevation data is used and there is less reason to use 3D software.

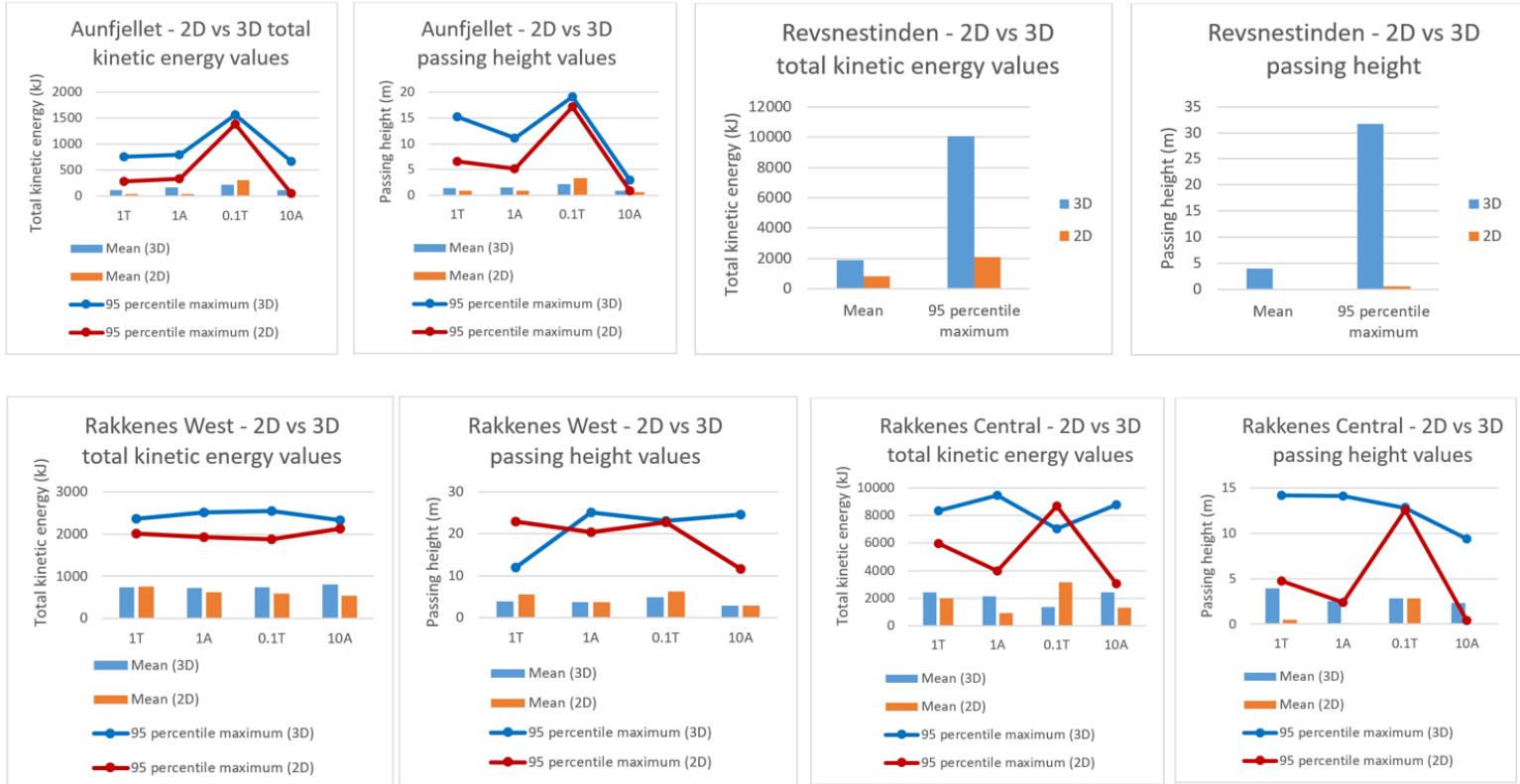


Figure 92: Summarizing statistics from all simulations except those applying a 3 m resolution model (3 m resolution was not tested in 2D simulations).

### 6.4 Rakkenes East mitigation suggestion

Since this is a projected tunnel exit it seems most practical to extend the tunnel portal so far that boulders don't reach the road. Presumably the tunnel will redistribute traffic from Europe Road 6 through Rakkenes. A unit stretch called 1900 EV6 HP26 m4034 – 8619 (a 1 km section of E6 that passes Rakkenes) is traversed by a yearly average of 600 daily (Vegvesenet). According to Norwegian regulations, tunnel type 8.5 should be constructed for this extent of traffic (Vegdirektoratet, 2016). This tunnel design has a 8.5 m wide and 4.6 m tall aperture and its portal is required to deter natural hazards with under 200 year return times (Vegdirektoratet, 2016).

A tunnel portal that corresponds to these specifications was modelled in ArcMap using Esri shapefiles. It was extended a distance that supersedes the majority of output settling locations (See figure 73 and 74 for the simulation this mitigation suggestion is based on). A ditch was also modelled to avoid low energy boulders emerging from the east (see figure 93-95 and table 30).

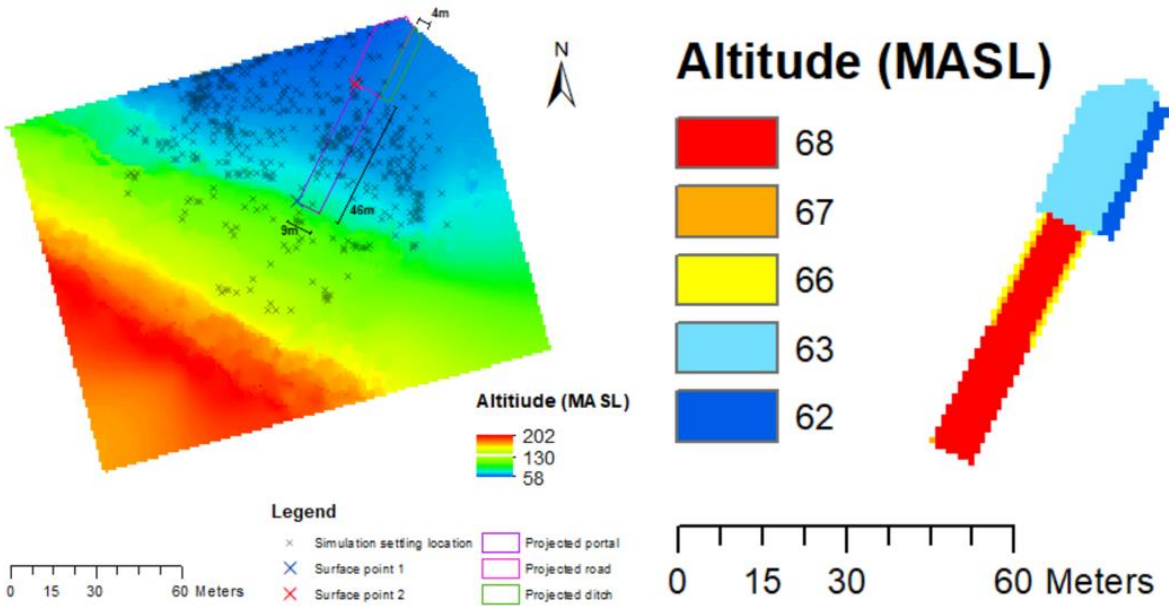


Figure 93: Mitigation design. The left figure shows simulation settling location and planned areas for road, portal and ditch placement. The right figure is the raster that will be merged with the digital elevation model

Table 29: Surface points that can be used to correctly place and orient the portal during potential construction.

	North (m)	East (m)
Surface point 1 (UTM 33N)	7 766 557.78	758 554.35
Surface point 2 (UTM 33N)	7 766 598.95	758 574.80

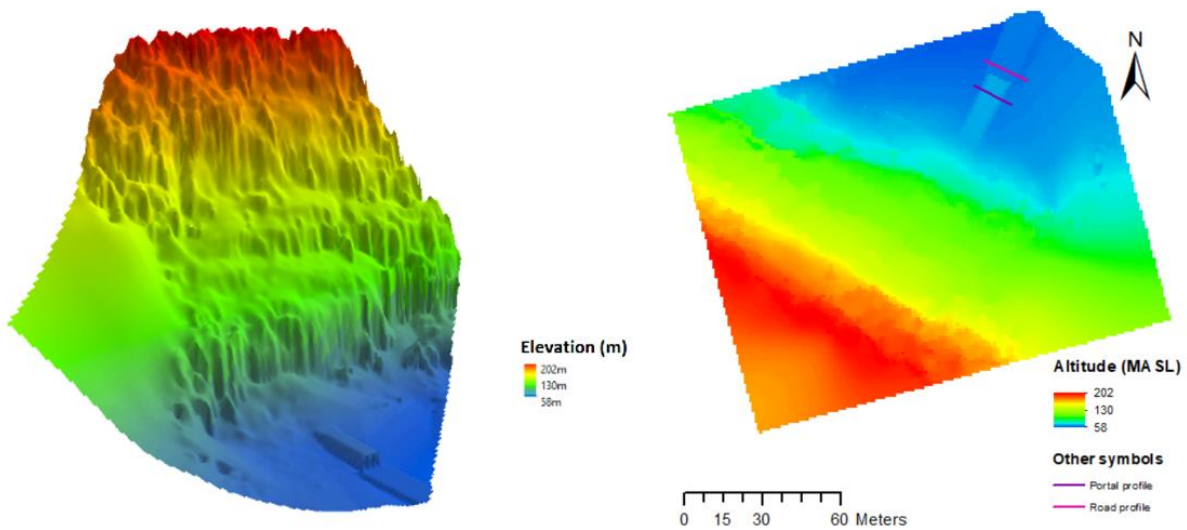


Figure 94: Digital elevation model with portal, road and ditch implemented. 3D rendered figure (left) and 2D color coded raster with elevation profile sections (right).

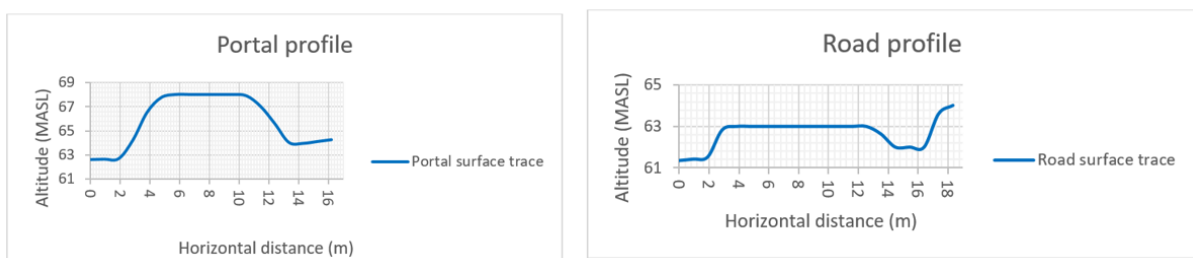


Figure 95: Portal (left) and road (right) surface trace profiles. See figure 94.

A final simulation was then done with the same input as described in chapter 4.5.1. Simulation results show the mitigation to be effective. Incoming boulders are deflected by the portal roof or caught in the modelled ditch (see figure 96).

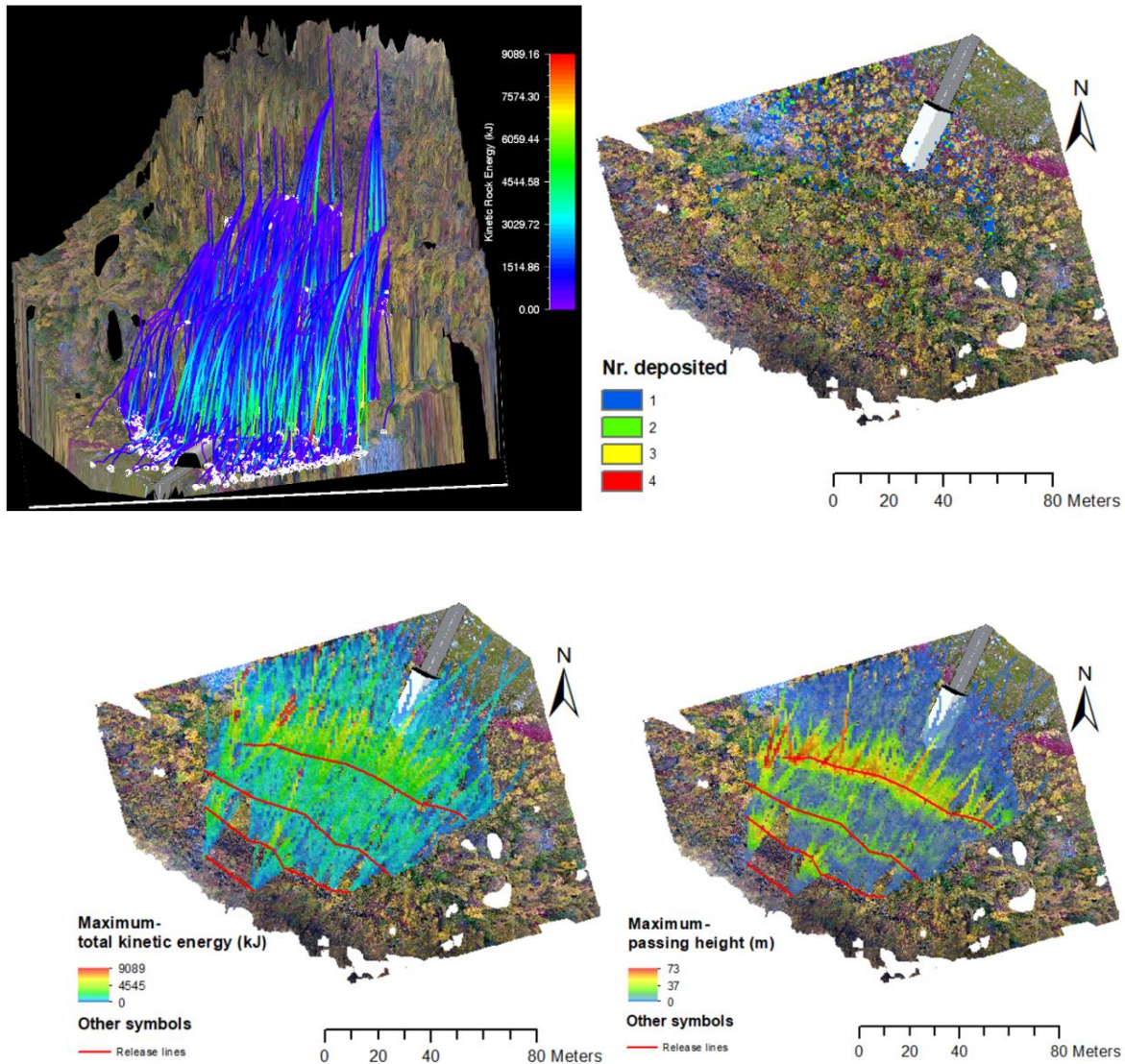


Figure 96: Trajectories (upper left), output setting locations (upper right), maximum total kinetic energy values (lower left) and passing height (lower right) for the rockfall simulation.

Simulations have thereby shown that a 5 m tall solid curved surface extended 46 m from the cliff wall combined with ditches of at least 1 m depth east and west of road will deter any boulder falling from any elevation, assuming the boulders are not larger than those sampled in the talus, that material properties are accurate, and that random orientations and source locations have sufficiently displayed the range of possible trajectories. Larger boulders could certainly be expected but is unlikely with a return time of 200 years. Since many taluses has seen low deposition rates since the end of the last glacial maximum (Luckman, 2013) the boulder sampled in field are expected to constitute close to size maximum for the given return time.

## 7 Conclusion

- 3D modelling will generally calculate higher bounce heights and total kinetic energies than 2D. This trend is particularly noteworthy on gentle slopes like taluses. Where 2D modelling show rolling/sliding motion, 3D models often calculate bounces.
- 2D software can be used for a good run estimate using literature values if no significant lateral elevation variance exists downslope. Steepest paths run out lengths usually encompass 3D simulation maximum in terms of kinetic energy, bounce height and run-out distance. Cautiously extrapolating a 2D simulation run out distance, where slope is derived from steepest path elevation data, into a cone shape can therefore produce a sound worst case run out estimate.
- 2D modelling produce a good kinetic energy estimate on steep rock slopes without developed taluses, using resolutions down to 10 m. Bounce height and kinetic energy estimates based on 2D simulations on gentle slopes like taluses produce low output values.
- Higher resolutions generally produce higher output kinetic energies and bounce heights for both 2D and 3D software. Simulations using digital elevation models with resolution much higher than 1 m calculates high end bounce height and kinetic energy values. However, simulations also output unrealistic settling locations in steep slope sections even when low friction/high restitution coefficients are assigned substrate.
- Simulations using 1 m and 3 m resolution digital elevation models produce sound output using literature values.
- 10 m resolution digital elevation models can be used for run-out estimates where such low detail does not obscure important terrain structures such as steep slopes and obstacles.
- Digital elevation models produced with aircraft based LIDAR are consistently less steep than those produced with more local survey models, likely due to parallel incident angles and/or enhanced vertical error stemming from GPS systems. Notably higher bounce heights will be calculated from a local terrestrial survey derived digital elevation model while total kinetic energy is less effected by model origin (remote sensing technique).

## Bibliography

- AGLIARDI, F. & CROSTA, G. 2003. High resolution three-dimensional numerical modelling of rockfalls. *International Journal of Rock Mechanics and Mining Sciences*, 40, pp. 455-471.
- AZZONI, A. & DE FREITAS, M. 1995. Experimentally gained parameters, decisive for rock fall analysis. *Rock mechanics and rock engineering*, 28, pp. 111-124.
- BARTELT, P., BIELER, C., BÜHLER, Y., CHRISTEN, M., CHRISTEN, M., DREIER, L., GERBER, W., GLOVER, J., SCHNEIDER, M., GLOCKER, C., LEINE, R. & SCHWEIZER, A. 2016. RAMMS::ROCKFALL User Manual v1.6. WSL Institute for Snow and Avalanche Research SLF.
- BOZZOLO, D. & PAMINI, R. 1986. Simulation of rock falls down a valley side. *Acta Mechanica*, 63, pp. 113-130.
- CHEN, G., ZHENG, L., ZHANG, Y. & WU, J. 2013. Numerical simulation in rockfall analysis: a close comparison of 2-D and 3-D DDA. *Rock mechanics and rock engineering*, 46, pp. 527-541.
- CLAGUE, J. J. & ROBERTS, N. J. 2012. 1 Landslide hazard and risk. In: CLAGUE, J. J. & STEAD, D. (eds.) *Landslides - Types, Mechanisms and Modeling*. New York, NY: Cambridge University Press.
- DEVOLI, G., EIRKENÆS, O. & TAURISANO, A. 2011. Plan for skredfarekartlegging - Delrapport steinsprang, steinskred og fjellskred In: DEVOLI, G. (ed.).
- DOMAAS, U. & GRIMSTAD, E. 2014. Fjell- og steinskred. In: HØEG, K., K., K. & LIED, K. (eds.) *Skred: skredfare og sikringstiltak: praktiske erfaringer og teoretiske prinsipper*. Oslo: Universitetsforlaget.
- DORREN, L., DOMAAS, U., KRONHOLM, K. & LABIOUSE, V. 2013. Methods for Predicting Rockfall Trajectories and Run-out Zones In: LAMBERT, S. & NICOT, F. (eds.) *Rockfall engineering*. Hoboken, NJ: John Wiley & Sons.
- DORREN, L. K. 2003. A review of rockfall mechanics and modelling approaches. *Progress in Physical Geography*, 27, pp. 69-87.
- DORREN, L. K. & SEIJMONSBERGEN, A. C. 2003. Comparison of three GIS-based models for predicting rockfall runout zones at a regional scale. *Geomorphology*, 56, pp. 49-64.
- FANOS, A. M. & PRADHAN, B. 2018. Laser Scanning Systems and Techniques in Rockfall Source Identification and Risk Assessment: A Critical Review. *Earth Systems and Environment*, pp. 1-20.
- FRATTINI, P., CROSTA, G. B. & AGLIARDI, F. 2012. Rockfall characterization and modeling. In: CLAGUE, J. J. & STEAD, D. (eds.) *Landslides - Types, Mechanisms and Modeling*. New York, NY: Cambridge University Press.
- GUSTAVSON, M. 1974. *Berggrunnskart Narvik M 1:250 000*. NGU.
- HAU, K. T., WONG, R. H. C. & LEE, C. F. 1996. Rockfall Problems in Hong Kong and some new experimental results for coefficients of Restitution. *International Journal of rock mechanics and mining sciences and geomechanics*, 35, pp. 662-663.
- HEIDENREICH, B. 2004. *Small-and half-scale experimental studies of rockfall impacts on sandy slopes*. PhD, École Polytechnique Fédérale De Lausanne.
- HODGSON, M. E. & BRESNAHAN, P. 2004. Accuracy of airborne LiDAR-derived elevation. *Photogrammetric Engineering & Remote Sensing*, 70, pp. 331-339.
- JABOYEDOFF, M. & LABIOUSE, V. 2011. Preliminary estimation of rockfall runout zones. *Natural Hazards and Earth System Sciences*, 11, pp. 819-828.

- JABOYEDOFF, M., OPPIKOFER, T., ABELLÁN, A., DERRON, M.-H., LOYE, A., METZGER, R. & PEDRAZZINI, A. 2012. Use of LIDAR in landslide investigations: a review. *Natural hazards*, 61, pp. 5-28.
- KARTVERKET. *Høydedata* [Online]. Available: <https://hoydedata.no/LaserInnsyn/> [Accessed 9 September 2017].
- KARTVERKET. *Høydedata og terrengmodeller fra Kartverket* [Online]. Available: <https://www.kartverket.no/data/laserskanning/> [Accessed 9 May 2018].
- KARTVERKET. *N2000 Kartdata* [Online]. Kartverket. Available: <https://kartkatalog.geonorge.no/metadatas/kartverket/n2000-kartdata/8d52075d-6ef6-4120-8041-d0c0901f21f7> [Accessed 9 April 2018].
- KARTVERKET. *N5000 Kartdata* [Online]. Kartverket. Available: <https://kartkatalog.geonorge.no/metadatas/kartverket/n5000-kartdata/c777d53d-8916-4d9d-bae4-6d5140e0c569> [Accessed 9 April 2018].
- KARTVERKET. *Norgebilder* [Online]. Available: <https://www.norgebilder.no/> [Accessed 9 May 2018].
- KELLER, E. A. 2011. *Environmental Geology*, Upper Saddle River, NJ, Pearson Education.
- KHORRAM, S., KOCH, F. H., VAN DER WIELE, C. F. & NELSON, S. A. 2012. *Remote sensing*, New York, NY, Springer Science & Business Media.
- LUCKMAN, B. H. 2013. Talus Slopes. In: S.A., E. (ed.) *The Encyclopedia of Quaternary Science*. Amsterdam: Elsevier.
- MARSHAK, S. 2011. *Earth: Portrait of a Planet: Fourth International Student Edition*, New York, NY, WW Norton & Company.
- MARTINSEN, J. O., NØTTVEDT, A. & PEDERSEN, R.-B. 2013. Av hav stiger landet - Paleogen og neogen, kontinentene av i dag formes; 66-2,6 Ma. In: RAMBERG, I. B., BRYHNI, I., NØTTVEDT, A. & RANGNES, K. (eds.) *Landet blir til - Norges geologi*. 2nd ed. Trondheim: Norges geologiske forening.
- PFEIFFER, T. J. & BOWEN, T. D. 1989. Computer Simulation of Rockfalls. *Bulletin of Association of Engineering Geologists*, 26, pp. 135-146.
- REDWEIK, P. 2012. Photogrammetry. In: XU, G. (ed.) *Sciences of Geodesy-II: Innovations and Future Developments*. New York, NY: Springer Science & Business Media.
- RITCHIE, A. M. 1963. Evaluation of rockfall and its control. *Highway research record*, pp 13-38.
- ROBOTHAM, M. E., WANG, H. & WALTON, G. 1995. Assessment of risk from rockfall from active and abandoned quarry slopes. *Institution of mining and Metallurgy*, 5, pp. A25-A33.
- ROCSCIENCE. *What's New in RocFall Version 6.0* [Online]. Available: <https://www.rocscience.com/help/rockfall/webhelp6/RocFall.htm> [Accessed 9 may 2018].
- STEIWER, G. W. H. 2017. *Nasjonal detaljert høydemodell-homogenitetsanalyse av terrengmodell fra flybåren laserskanning*. Master, NTNU.
- STEVENS, W. D. 1998. *RocFall, a tool for probabilistic analysis, design of remedial measures and prediction of rockfalls*. Master, University of Toronto.
- TENZER, R., SIRGUEY, P., RATTENBURY, M. & NICOLSON, J. 2011. A digital rock density map of New Zealand. *Computers & geosciences*, 37, pp. 1181-1191.
- TWISS, R. J. & MOORES, E. M. 1992. *Structural geology*, New York, NY, W. H. Freeman and Company.
- VEGDIREKTORATET. 2016. *Vegtunneler - Håndbok N500* [Online]. Statens Vegvesen. Available: [https://www.vegvesen.no/\\_attachment/61913](https://www.vegvesen.no/_attachment/61913) [Accessed 9 April 2018].

- VEGVESNET. *Vegkart* [Online]. Available:  
<https://www.vegvesen.no/vegkart/vegkart/#kartlag:geodata/@600000,7225000,3>  
[Accessed 9 April 2018].
- VEGVESNET 2014a. 50857-GEOL-04 Kjerringstølen skredfarevurdering. Fv. 83, SVV rapport 2016».
- VEGVESNET 2014b. 2014005900-9 Stabilitetsvurdering etter steinskred 18.06.2014 Rakkenesura. E6, SVV rapport 2014
- VEGVESNET. 2017. *Fv. 2 Aunfjellet - informasjonsmøte om rassikring* [Online]. Statens Vegvesen. Available:  
<https://www.vegvesen.no/om+statens+vegvesen/presse/nyheter/lokalt/Region+Nord/Troms/fv.2-aunfjellet-informasjonsm%C3%B8te-om-rassikring> [Accessed 9 May 2018].
- VOLKWEIN, A., SCHELLENBERG, K., LABIOUSE, V., AGLIARDI, F., BERGER, F., BOURRIER, F., DORREN, L. K., GERBER, W. & JABOYEDOFF, M. 2011. Rockfall characterisation and structural protection-a review. *Natural Hazards and Earth System Sciences*, 11, pp. 2617-2651.
- VORREN, T. O., MANGERUD, J., BLIKRA, L. H., NESJE, A. & SVEIAN, H. 2013. Norge trer fram - De siste 11 700 år - Holocen. In: RAMBERG, I. B., BRYHNI, I., NØTTVEDT, A. & RANGNES, K. (eds.) *Landet blir til - Norges geologi*. 2nd ed. Trondheim: Norges geologiske forening.
- WYLLIE, D. C. 2014. *Rock fall engineering*. Boca Rator, FL, CRC Press.
- WYLLIE, D. C. & MAH, C. W. 2004. *Rock slope engineering - Civil and Mining*, Oxfordshire, Taylor and Francis group.
- ZWAAN, K. B. 1988. *Berggrunnskart Nordreisa M 1:250 000*. NGU.

## Appendix A – Slope profiles used in Rocfall 6.0

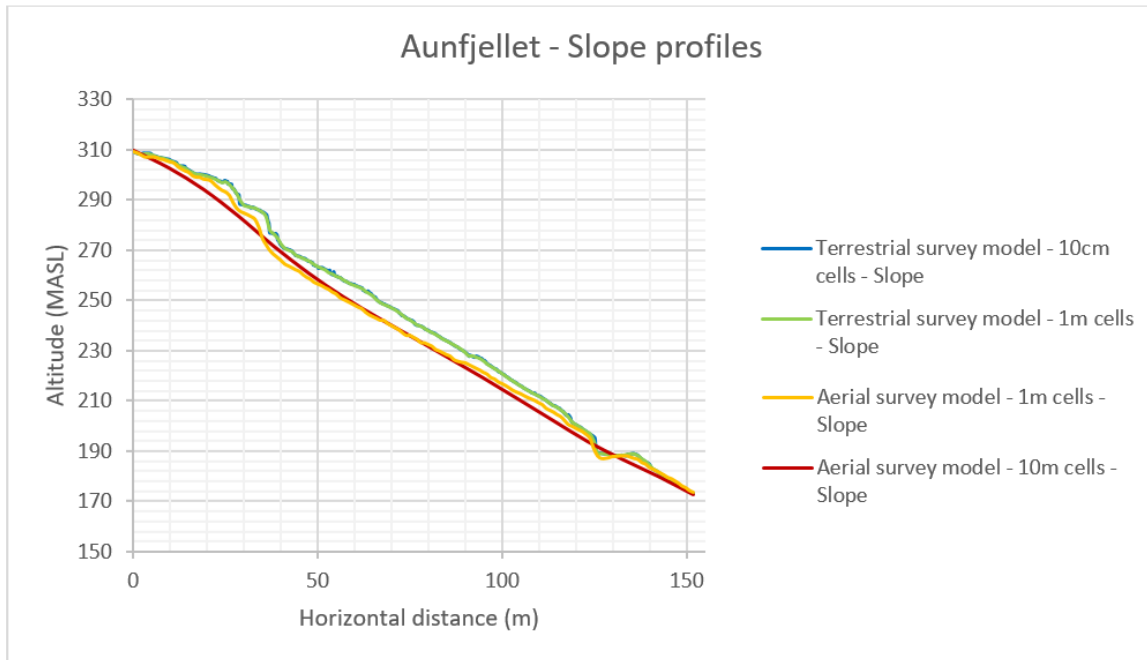


Figure 97: Aunfjellet 2D slope profiles.

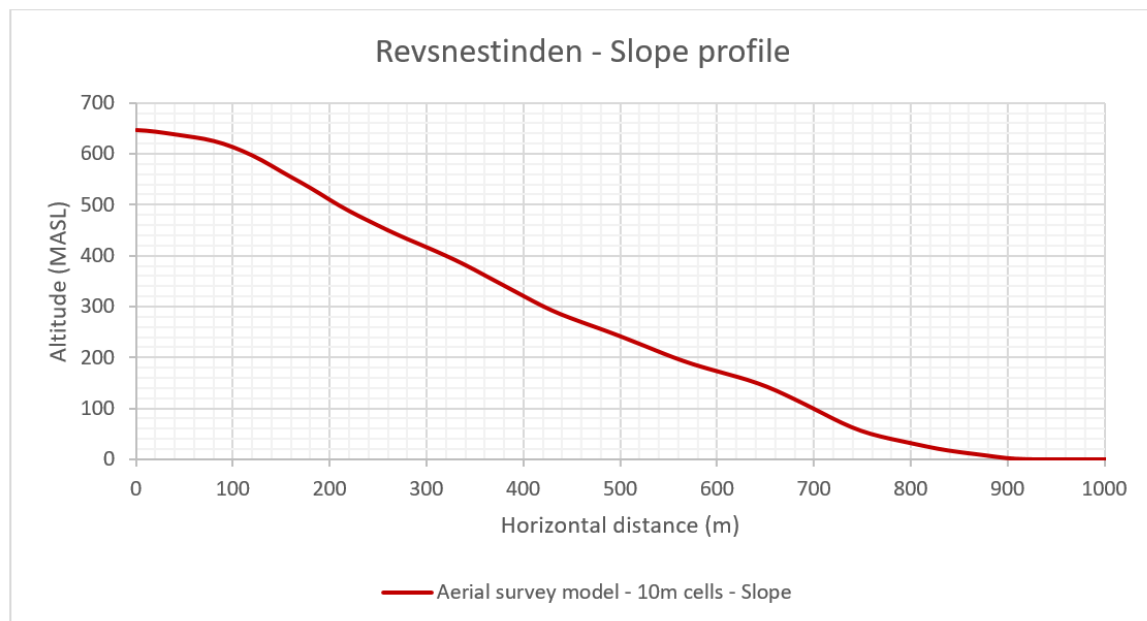


Figure 98: Revsnestinden 2D slope profile.

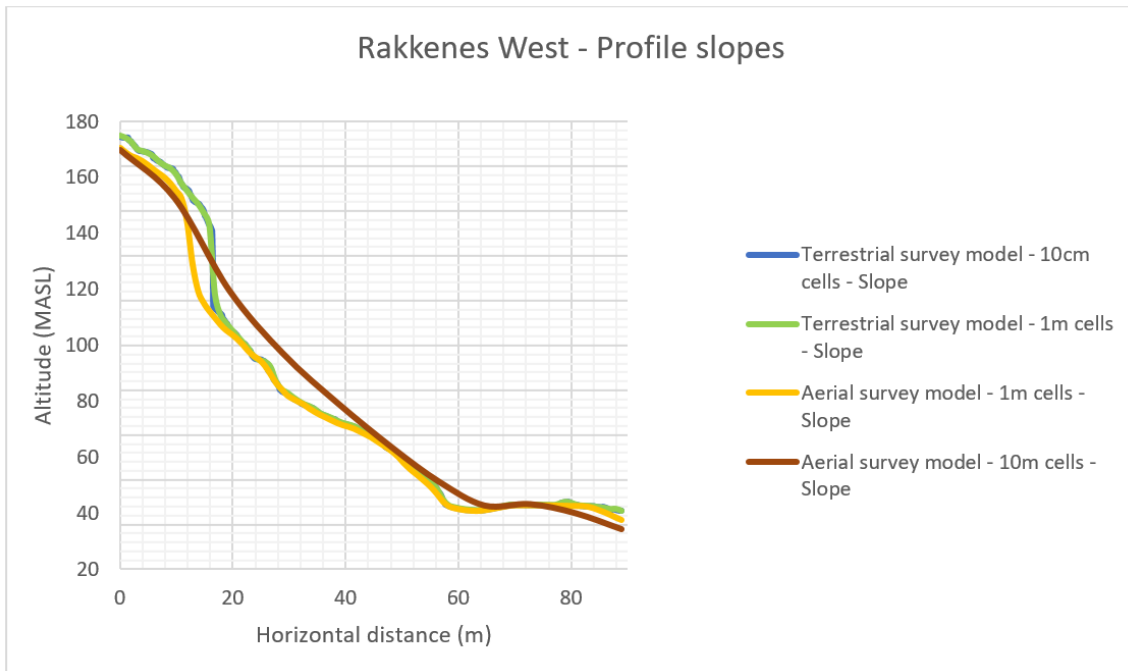


Figure 99: Rakkenes West 2D slope profiles.

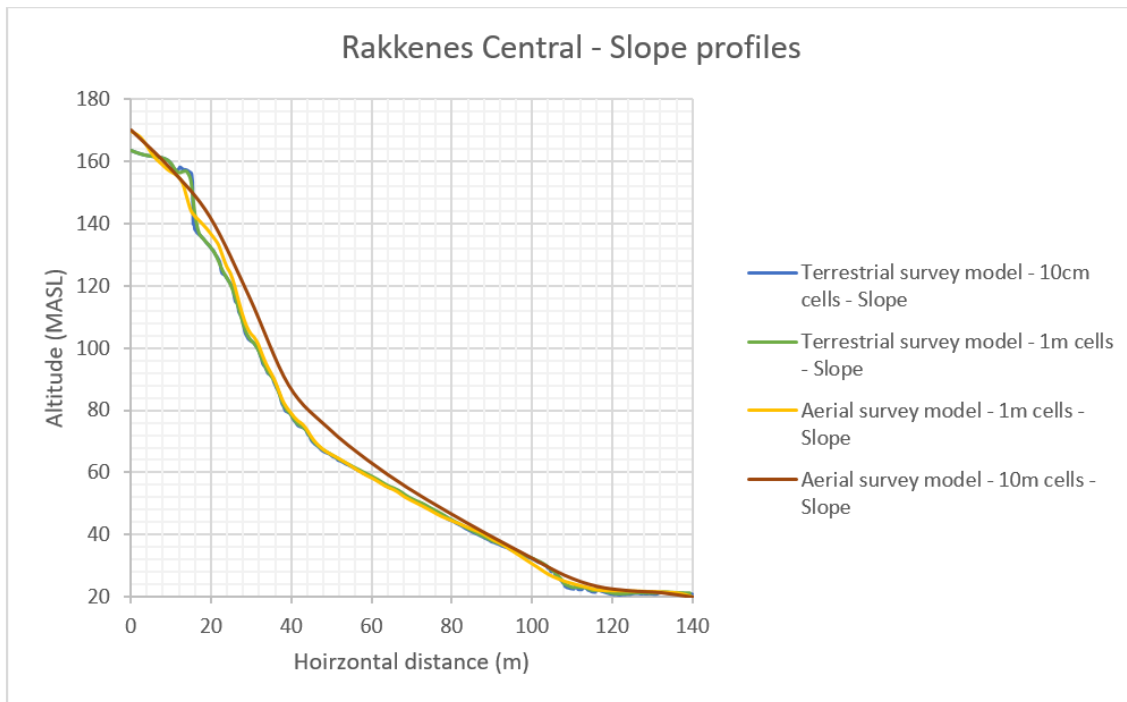


Figure 100: Rakkenes Central 2D slope profiles.

## Appendix B – Release point coordinates

Table 30: Release coordinates. Release point 1 and 2 on Rakkenes Central were disproved during calibration. Only release point 2 was used to produce results on simulations on Rakkenes Central. Coordinates are based on UTM33N projection.

Case area	Name	Location (North) (m)	Location (East) (m)	Altitude (m)
Aunfjellet	Release point	7641039	553713	276
Revsnestinden	Release point	7620896	543117	551
Rakkenes West	Release point 1	7766937	757394	138
	Release point 2	7766934	757394	138
Rakkenes Central	Release point 1	7766854	757708	76
	Release point 2	7766843	757703	104
	Release point 3	7766843	757703	139

## Appendix C – Historical rockfall settling locations and size

Table 31: Historical rockfall properties. Coordinates are based on UTM33N projection.

Case area	Na me	Dmax (m)	Dmid (m)	Dmin (m)	Settling location (North) (m)	Settling location (East) (m)
Revsnesti nden	R1	2.4	1.8	1.4	7621120	542527
Rakkenes central	C1	NA	NA	NA	7766921	757746
Rakkenes East	E1	2.5	1.3	1	7766583	758573
	E2	2.1	1.1	1	7766590	758569
	E3	1	0.9	0.3	7766580	758568
	E4	2.5	1.5	1.2	7766579	758568
	E5	1.6	1.6	1.1	7766574	758579
	E6	1.3	1	0.6	7766572	758580
	E7	2.1	1.1	0.75	7766566	758590
	E8	0.8	0.45	0.45	7766570	758596
	E9	1.6	1	0.45	7766574	758590
	E10	NA	NA	NA	7766579	758573

## Appendix D - RAMMS:Rockfall material input

### *Aunfjellet*

Table 32: Input for back calculation. 1T and 10A did not result in successful back calculation.

DEM name	Area (see figure 44)	Material	Properties
1T	MD1	Bedrock	Hard
	MD2	Talus	Extra soft
	MD3	Soil	Extra soft
	MD4	Asphalt	Hard
	Enhanced drag	Forest	Open
1A	MD1	Bedrock	Hard
	MD2	Talus	Extra soft
	MD3	Soil	Extra soft
	MD4	Asphalt	Hard
	Enhanced drag	Forest	Open
3T	MD1	Bedrock	Extra soft
	MD2	Talus	Extra soft
	MD3	Soil	Extra soft
	MD4	Asphalt	Hard
	Enhanced drag	Forest	Open
3A	MD1	Bedrock	Extra soft
	MD2	Talus	Extra soft
	MD3	Soil	Extra soft
	MD4	Asphalt	Hard
	Enhanced drag	Forest	Open
0.1T	MD1	Bedrock	Extra hard
	MD2	Talus	Extra hard
	MD3	Soil	Medium
	MD4	Asphalt	Hard
10A	Entire slope	NA	Extra soft

### *Revsnestinden*

Table 33: Input for successful back calculation.

Area (see figure 45)	Material	Properties
MD1	Bedrock	Extra hard
MD2	Talus	Hard
Enhanced drag	Forest	Open

### *Rakkenes West*

Table 34: Input for successful back calculation.

DEM name	Area (see figure 46)	Material	Properties
1T	MD1	Bedrock	Hard
	MD2	Soil	Medium soft
	MD3	Asphalt	Hard
1A	MD1	Bedrock	Hard
	MD2	Soil	Medium soft
	MD3	Asphalt	Hard
3T	MD1	Bedrock	Hard
	MD2	Soil	Medium soft
	MD3	Asphalt	Hard
3A	MD1	Bedrock	Hard
	MD2	Soil	Medium soft
	MD3	Asphalt	Hard
0.1T	MD1	Bedrock	Hard
	MD2	Soil	Medium
	MD3	Asphalt	Hard
10A	MD1	Bedrock	Medium hard
	MD2	Soil	Extra soft
	MD3	Asphalt	Extra soft

## *Rakkenes Central*

Table 35: Input for successful back calculation.

DEM name	Area (see figure 47)	Material	Properties
1T	MD1	Bedrock	Extra hard
	MD2	Talus	Medium hard
	MD3	Soil	Medium
	MD4	Asphalt	Hard
	Enhanced drag	Forest	Open
1A	MD1	Bedrock	Extra hard
	MD2	Talus	Medium
	MD3	Soil	Medium
	MD4	Asphalt	Hard
	Enhanced drag	Forest	Open
3T	MD1	Bedrock	Extra hard
	MD2	Talus	Medium
	MD3	Soil	Medium
	MD4	Asphalt	Hard
	Enhanced drag	Forest	Open
3A	MD1	Bedrock	Extra hard
	MD2	Talus	Medium
	MD3	Soil	Medium
	MD4	Asphalt	Hard
	Enhanced drag	Forest	Open
0.1T	MD1	Bedrock	Hard
	MD2	Talus	Medium
	MD3	Soil	Medium
	MD4	Asphalt	Hard
	Enhanced drag	Forest	Open
10A	MD1	Bedrock	Hard
	MD2	Talus	Medium
	MD3	Soil	Medium
	MD4	Asphalt	Hard
	Enhanced drag	Forest	Open

## ***Rakkenes East***

*Table 36: Simulation material input.*

DEM	Area (see figure 48)	Material	Properties
1T – No portal	MD1	Bedrock	Medium hard
	MD2	Talus	Medium
	MD3	Soil	Medium soft
	Enhanced drag	Forest	Open
1T – Portal implemented	MD1	Bedrock	Medium hard
	MD2	Talus	Medium
	MD3	Soil	Medium soft
	MD4	Portal roof	Medium hard
	MD5	Road	Hard
	Enhanced drag	Forest	Open

## Appendix E – Rocfall 6.0 material input

### *Aunfjellet*

Table 37: Input for back calculation. 0.1T did not result in a successful back calculation.

DEM name	Section (see figure 49)	Material	Normal restitution coefficient (SD)	Tangential restitution coefficient (SD)	Dynamic friction (SD)	Rolling friction (SD)
1T	MD1	Bedrock	0.35 (0.04)	0.85 (0.04)	0.5 (0.04)	0.1 (0.02)
	MD2	Talus	0.30 (0.04)	0.61 (0.04)	0.5 (0.04)	0.1 (0.02)
	MD3	Soil	0.39 (0.04)	0.57 (0.03)	0.5 (0.04)	0.1 (0.02)
	MD4	Asphalt	0.9 (0.04)	0.4 (0.03)	0.5 (0.04)	0.1 (0.01)
1A	MD1	Bedrock	0.35 (0.04)	0.85 (0.04)	0.5 (0.04)	0.1 (0.02)
	MD2	Talus	0.30 (0.04)	0.61 (0.04)	0.5 (0.04)	0.1 (0.02)
	MD3	Soil	0.39 (0.04)	0.57 (0.03)	0.5 (0.04)	0.1 (0.02)
	MD4	Asphalt	0.9 (0.04)	0.4 (0.03)	0.5 (0.04)	0.1 (0.01)
0.1T	MD1	Bedrock	0.30 (0.04)	0.75 (0.02)	0.5 (0.04)	0.1 (0.02)
	MD2	Talus	0.30 (0.04)	0.75 (0.02)	0.03 (0.01)	0.01 (0)
	MD3	Soil	0.39 (0.04)	0.57 (0.03)	0.5 (0.04)	0.1 (0.02)
	MD4	Asphalt	0.9 (0.04)	0.4 (0.03)	0.5 (0.04)	0.1 (0.01)
10A	Entire slope	NA	0.1 (0)	0.1 (0)	0.9 (0)	0.7 (0)

### *Revsnestinden*

Table 38: Input for successful back calculation.

Section (see figure 50)	Material	Normal restitution coefficient (SD)	Tangential restitution coefficient (SD)	Friction angle in degrees (SD)
MD1	Bedrock	0.42 (0.04)	0.91 (0.02)	30 (0)
MD2	Slope	0.35 (0.02)	0.85 (0.02)	28 (0)

## *Rakkenes West*

Table 39: Input for successful back calculation.

DEM name	Section (see figure 51)	Material	Normal restitution Coefficient (SD)	Tangential restitution coefficient (SD)	Dynamic friction (SD)	Rolling friction (SD)
1T	MD1	Bedrock	0.35 (0.04)	0.85 (0.04)	0.5 (0.04)	0.1 (0.02)
	MD2	Soil	0.39 (0.04)	0.57 (0.03)	0.5 (0.04)	0.1 (0.02)
	MD3	Asphalt	0.9 (0.04)	0.4 (0.03)	0.5 (0.04)	0.1 (0.01)
1A	MD1	Bedrock	0.35 (0.04)	0.85 (0.04)	0.5 (0.04)	0.1 (0.02)
	MD2	Soil	0.39 (0.04)	0.57 (0.03)	0.5 (0.04)	0.1 (0.02)
	MD3	Asphalt	0.9 (0.04)	0.4 (0.03)	0.5 (0.04)	0.1 (0.01)
0.1T	MD1	Bedrock	0.32 (0.06)	0.71 (0.12)	0.5 (0.04)	0.1 (0.02)
	MD2	Soil	0.39 (0.04)	0.57 (0.03)	0.5 (0.04)	0.1 (0.02)
	MD3	Asphalt	0.9 (0.04)	0.4 (0.03)	0.5 (0.04)	0.1 (0.02)
10A	MD1	Bedrock	0.9 (0.02)	0.1 (0.02)	0.5 (0.04)	0.1 (0.02)
	MD2	Soil	0.39 (0.04)	0.57 (0.03)	0.5 (0.04)	0.1 (0.02)
	MD3	Asphalt	0.9 (0.04)	0.4 (0.03)	0.5 (0.04)	0.1 (0.02)

### *Rakkenes Central*

Table 40: Input for successful back calculation.

DEM name	Section (see figure 52)	Material	Normal restitution coefficient (SD)	Tangential restitution coefficient (SD)	Friction angle in degrees (SD)
1T	MD1	Bedrock	0.35 (0.04)	0.85 (0.04)	30
	MD2	Talus	0.32 (0.04)	0.85 (0.04)	30
	MD4	Asphalt	0.9 (0.04)	0.4 (0.03)	30
1A	MD1	Bedrock	0.35 (0.04)	0.85 (0.04)	30
	MD2	Talus	0.32 (0.04)	0.85 (0.04)	28
	MD4	Asphalt	0.9 (0.04)	0.4 (0.03)	30
0.1T	MD1	Bedrock	0.42 (0.04)	0.91 (0.02)	30
	MD2	Talus	0.30 (0.04)	0.80 (0.04)	30
	MD4	Asphalt	0.9 (0.04)	0.4 (0.03)	30
10A	MD1	Bedrock	0.35 (0.04)	0.85 (0.04)	30
	MD2	Talus	0.32 (0.04)	0.85 (0.04)	28
	MD4	Asphalt	0.9 (0.04)	0.4 (0.03)	30

# Appendix F - RAMMS:Rockfall output deposit locations

*Aunfjellet*

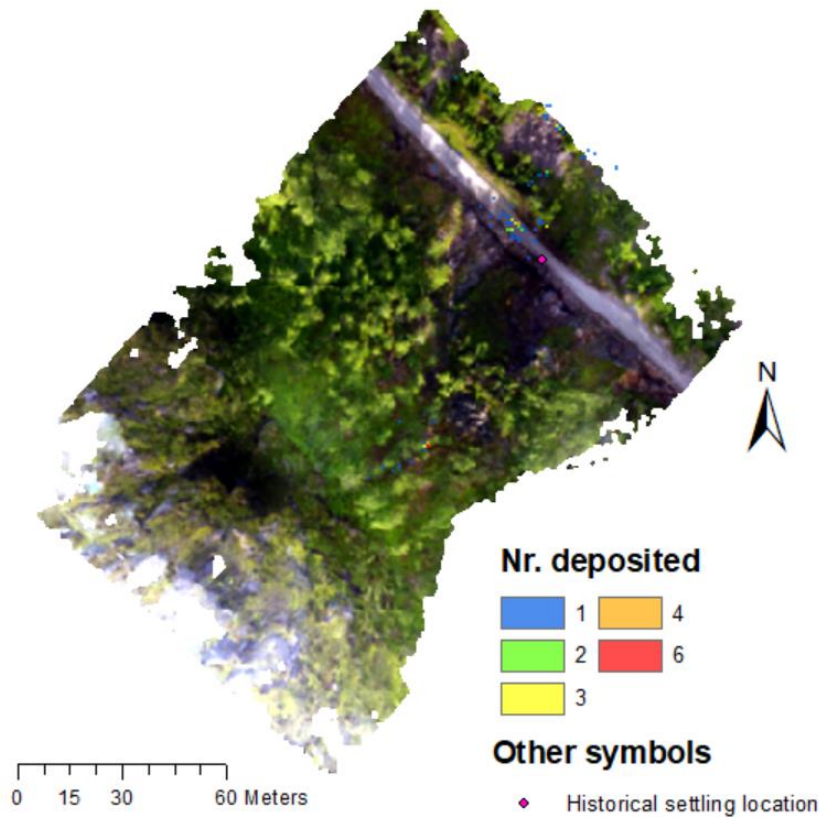


Figure 101: Model 1T.

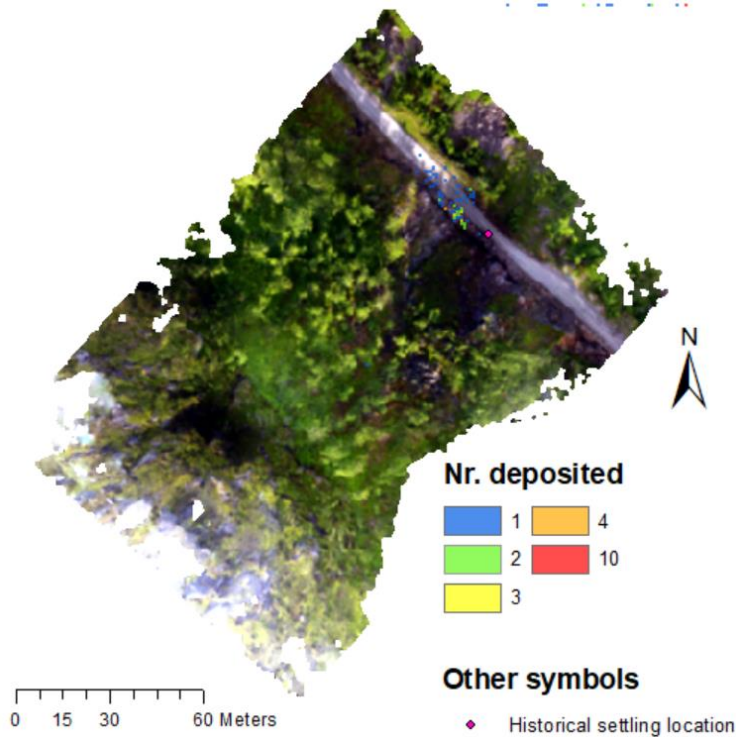


Figure 102: Model 1A.

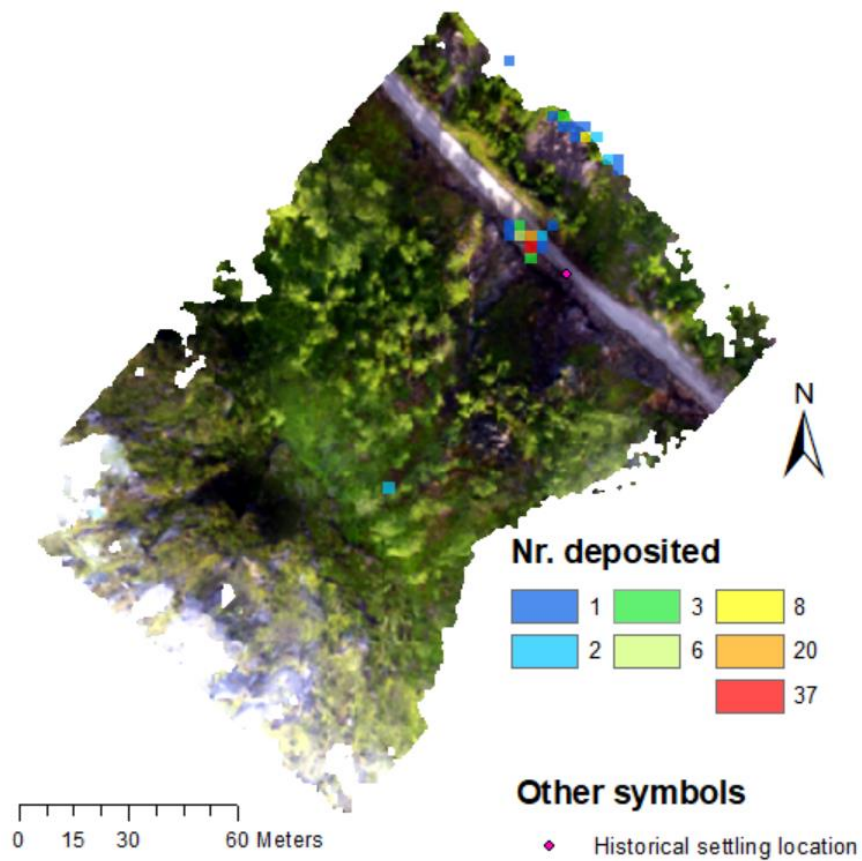


Figure 103: Model 3T.

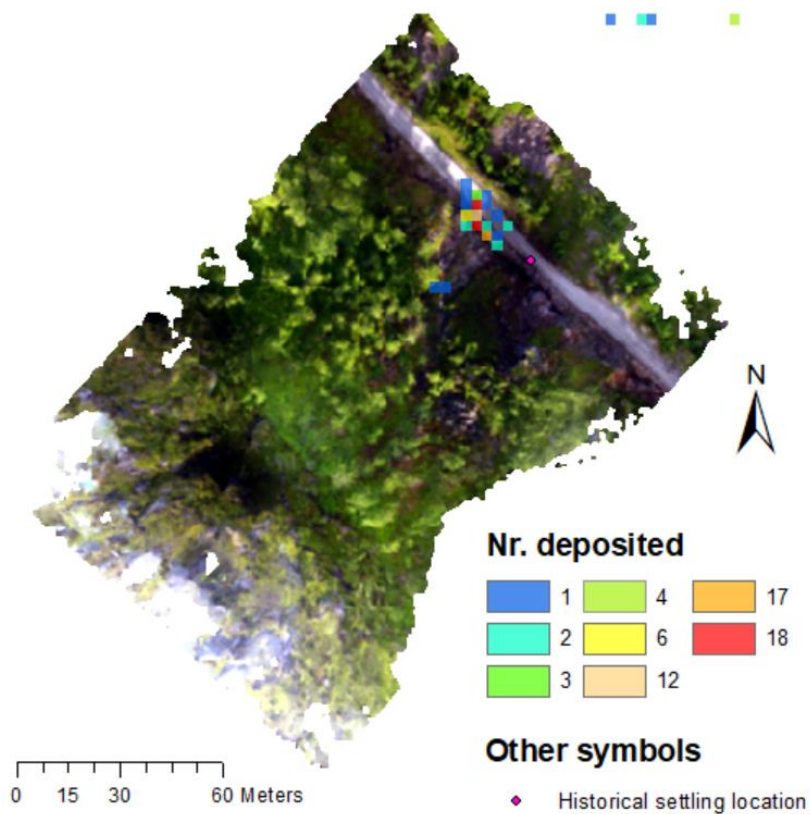


Figure 104: Model 3A.

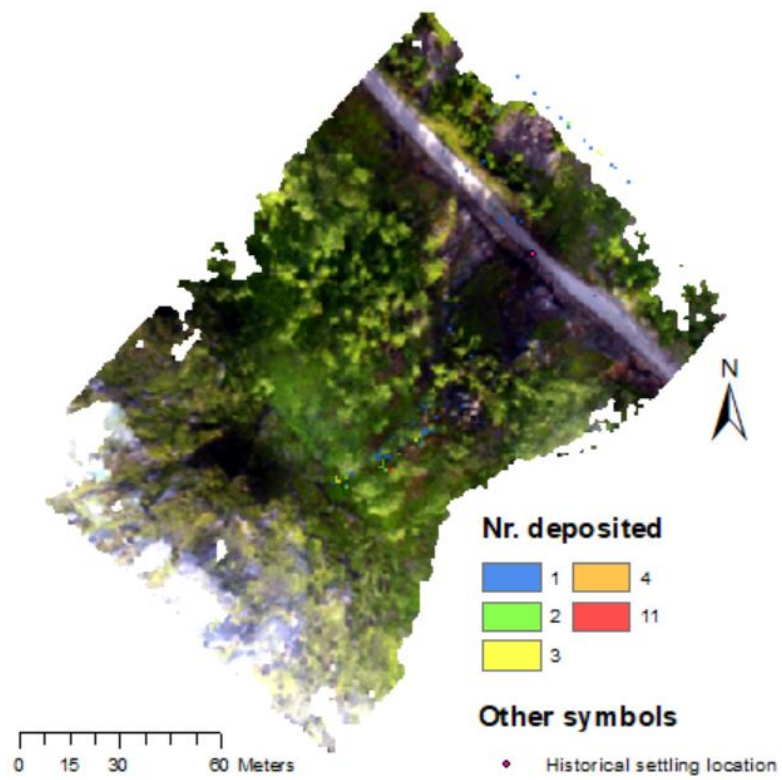


Figure 105: Model 0.1T.

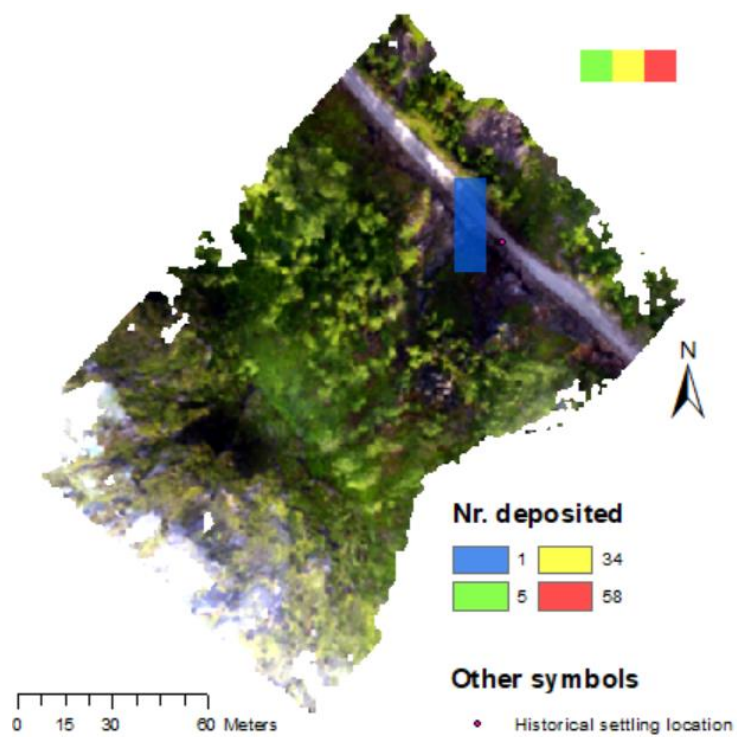
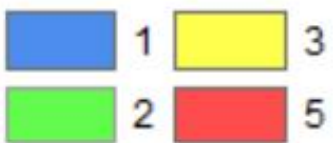


Figure 106: Model 10A.

*Revsnestinden*



**Nr. deposited**



**Other symbols**

-  Historical settling location

*Figure 107: Model 10A.*

*Rakkenes West*

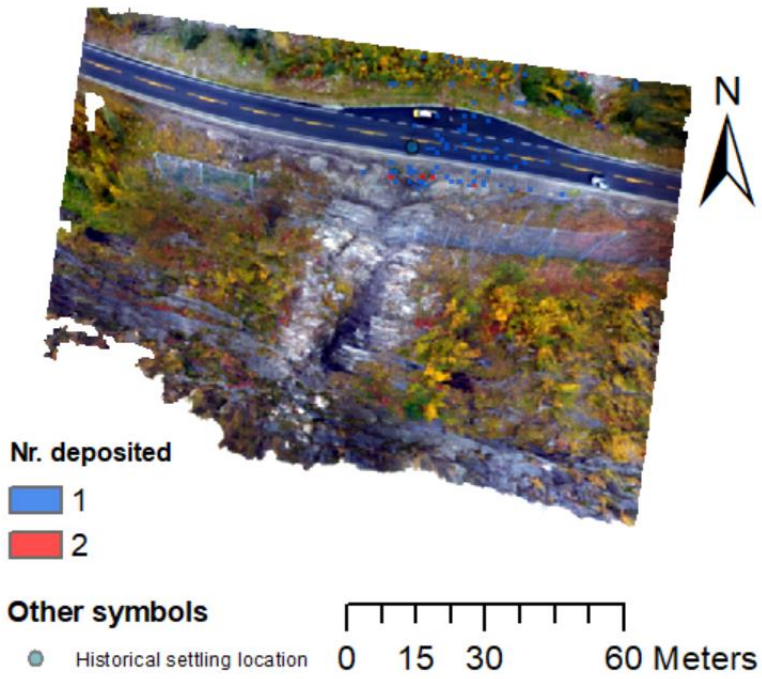


*Figure 108: Model 1T.*

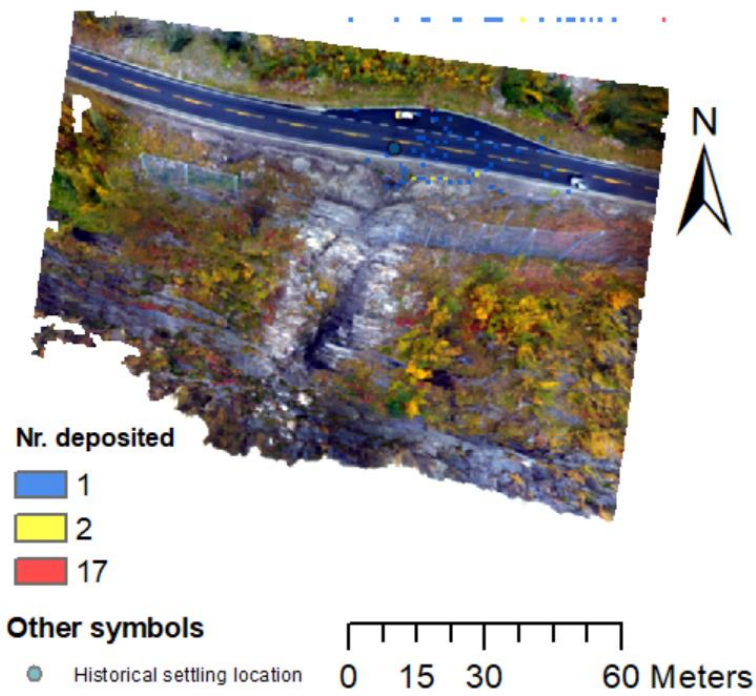


*Figure 109: Model 1A.*

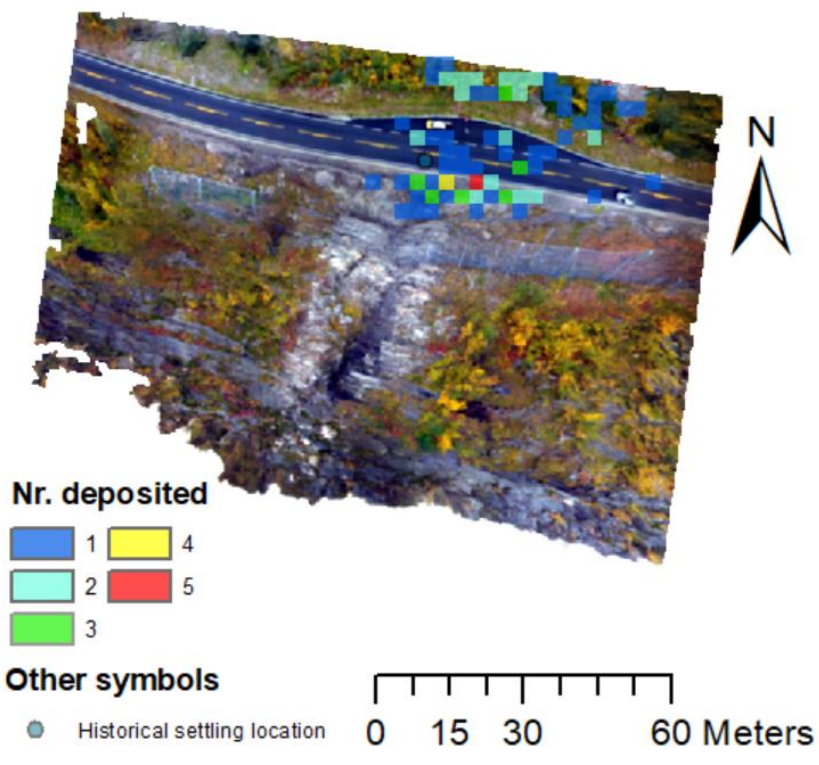


Figure 110: Model 3T.

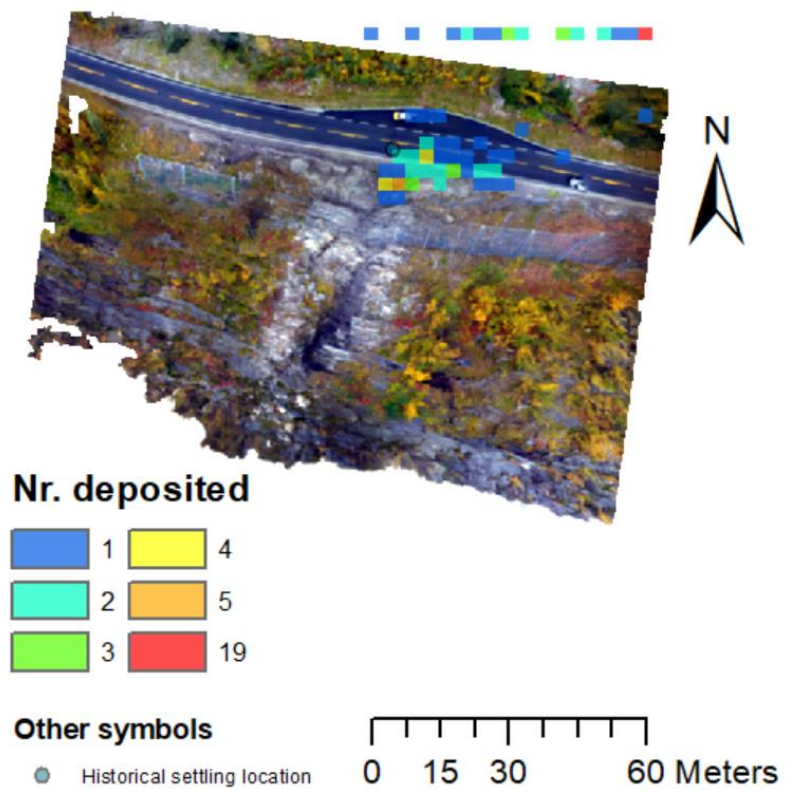


Figure 111: Model 3A.

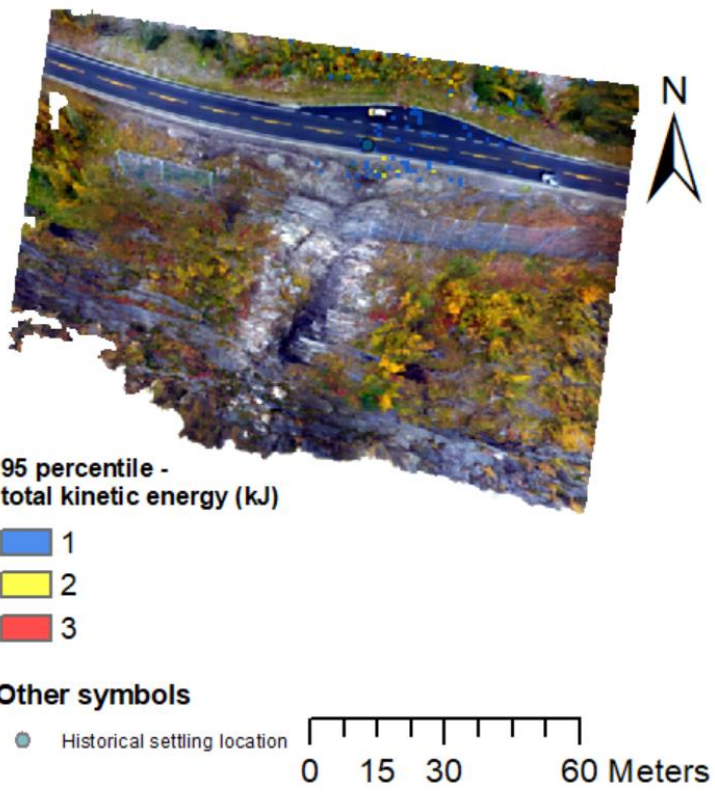


Figure 112: Model 0.1T.

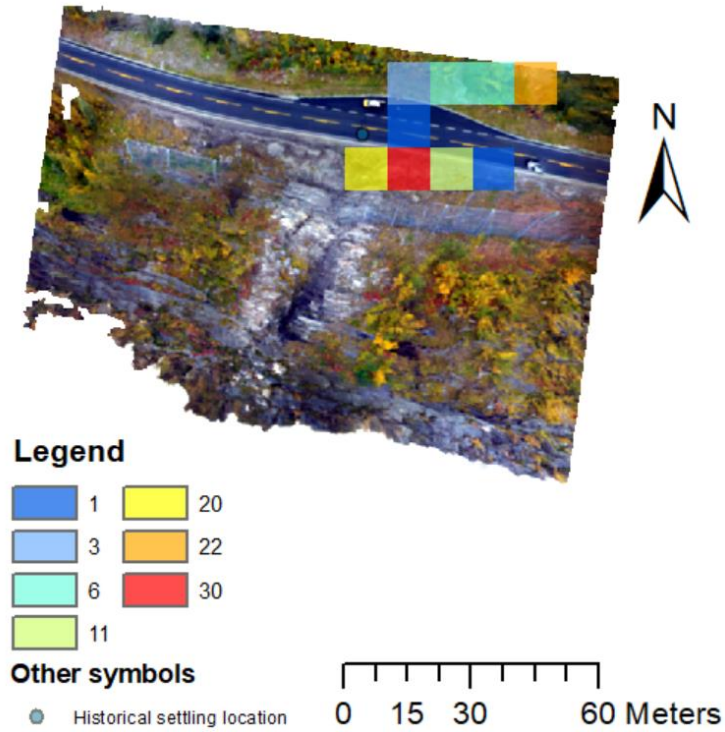
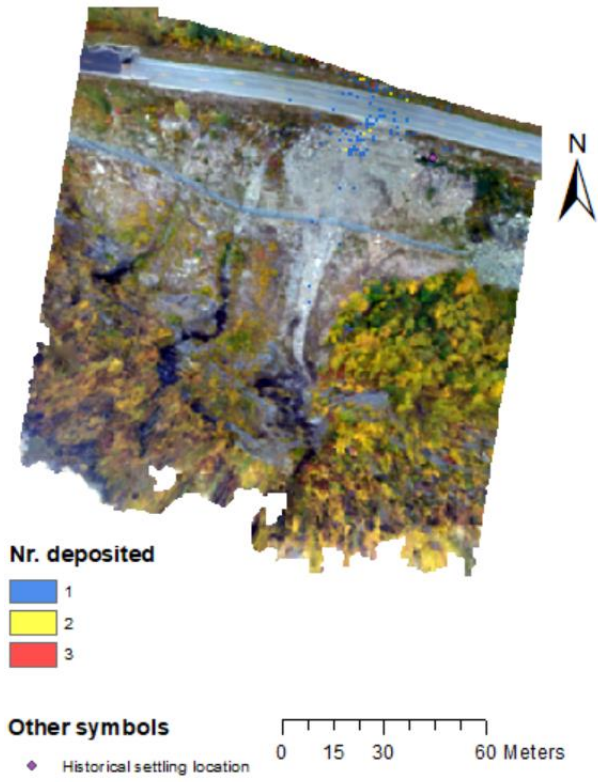
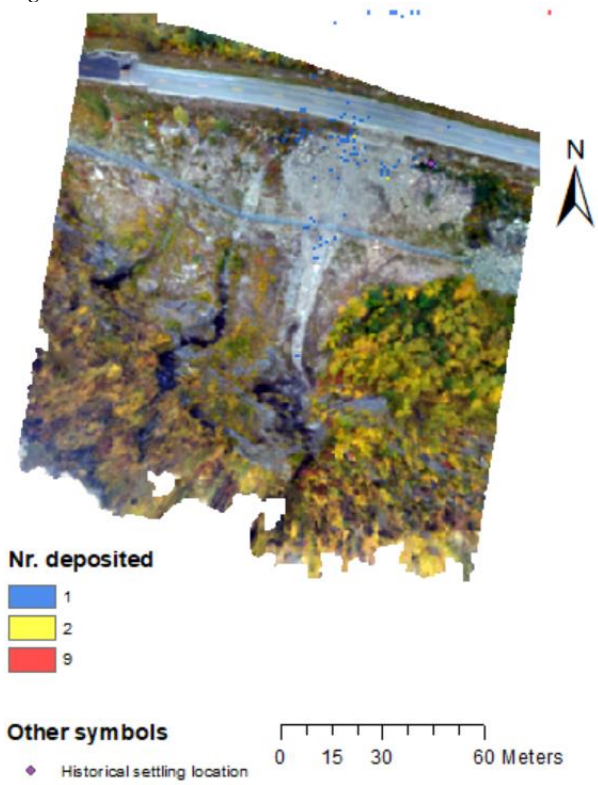


Figure 113: Model 10A.

*Rakkenes Central*



*Figure 114: Model 1T.*



*Figure 115: Model 1A.*

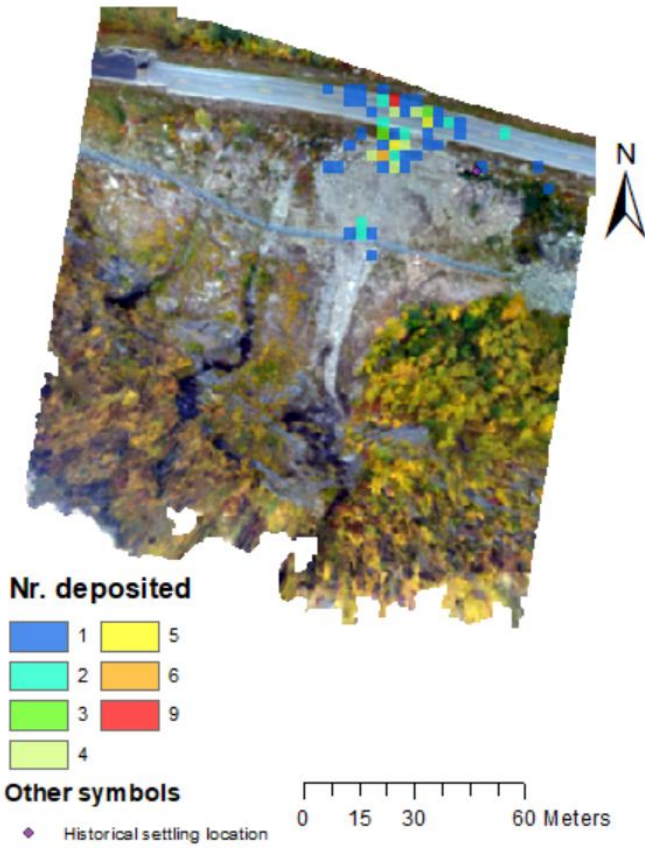


Figure 116: Model 3A.

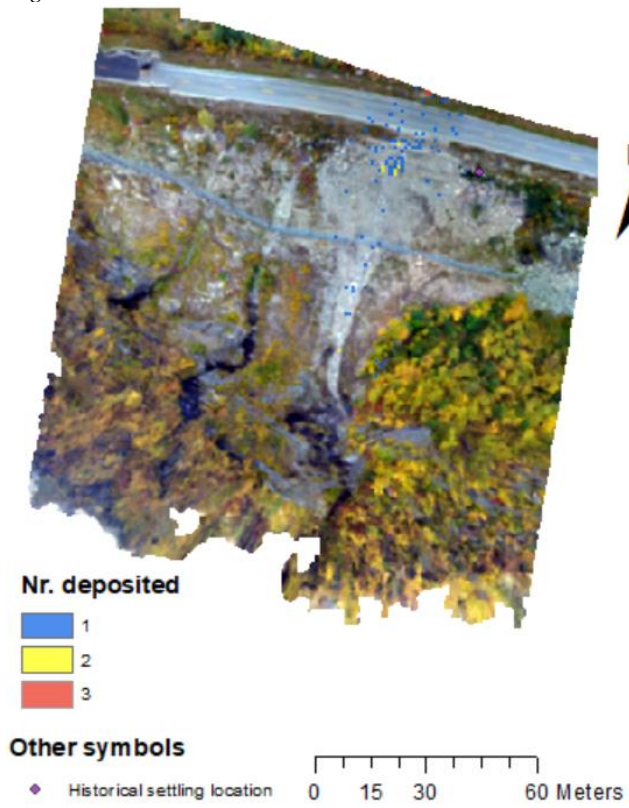


Figure 117: Model 0.1T.

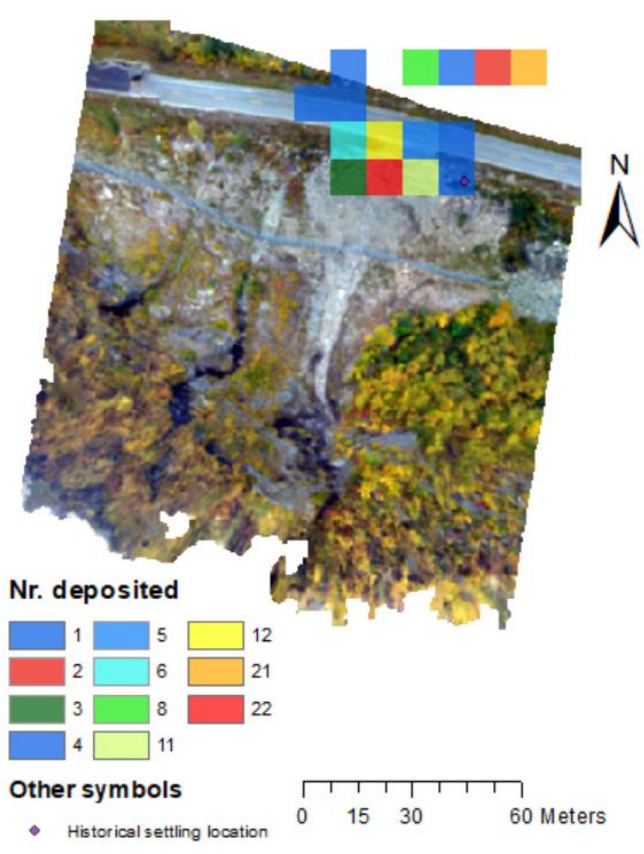


Figure 118: Model 10A.

# Appendix G - Rocfall 6.0 output deposit locations

## Aunfjellet

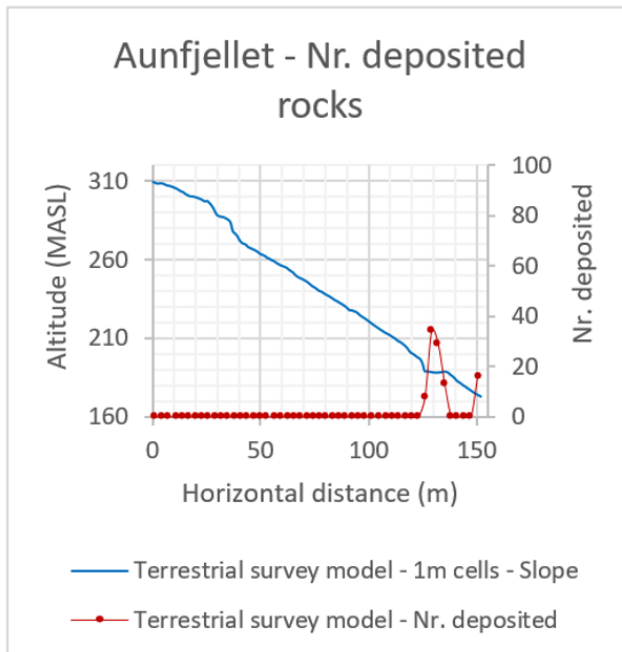


Figure 119: Simulation deposit locations. Model 1T.

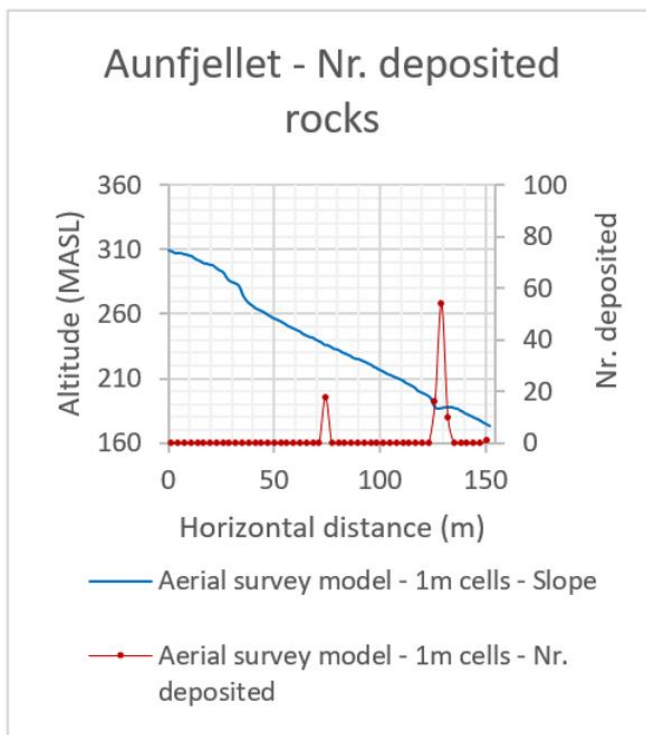


Figure 120: Simulation deposit locations. Model 1A.

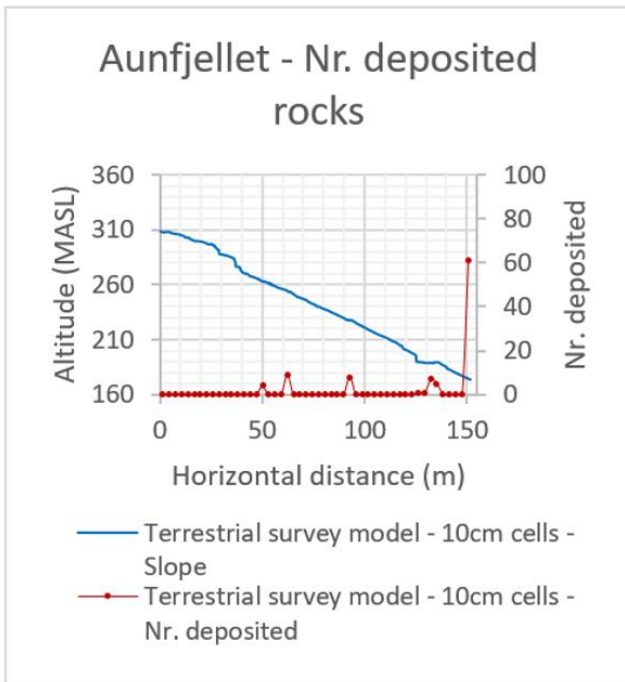


Figure 121: Simulation deposit locations. Model 0.1T.

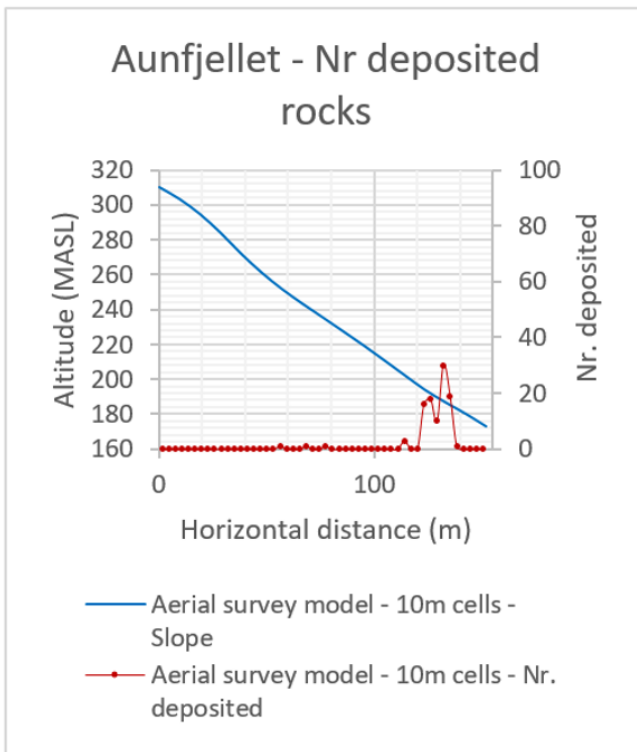


Figure 122: Simulation deposit locations. Model 10A.

### Revsnestinden

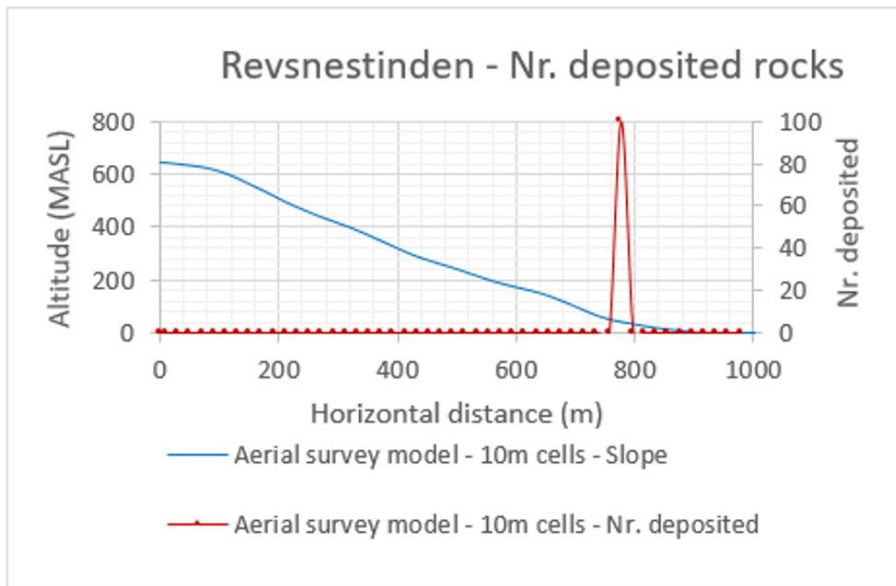


Figure 123: Simulation deposit location. Model 10A.

### Rakkenes West

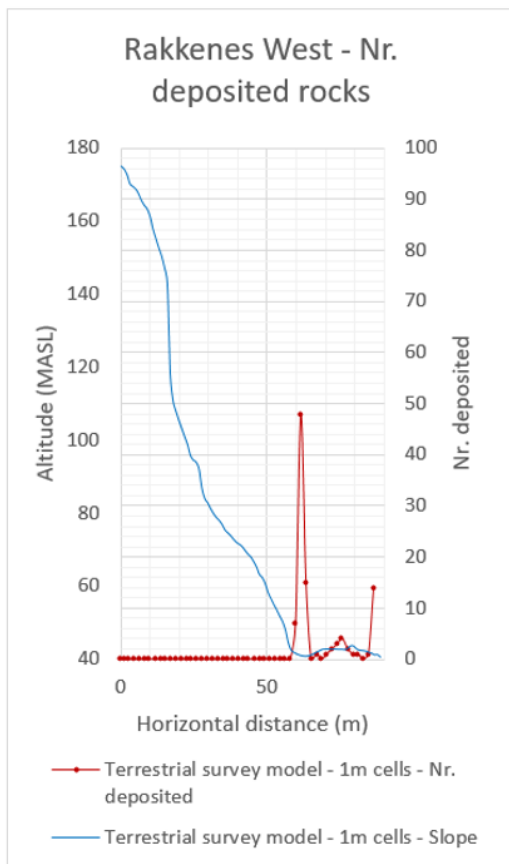


Figure 124: Simulation deposit locations. Model 1T.

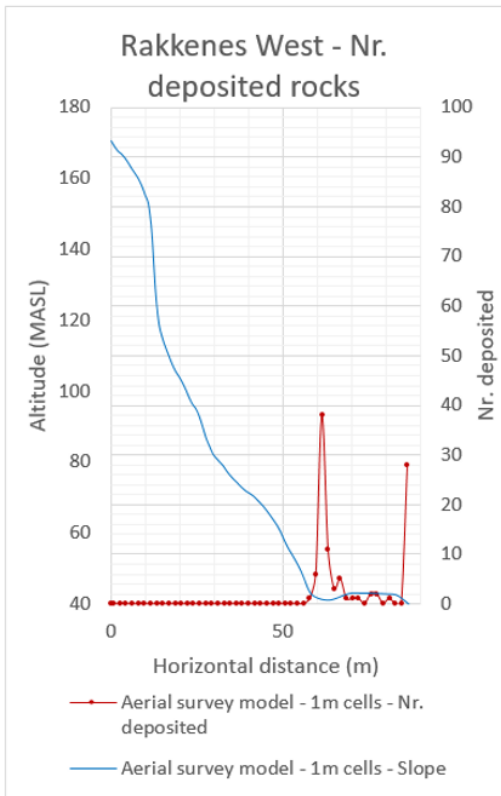


Figure 125: Simulation deposit locations. Model 1A.

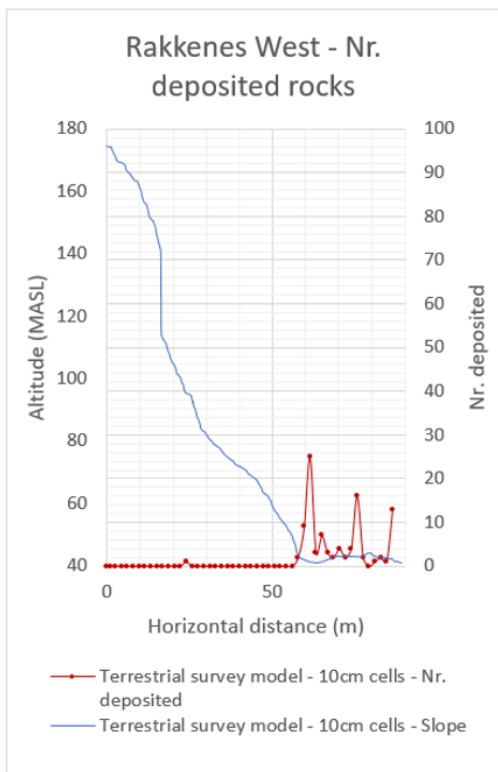


Figure 126: Simulation deposit locations. Model 0.1T.

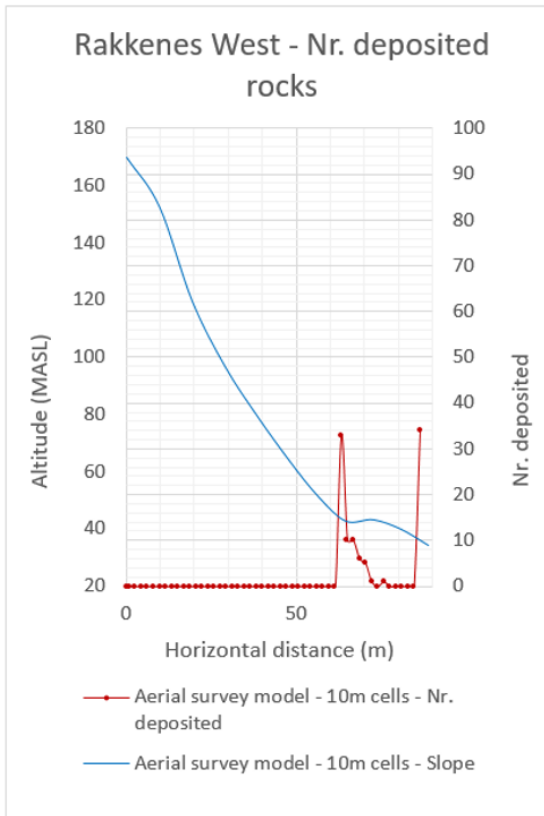


Figure 127: Simulation deposit locations. Model 10A.

**Rakkenes Central**

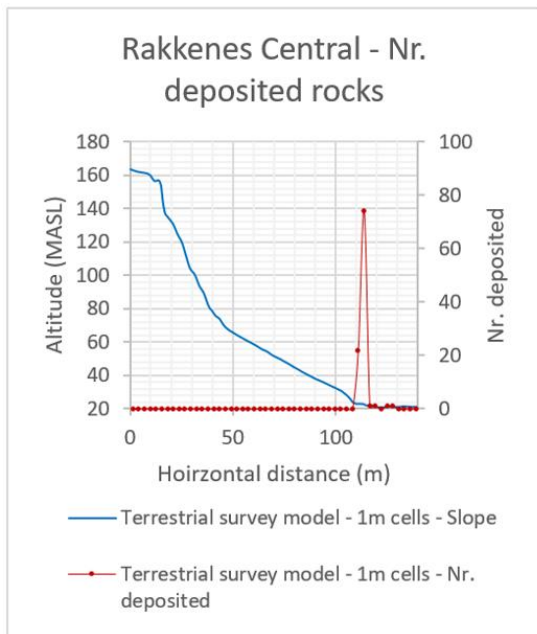


Figure 128: Simulation deposit locations. Model 1T.

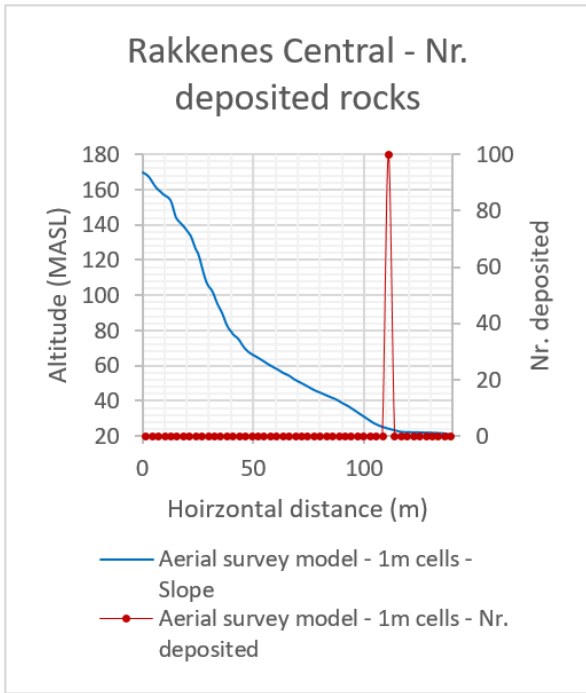


Figure 129: Simulation deposit locations. Model 1A.

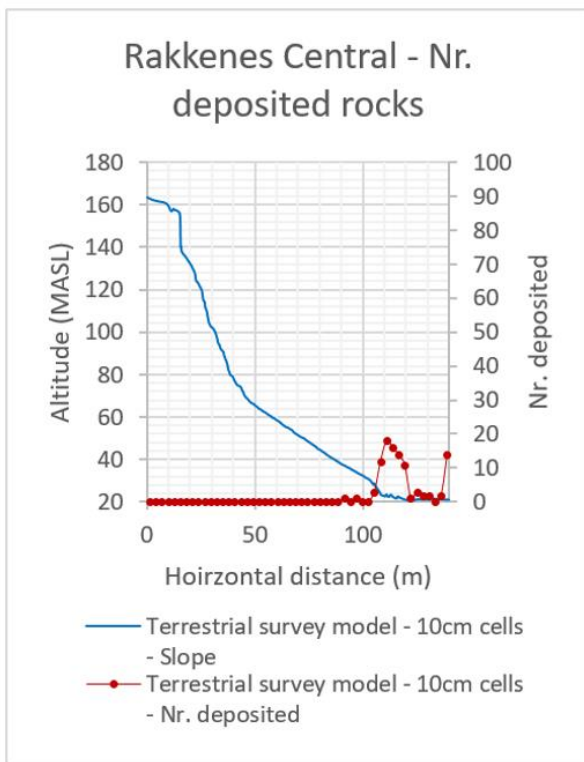


Figure 130: Simulation deposit locations. Model 0.1T.

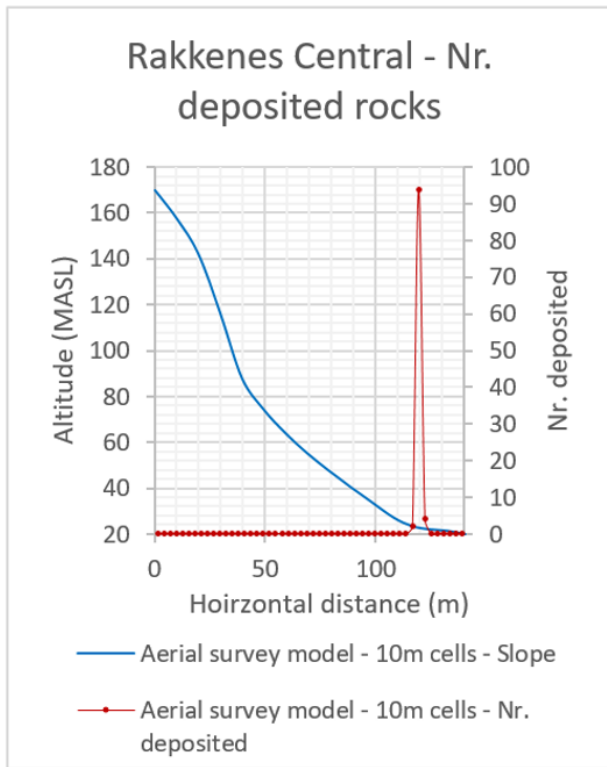


Figure 131: Simulation deposit locations. Model 10A.